Time-Resolved Infrared Spectroscopy of Photoswitchable Thioxopeptides

---

Dissertation
zur
Erlangung der naturwissenschaftlichen Doktorwürde
(Dr. sc. nat.)

vorgelegt der
Mathematisch-naturwissenschaftlichen Fakultät
der
Universität Zürich

von
Harald Bregy
aus
Niedergesteln (VS)

Promotionskomitee
Prof. Dr. Peter Hamm (Vorsitz)
Prof. Dr. Stefan Seeger
Prof. Dr. Jürg Hutter

Zürich, 2009

To my parents

List of publications

Parts of the results in this thesis have been or will be published in the following articles:

- **Harald Bregy**, Peter Hamm and Jan Helbing
  Transient Two-Dimensional Spectroscopy of a Small β-turn forming Thioxopeptide: Experiment and Simulation
  in preparation

- **Harald Bregy**, Heinz Heimgartner and Jan Helbing
  A Time-resolved Spectroscopic Comparison of the Photoisomerization of Small β-turn forming Thioxopeptides
  J. Phys. Chem. B, 113, 1756 (**2009**)

- Valetina Cervetto, Rolf Pfister Christoph Kolano, **Harald Bregy**, Heinz Heimgartner and Jan Helbing
  Coexistence of Hydrogen-Bonded Loop and Extended Tetrapeptide Conformations
  Chem. Eur. J., 13, 9004 (**2007**)

- Valetina Cervetto, **Harald Bregy**, Peter Hamm and Jan Helbing
  Time-resolved IR spectroscopy of N*-Methylthioacetamide: cis→trans isomerization and n-π* excitation*
  J. Phys Chem. A, 110, 11473 (**2006**)

- Jan Helbing, **Harald Bregy**, Jens Bredenbeck, Rolf Pfister, Peter Hamm, Robert Huber, Josef Wachtveitl, Luca De Vico and Massimo Olivucci
  A Fast Phiotoswitch for Minimally Perturbed Peptides: Investigation of the cis→trans Photoisomerization of N*-Methylthioacetamide*
  J. Am. Chem. Soc., 126, 8823 (**2004**)

Contents

Abstract

Proteins are important biomolecules. Knowledge of their conformations and conformational dynamics is essential to understand their biological functionality. While there exist established methods to investigate the structure of a protein, methods to explore the dynamics like protein folding, allosteric regulations and catalysis are relatively new and still in development. Processes which happen on a millisecond or slower time scale can be efficiently studied by NMR spectroscopy. To investigate faster dynamical processes, other spectroscopic methods are needed. In this work, time-resolved infrared spectroscopy on small peptides reveals information about dynamics on the picosecond time scale. Two-dimensional infrared spectroscopy (2D-IR) obtains structural information like coupling and relative dipole orientations between molecular groups in a protein/peptide in equilibrium. This method can also be applied to a system being not in equilibrium, e.g a peptide undergoing conformational change (transient 2D-IR). Transient (2D-)IR experiments require a trigger to induce structural changes at a well defined time. This trigger can be e.g. a temperature-jump or a molecular photoswitch in the peptide. In this work, the substitution of the carbonyl oxygen in one peptide bond by a sulfur atom is used to create a photoswitch in the peptide. The resulting thioamide bond then can be excited selectively by ultraviolet light ($\pi \rightarrow \pi^*$ excitation red-shifted in regard with an amide bond). This moiety then isomerizes and forces the peptide to change its structure. To investigate the functioning of the thioamide bond as photoswitch, *N*-Methylthioacetamide has been investigated by different methods revealing trans $\rightarrow$ cis isomerization with a high yield which is completed within one nanosecond. In this work, a thioamide containing peptide, Boc-Ala-Pro-ψ(SC-NH)-Aib-Ala-OMe, is synthesized. This thioxopeptide has well-resolved bands in the amide I region which makes the interpretation of transient spectra easier. Furthermore, it contains a -Pro-Aib- amino acid sequence which is known to form stable β-turn structure, characterized by a $i \rightarrow i+3$ hydrogen-bond. The breaking of this hydrogen-bond, induced by the photoswitch, is investigated by transient infrared spectroscopy (UV-pump/IR-probe spectroscopy). The dynamics is compared to other -Aib-containing thioxopeptides which tend to form β-turns as well. All thioxopeptides show very similar photoisomerization dynamics, while there are significant differences for the re-

laxation in the thermal ground state. Furthermore, structural properties are revealed from the time-resolved measurements, which show very rigid structure in the inner part of all the thioxopeptides (-ψ(SC-NH)-Aib-), while the tails are flexible. Finally, the investigation on the $i \rightarrow i{+}3$ hydrogen-bond breaking of thioxopeptide Boc-Ala-Pro-ψ(SC-NH)-Aib-Ala-OMe is extended to transient 2D-IR spectroscopy. For detailed interpretation of the spectra, they are compared to additionally performed computer simulations.

Zusammenfassung

Proteine sind wichtige Biomoleküle. Kenntnisse über deren Konformation und Konformationsdynamik ist essentiell, um ihre biologische Funktion zu verstehen. Während Methoden zur Strukturbestimmung von Proteinen etabliert sind, sind deren zur Untersuchung der Dynamik wie Proteinfaltung, allosterische Regulationen und Katalyse relativ neu und noch in Entwicklung. Prozesse, welche auf einer Zeitskala von Millisekunden oder langsamer stattfinden, können mit NMR-Spektroskopie untersucht werden. Um schnellere Prozesse zu untersuchen, werden andere spektroskopische Methoden gebraucht. In dieser Arbeit wird zeitaufgelöste Infrarotspektroskopie gebraucht, um Informationen über die Dynamik von kleinen Peptiden auf einer Pikosekunden-Zeitskala zu erhalten. Zweidimensionale Infrarotspektroskopie (2D-IR) erlaubt es, Strukturinformationen wie Kopplungen und relative Dipolorientierungen zwischen molekularen Gruppen in Proteinen/ Peptiden im Gleichgewicht zu untersuchen. Diese Methode kann auf Systeme, welche nicht im Gleichgewicht sind, z.B. ein Peptid während einer Konformationsänderung, angewandt werden (Transiente 2D-IR). Diese Experimente benötigen einen Auslöser, um die Konformationsänderung zu einem definierten Zeitpunkt zu induzieren. Dieser Auslöser kann zum Beispiel ein Temperatursprung oder ein molekularer Fotoschalter in einem Peptid sein. In dieser Arbeit wird die Ersetzung eines Carbonyl-Sauerstoffatom in einer Peptidbindung mit einem Schwefelatom benutzt, um einen Fotoschalter zu erzeugen. Die so erhaltene Thioamidbindung kann dann mit ultraviolettem Licht selektiv angeregt werden (die $\pi \rightarrow \pi^*$ Anregung is gegenüber einer Amidbindung rotverschoben). Dieser Teil des Moleküls isomerisiert dann und zwingt das Peptid, seine Struktur zu ändern. Um die Funktionalität der Thioamidbindung zu untersuchen, wurde N-Methylthioacetamid mit verschiedenen Methoden untersucht, was eine trans $\rightarrow$ cis Isomerisierung mit hoher Ausbeute zeigte, die innerhalb einer Nanosekunde vollendet ist. In dieser Arbeit wird ein thioamidhaltiges Peptid, Boc-Ala-Pro-ψ(SC-NH)-Aib-Ala-OMe, synthetisiert. Dieses Thioxopeptid hat aufgelöste Banden in der Amid I-Region, was die Interpretation von transienten Spektren leichter macht. Zudem enthält es eine -Pro-Aib-Aminosäuresequenz, von welcher man weiss, dass sie stabile β-Turns bildet, welche mit einer $i \rightarrow i{+}3$ Wasserstoffbrücke charakterisiert sind. Das Aufbrechen dieser Wasserstoffbrücke, welche mit

dem Fotoschalter herbeigeführt wird, wird mit transienter Infrarotspektroskopie untersucht (UV-pump/IR-probe Spektroskopie). Die Dynamik wird mit anderen -Aib-haltigen Thioxopeptiden verglichen, welche auch zur Bildung von β-Turns tendieren. Währen alle Thioxopeptide vegleichbare Fotoisomerisierungsdynamik zeigen, gibt es signifikante Unterschiede für die Relaxation im thermischen Grundzustand. Des Weiteren können strukturelle Eigenschaften mit den zeitaufgelösten Messungen untersucht werden, welche für alle Thioxopeptide eine starre Struktur im inneren Teil des Moleküls zeigen (-ψ(SC-NH)-Aib-), während deren Enden flexibel sind. Schliesslich wird die Untersuchung über das Aufbrechen der $i \rightarrow i{+}3$ Wasserstoffbrücke in Boc-Ala-Pro-ψ(SC-NH)-Aib-Ala-OMe auf transiente 2D-IR Spektroskopie erweitert. Für die genaue Interpretation der Spektren werden sie mit zusätzlich durchgeführten Computersimulationen verglichen.

Chapter 1

Introduction

Protein and Peptide Dynamics

Proteins are the molecular machines for many processes in living cells. Ion transport, cell signaling, structuring (e.g. collagen) and catalysis of biochemical reactions (enzymes) are a few of their functions. The properties and function of a protein are largely determined by its three-dimensional structure, which already was recognized at the end of the 19th century [1].

When a protein is produced in a cell, the amino acid sequence, which is coded on the DNA, is built up in the ribosomes. Twenty different amino acids with individual physical properties are used. The size of such a sequence ranges from short peptides (molecules with less than 100 amino acids) like insulin (hormone, about 50 amino acids) up to 30'000 amino acids (titin, muscle filament). The sequence of the amino acids is called the primary structure. Local hydrogen-bonding between amino acids leads to well defined motifs which are known as the secondary structure. The most prominent ones are the α-helix, the (anti-)parallel β-sheet and the β-turn. Packing of different motifs into one domain is called the tertiary structure, and possibly one step further packing of different domains leads to the quaternary structure. For the last two structure levels, interactions like disulfide bridges and other, non-covalent interactions in addition to hydrogen-bonding are important too. The complex process of structure formation is known as protein folding. Failure to fold into the correct shape usually produces inactive proteins with different properties. Diseases like Creutzfeldt-Jakob and Alzheimer are believed to result from the accumulation of incorrectly folded proteins. Studies about the relation of dynamics (not only in case of protein folding but also of ATP-driven motors [2, 3], catalytic functions or allosteric regulations [4–9]) and the structure/ function of a proteins and peptides has grown its importance only in the last decades. Dynamical processes can be studied with NMR spectroscopy in real time, if the process is sufficiently slow (microseconds, with

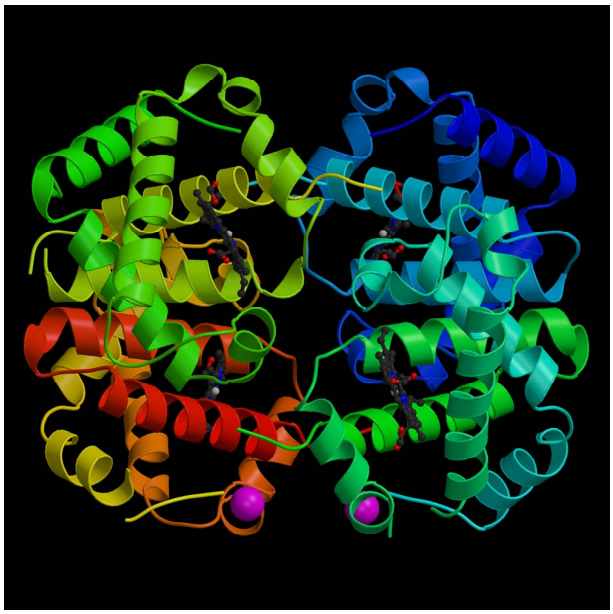

Figure 1.1: The protein Hemoglobin (PDB ID 4hhb) in its final 3-dimensional structure.

special NMR-techniques nanoseconds).

However, in many biomolecular systems a significant part of the dynamics takes place on much faster time scales. An important case are small peptides in solution, which are very flexible, and which strongly interact with the solvent. Such small peptides are considered good model systems for investigating the elementary steps of protein folding (secondary structure formation) and thus are the subject in this work. Parts of the dynamics of these molecules occurs on a (sub-)picosecond time scale which is difficult to access with NMR. Therefore, other techniques like time-resolved infrared spectroscopy are applied to access these time scales.

Experimental Idea

While there are already standardized methods for the determination of the protein structure like multidimensional NMR and x-ray crystallogrpahy [10,11], developing methods to follow protein dynamics is still a challenging research field, especially on time scales below microseconds. In this thesis time-resolved infrared (IR) spectroscopy is used to follow structure dynamics on the level of peptides. This technique uses IR pulses with a temporal width of about 100 fs. Using them, triggered conformational changes which take place on a (sub-)ps timescale can be investigated. The big advantage of this method compared to NMR-techniques is the higher time resolution, on the other hand IR bands are less resolved than NMR-peaks due to the much less distinct motional narrowing [12,13]. Due

to their properties, these two methods give different information about a system. Thus, they should be viewed as complementary rather than competing methods.

An extension to time-resolved IR spectroscopy is 2D-IR spectroscopy (more detailed description in chapter 2) [14–16]. In this technique a narrow (~ 10 cm^{-1}) IR-pump pulse is used to excite an IR band while the following IR-probe pulse is used to investigate coupling and anisotropy between the excited band and the others. From these measurements structural parameters can be deduced [13, 17–21].

A further extension can be made to transient 2D-IR spectroscopy where a conformational change in a peptide is induced and the structural change is observed by 2D-IR spectroscopy [22, 23].

Conformational changes in a peptide can be induced by either a temperature-jump [24–27] or (as is done in this work) by a built-in photo switch which can be isomerized by a visible or ultraviolet light pulse.

Photoswitches and their Applications to Peptide Folding

Azobenzene: A widely used photo switch is azobenzene which has been investigated extensively. Its cis→trans isomerization is ultrafast (< 1 ps) [28] with a high quantum yield of 50 %. Azobenzene has been integrated [29–34] into peptides and the conformational change after isomerization of the photo switch has been investigated among others by time-resolved IR spectroscopy [35–41]. Furthermore, transient 2D-IR spectroscopy has been applied [42].

Disulfidebridges: It has been shown that disulfide bridges in peptides can be easily cleaved by irradiation of ultraviolet light [43, 44] and thus a conformational change can be induced. Disulfide bridge-containing peptides which define a very rigid β-turn structure have been synthesized [45] and it has been shown that the opening of a β-turn can be investigated by time-resolve IR spectrscopy [46]. With transient 2D-IR spectroscopy the opening of the intramolecular hydrogen-bond could be observed directly after opening the β-turn with ultraviolet light [47].

Thioamide: In peptides the neighboring amino acids are covalently bound via amide bonds which are predominantly in their trans conformations and can be isomerized upon UV excitation [48]. Substitution of one oxygen atom with a sulfur atom leads to a thioamide bond (see Figure 1.2). The $\pi \rightarrow \pi^*$ excitation energy of a thioamide is red-shifted (maximum at 255 nm [49]) compared to the one of an amide bond (center at 186 nm [50]). Thus, photoisomerization can now be induced at one certain position in the peptide. This modification leads to the least invasive photo switch for peptides. It has been shown that this substitution does not change the secondary structure of a pep-

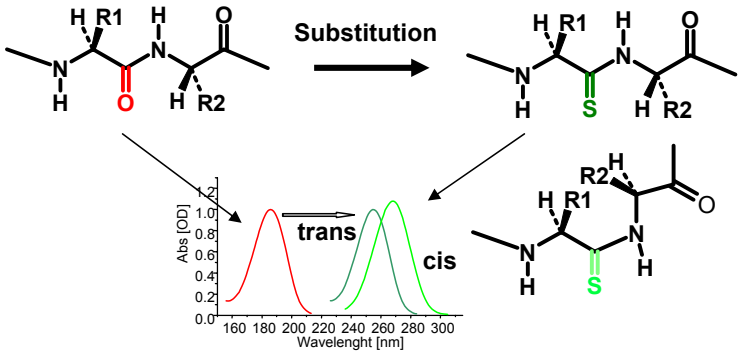

Figure 1.2: Substitution of an oxygen in one peptide bond leads to a thioamide whose $\pi \rightarrow \pi^*$ excitation leads to a read shift compared to an amide bond. Thus the thioamide bond can be excited selectively.

tide significantly [51, 52]. The ability of this moiety to isomerize is described in detail in chapter 4. There, results of time-resolved IR spectroscopy and additional methods (time-resolved UV/Vis spectroscopy and *ab initio* computer simulations) on the isomerization of *N*-Methylthioacetamide, which is the simplest photoswitchable thioamide, after $\pi \rightarrow \pi^*$ excitation are presented. In this thesis work this thioamide photo switch moiety is used to trigger the peptides.

In earlier work the ability of isomerizing thioxopeptides (peptides which contain at least one sulfur-substituted carbonyl group in a peptide bond) has been studied with steady state methods [53, 54] and also transient IR and UV measurements have been used to investigate the isomerization in real time [55–57].

One goal of this work was to synthesize a thioxopeptide which is an optimal model for the investigation of conformational dynamics with time-resolved infrared spectroscopy, especially for the transient 2D-IR measurements. Therefore, the amino acid sequence is chosen so that the thioxopeptide is as small as possible (minimize amount of infrared bands and the complexity of interactions), have a defined secondary structure in its thermal equilibrium, namely a β-turn form, and well-resolved bands in the infrared amide I region (see Figure 1.3). However, the synthesis of α-aminoisobutyric acid (Aib)-containing thioxopeptides has been a challenging research field for the last decades.

Difficulties involved in the Synthesis of Thioxopeptides

Since the 1950s the change of biological activity of modified proteins have been investigated. Biologically active proteins with a built-in sulfur atom in one peptide bond can show protease resistance, in- or decreased biological activity or better receptor selectivity [58–61].

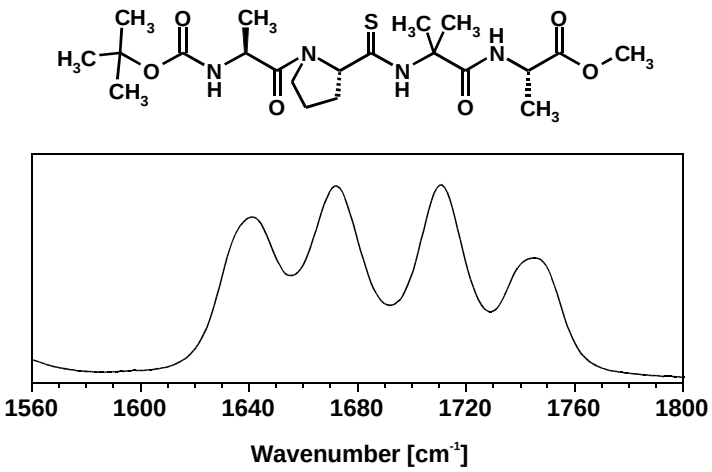

Figure 1.3: Synthesized thioxopeptide with its thioamide photoswitch and the resolved bands in the amide I region.

One possibility to synthesize thioxopeptides is the use of thionation [62, 63] or thioacylation reagents [64, 65], which exchange the oxygen atom in an amide bond of a N- and O-terminal protected dipeptide with a sulfur atom. Theoretically, the dithioxopeptide then can be built in a bigger peptide after de-protection based on normal solid-phase reaction [66–70]. If acid labile protection groups are used at the N-terminal site one has to use mild acid reagents because the thioamide undergoes acid-catalyzed hydrolysis too. Successful cleavages with different mild acid reagents have been reported [71]. The bigger problem is de-protection on the C-terminus site. As soon as it is de-protected the so called 1,3-thiazol-5(4*H*) is formed which is only little reactive and the residue of the N-terminal amino acid undergoes racemization (see Figure 1.4). The racemization can be suppressed by fast reaction conditions.

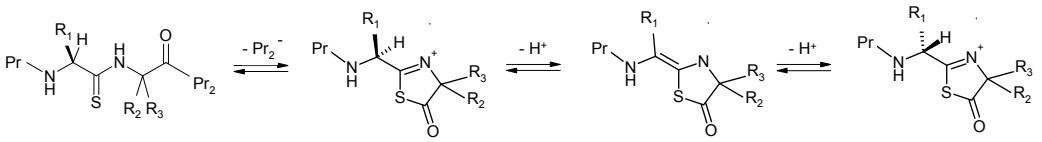

Figure 1.4: Probable reaction mechanism for the racemization after C-terminal deprotection of a dithioxopeptide.

In addition, the peptides contain Aib. This bi-substituted amino acid is known to induce β-turns and helices in peptides [72]. The amino acid Aib which is spatially ambitious prevents the bonding on its N-terminal site to another amino acid resp. peptide. This and the possible racemization of 1,3-thiazol-5(4*H*) are the challenging steps in the synthesis of Aib-containing thioxopeptides. An elegant way to do this is the 'Azirine/Oxazolone

method' which was developed in the 1980s and 1990s by Heimgartner's group [73, 74].

A-Pro-Aib-containing thioxopeptide has been synthesized during this work. The procedure is presented in chapter 3 in detail. The isomerization dynamics of this thioxopeptide then is compared to other -Aib-containing thioxopeptides which were synthesized according the same procedure and were provided directly by the Heimgartner group [75–77].

Outline of the Experiments

The measurements mainly focus on the thioxopeptide Boc-Ala-Pro-ψ(SC-NH)-Aib-Ala-OMe. The isotope labelled analogue Boc-Ala-ψ(O^{13}C-NH)-Pro-ψ(SC-NH)-Aib-Ala-OMe and the thioxopeptides provided by Heimgartner's group, Z-Gly-ψ(SC-NH)-Aib-Ile-OMe, Z-Ala-ψ(SC-NH)-Aib-Ile-OMe, Z-Ile-ψ(SC-NH)-Aib-Gly-OMe and Boc-Phe-Ile-ψ(SC-NH)-Aib-Phe-OMe are investigated to see how general the results obtained from Boc-Ala-Pro-ψ(SC-NH)-Aib-Ala-OMe are.

It is known that small Aib- and specifically Pro-Aib-containing peptides tend to form β-turns whose most specific property is a $i \rightarrow i+3$ hydrogen-bond. In chapter 5 the investigations of the conformations of Boc-Ala-Pro-ψ(SC-NH)-Aib-Ala-OMe are shown, with the aim to identify molecules folded in the β-turn conformation. For this purpose, (2D-)IR,^{13}C- and temperature-dependent ^{1}H-NMR measurements are used.

In the following chapter (6) the results of the time-resolved infrared measurements on the conformational change of Boc-Ala-Pro-ψ(SC-NH)-Aib-Ala-OMe, initiated by the isomerization of the built-in photoswitch, are presented. It is assumed that the isomerized conformation of the photoswitch (cis form) hinders the peptide to form a β-turn. Therefore, investigation of the β-turn opening is possible.

In chapter 7 the conformation and isomerization properties of Boc-Ala-Pro-ψ(SC-NH)-Aib-Ala-OMe are compared to other Aib-containing thioxopeptides. Additionally, results on the backreaction on the electronic ground state after isomerization are shown.

When performing polarization dependent (parallel and perpendicular orientation between the different pulses) 2D-IR, transient 1D- and 2D-IR it is possible to obtain structural properties of the system. These structural parameters are presented in chapter 8 and compared to a crystal structure performed by Lehmann et al. [77]. These structural parameters are also needed to simulate 2D-IR and transient 2D-IR spectra (see chapter 9).

The main goal of this work is to investigate conformational changes (specifically changes in coupling) with transient 2D-IR spectroscopy. This method is still in development and the interpretation of transient 2D-IR spectra is challenging. The method has already been applied to another small thioxopeptide, but the partial overlap of the amide I bands and

the coexistence of different equilibrium-structures made the spectroscopic investigation and interpretation quite difficult [57]. The thioxopeptide Boc-Ala-Pro-ψ(SC-NH)-Aib-Ala-OMe it is a model system with fully-resolved bands in the amide I region and strong structural constraints. Chapter 9 shows the measured spectra, which then are compared to computer-simulated spectra.

Chapter 2

Principle of 2D-IR Spectroscopy

2D-IR spectroscopy used here is based on the excitation of a vibrational system with a narrow-band IR-pump pulse followed by a broad-band IR-probe pulse. Other 2D-IR techniques like time domain-pulsed Fourier transform spectroscopy have be devised as well and yielded similar information [78–83]. Additional variations are 2D-Raman [84–86] and DOVE [87, 88] spectroscopy.

Using an IR-pump pulse, a vibrational system can be excited to higher energy levels and thereafter probed by an IR-probe pulse (see Figure 2.2, top left). The resulting spectra are difference spectra by subtracting the spectrum without IR excitation from the spectrum with IR excitation (see Figure 2.2, bottom left, two vibrational systems are shown). Positive (red) and negative (blue) parts have three origins:

- Ground state bleaching (blue solid arrow in Figure 2.2, top left), $|0\rangle \rightarrow |1\rangle$ transition. It is observed when the IR-probe pulse detects a decrease of the ground state population which has been previously transferred to the first excited state by the IR-pump pulse.

- Stimulated emission (red dashed arrow in Figure 2.2, top left), $|1\rangle \rightarrow |0\rangle$ transition. It takes place when the IR-probe pulse stimulates the molecules in the excited state to return to the ground state.

- Excited state absorption (blue arrow in Figure 2.2, top left), $|1\rangle \rightarrow |2\rangle$ transition. This is observed when the excited molecules in the first energy level are excited to the second level by the IR-probe pulse.

Ground state bleaching and stimulated emission both contribute to the negative part of the signal, while the excited state absorption contributes to the positive part. If the system is harmonic the positive and the negative contributions would eliminate each other because the energy differences between the different vibrational states would be the same. Therefore it is essential that the vibrational system is anharmonic to observe positive and negative peaks.

The lineshape of the 2D-IR spectrum can give information about the internal dynamics

of the system. An inhomogeneously broadened band of one oscillator can for example arise from molecules having different solvent environments, provided that the exchange between them is slow enough. In Figure 2.1 (a) this is indicated with several sub-bands lying under the broad absorption band. Thus, exciting the band at different spectral positions with the IR-pump pulse results in a selective excitation. In this case, the 2D-IR shape is narrow in the IR-probe direction and tilted along the diagonal of the graph. In other words, the maximum of the absorption change varies with the frequency of the IR-pump pulse. If the exchange between the sub-states is sufficiently fast and/ or a band does not have any sub-structures, the maximum of the absorption change in the 2D-IR spectrum then would be independent of the spectral position of excitation (see Figure 2.1, b). In the mid-infrared range vibrational bands start to look homogeneous when increasing the time delay between the IR-pump and IR-probe pulse, due to spectral diffusion on a picosecond timescale.

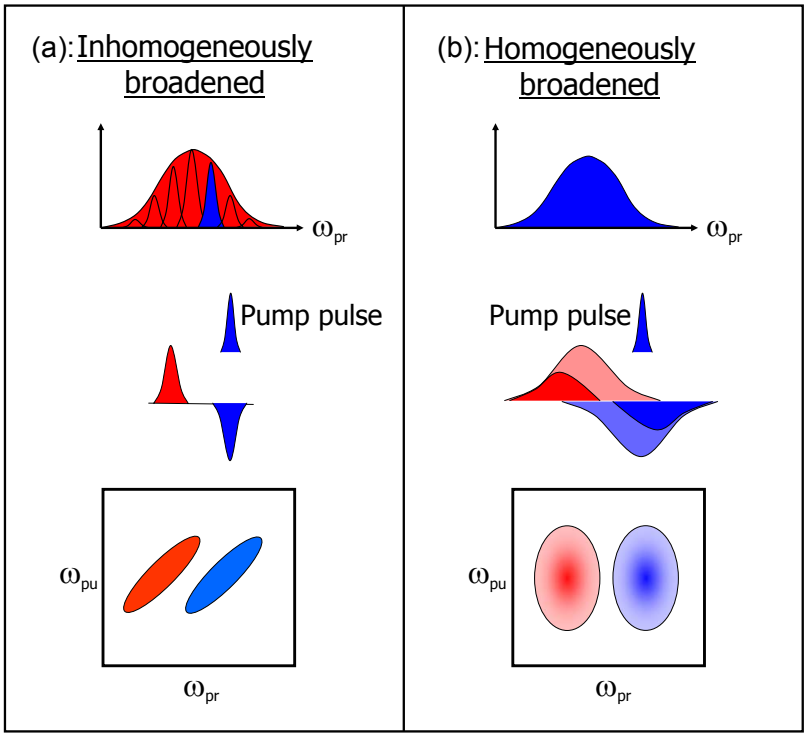

Figure 2.1: a: The 2D-IR shape in case of an inhomogeneously broadened band. b: The 2D-IR shape in case of an homogeneously broadened band.

Considering a system with more than one vibration 2D-IR spectroscopy is sensitive to the strength of the coupling and between oscillators and their anisotropies. In the following sections this is illustrated with one pair of oscillators.

2.1 Coupling

A pair of oscillators give rise to two absorption bands in the linear IR spectrum. Figure 2.2 (bottom) shows the oscillators between 1600 and 1700 cm^{-1}, but the theoretical description is completely general. If the two oscillators are not coupled, the 2D-IR spectrum shows two signals on the diagonal, each consisting of a positive (red) and a negative (blue) part (see Figure 2.2, bottom left). Coupling of these two oscillators leads to two additional features in the 2D-IR spectrum, arising at the IR-pump frequency of one band and the IR-probe frequency of the other. These features are called off-diagonal or cross peaks (see Figure 2.2, bottom right). To understand these features, the vibrational energy of a molecule can be expanded on powers of the excitation level n_i of each normal mode [89]:

$$E = \sum_i \epsilon_i (n_i + \frac{1}{2}) - \sum_{i \leq j} \chi_{ij} (n_i + \frac{1}{2})(n_j + \frac{1}{2}) + \cdots. \tag{2.1}$$

In this picture, the state $|mn\rangle$ describes the system with m quanta in mode 1 and n quanta in mode 2 (see Figure 2.2 top right). The diagonal signals arise from the $|00\rangle \rightarrow |10\rangle$ (8, ground state bleaching), $|10\rangle \rightarrow |00\rangle$ (4, stimulated emission), $|10\rangle \rightarrow |20\rangle$ (3, excited state absorption), $|00\rangle \rightarrow |01\rangle$ (2, ground state bleaching), $|01\rangle \rightarrow |00\rangle$ (6, stimulated emission), $|01\rangle \rightarrow |02\rangle$ (5, excited state absorption) transitions. The $|10\rangle \rightarrow |20\rangle$ and $|01\rangle \rightarrow |02\rangle$ transition energies are lowered by a diagonal anharmonicity $2\chi_{ii}$ with regard to the $|00\rangle \rightarrow |10\rangle$ and $|00\rangle \rightarrow |01\rangle$ transition energies respectively. If the two oscillators now interact, a $|00\rangle \rightarrow |10\rangle$ (8) transition reduces the population of the common ground state $|00\rangle$, which results in a decrease of absorption (bleach) not only at the frequency of the $|00\rangle \rightarrow |10\rangle$ transition (8), but also at the frequency of the $|00\rangle \rightarrow |01\rangle$ transition (2) which is then observed as a negative off-diagonal signal. After excitation of the $|00\rangle$ state to the $|10\rangle$ state (8), a transition from the $|10\rangle$ state to the $|11\rangle$ (1) state is possible which then is seen as positive off-diagonal peak. Of course, this is true vice-versa: After $|00\rangle \rightarrow |01\rangle$ (2) excitation, additional features are observed in the off-diagonal region which are due to the $|00\rangle \rightarrow |10\rangle$ (8) and the $|00\rangle \rightarrow |01\rangle$ (5) transition. The $|10\rangle \rightarrow |11\rangle$ and $|01\rangle \rightarrow |11\rangle$ transition energies are lowered by a off-diagonal anharmonic factor χ_{ij} with regard to the $|00\rangle \rightarrow |01\rangle$ and $|00\rangle \rightarrow |10\rangle$ transition energies respectively. For uncoupled modes χ_{ij} is zero and the signals 1 and 2 exactly cancel (also 7 and 8).

When the normal modes are essentially linear combinations of localized vibrations (such as C=O stretch vibrations for amide I), the exciton model is often used as a simpler, more intuitive model. The coupling parameter β_{12} is introduced in this model and is directly related to the off-diagonal anharmonicity χ_{ij} as it is shown later (see equation 2.3). The Hamiltonian for two coupled anharmonic oscillators in the site basis is given

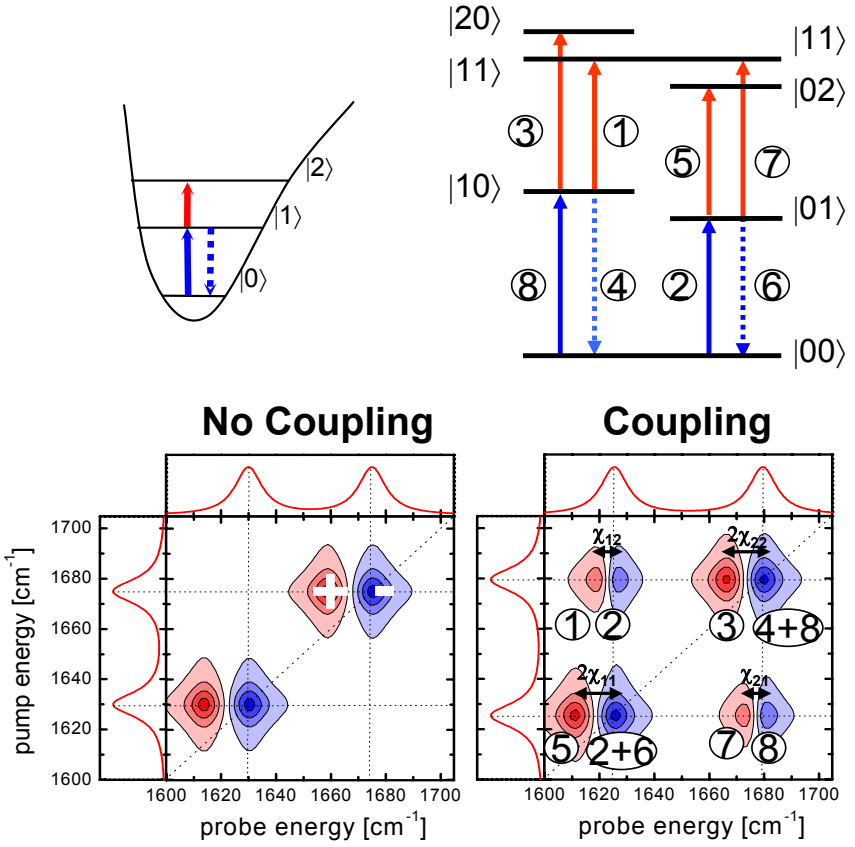

Figure 2.2: Top left: Anharmonic vibrational system with their vibrational states which can be reached with the 2D-IR method. Top right: A coupled two oscillator system with the possible states which can be reached with 2D-IR spectroscopy. Bottom left: 2D-IR spectrum of two oscillators which are not coupled. Bottom right: 2D-IR spectrum of two oscillators which are coupled.

by [14]:

$$H = \begin{pmatrix} 0 & & & & & \\ & \varepsilon_1 & \beta_{12} & & & \\ & \beta_{12} & \varepsilon_2 & & & \\ & & & 2\varepsilon_1 - \Delta & 0 & \sqrt{2}\beta_{12} \\ & & & 0 & 2\varepsilon_2 - \Delta & \sqrt{2}\beta_{12} \\ & & & \sqrt{2}\beta_{12} & \sqrt{2}\beta_{12} & \varepsilon_1 + \varepsilon_2 \end{pmatrix}. \tag{2.2}$$

The energies ε_1 and ε_2 correspond to the independent excitations of the localized vibrations 1 and 2 respectively, when the oscillators are not coupled. Anharmonicity is introduced by lowering the site energies of the doubly-excited site-states by an energy

Δ which has been determined from pump/probe experiments on the amide I band of an isolated peptide unit (N-Methylacetamide) [90]. Diagonalization of the Hamiltonian yields the frequencies E and transition dipoles of all possible transitions in the exciton basis. In the weak coupling limit ($\beta_{12} \ll \mid \varepsilon_1 - \varepsilon_2 \mid$) the diagonal anharmonicities are $\chi_{11} \approx \chi_{22} = -\frac{\Delta}{2}$ and the off-diagonal anharmonicity χ_{12} (and χ_{12}) can be calculated perturbatively [91]:

$$\chi_{12} = 4\Delta \frac{\beta_{12}^2}{(\varepsilon_1 - \varepsilon_2)^2}. \tag{2.3}$$

It can be easily seen that the off-diagonal anharmonicity χ_{12} decreases if the spectral separation of the two bands increases. Additionally, if the coupling β_{12} vanishes, the off-diagonal anharmonicity χ_{12} vanishes, too. In that case, both signals contributing to the cross peak appear at the same frequency and cancel exactly. Hence, the intensity of the cross peak is a direct measure of the coupling β_{12}.

The coupling of two oscillators is related to their relative orientation and distance. The simplest approach to relate the coupling constant β_{12} to geometrical properties is the transition dipole coupling model explored by Krimm et al. [92] and Torii et al. [93] This method is based on two approximations: the dipole approximation and neglect of through-bond effects. The resulting through-space-coupling is given by:

$$\beta_{12} = \frac{1}{r_{12}^3}(\widehat{\mu}_1 \cdot \widehat{\mu}_2 - 3(\widehat{r}_{12} \cdot \widehat{\mu}_1)(\widehat{r}_{12} \cdot \widehat{\mu}_2)), \tag{2.4}$$

where $\widehat{\mu}_1$ and $\widehat{\mu}_2$ are the transition dipoles moments of the two oscillators, r_{12} the distance between their centers and $\widehat{r}_{12}$ the unit vector along this distance. It can be easily seen that the coupling β_{12} decreases to the third power of the distance between the two oscillators.

In this thesis the measurements are mainly focused on the amide I modes in peptides (mainly C=O stretch vibration in the peptide bonds). It has been shown that for the amide I modes of adjacent peptide units this through-space-coupling is, however, a poor approximation, and *ab initio* calculations are needed to include through-bond-effects [14, 91]. A calculated nearest neighbor coupling map as a function of dihedral angles based on a HMR-B3LYP method is shown in Figure 2.3 [93].

2.1.1 Coupling calculation from delocalized modes

From orthogonal, delocalized amide I modes obtained e.g. via *ab initio* calculations, the coupling β_{12} between localized C=O stretch vibrations can be revealed by using the Hessian matrix reconstruction [94, 95]:

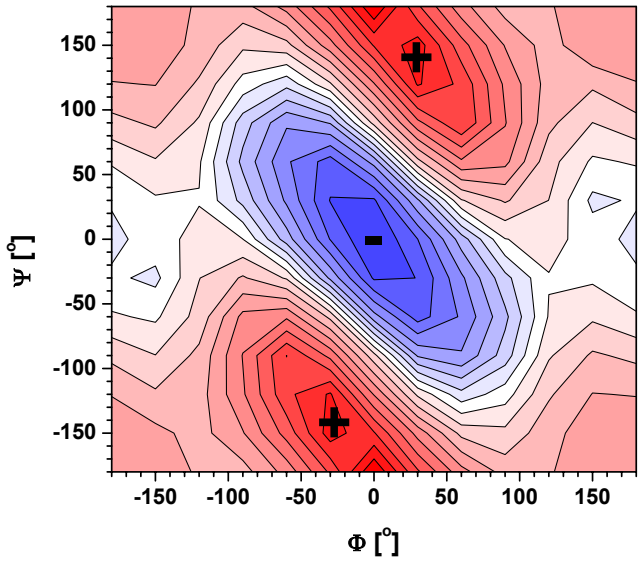

Figure 2.3: Calculated coupling map β_{12} in equation 2.2 based on a HMR-B3LYP method in dependence of the dihedral angles ϕ and ψ between two amide I transition dipole moments [93]. Scaled from -33 cm^{-1} (dark blue) to 45 cm^{-1} (dark red). Contour intervals are 4 cm^{-1}.

$$\begin{pmatrix} \varepsilon_1 & \beta_{12} \\ \beta_{12} & \varepsilon_2 \end{pmatrix} = U^{-1} \begin{pmatrix} E_1 & 0 \\ 0 & E_2 \end{pmatrix} U. \tag{2.5}$$

The eigenvector U can be deduced directly from the change of the C=O distances of the single normal modes, revealed from the *ab initio* output.

2.2 Anisotropy

The second set of structural information can be obtained by measuring 2D-IR spectra with the IR-pump pulse oriented perpendicular and parallel to the IR-probe pulse. In the case of parallel orientation, pumping one vibrational oscillator gives a stronger off-diagonal signal (which arises from the second vibrational oscillator) when the transition dipole moments are parallel oriented to each other and visa-versa. Calling the measurement signal with parallel orientation between the IR-pump and the IR-probe pulse $\Delta A_{2D,\parallel}(t)$ and the one with perpendicular orientation $\Delta A_{2D,\perp}(t)$ the so-called anisotropy $r(t)$ with a time delay t between the two IR pulses is given by [96, 97]:

$$r(t) = \frac{\Delta A_{2D,\parallel}(t) - \Delta A_{2D,\perp}(t)}{\Delta A_{2D,\parallel}(t) + 2\Delta A_{2D,\perp}(t)}, \tag{2.6}$$

which is defined to be a value between 0.4 and -0.2. When increasing the time delay between the two pulses, the anisotropy $r(t)$ decreases and finally goes to zero after a certain time t because of the rotational diffusion of the molecules. By extrapolating the anisotropy values $r(t)$ to $t = 0$, the anisotropy value directly reflects the angle θ between the two involved transition dipole moments, given by [96, 97]:

$$\theta \quad = \quad \arccos \sqrt{\frac{5r(0)+1}{3}}. \tag{2.7}$$

This equation results in a value θ between 0° (parallel, $r(0) = 0.4$) and 90° (perpendicular, $r(0) = -0.2$). The anisotropy gives only information about how the transition dipole moments are oriented to each other. Thus the angle θ, $(180 - \theta)°$, $(180 + \theta)°$, $-\theta$ give rise to the same anisotropy value.

2.3 Extension to Transient 2D-IR Spectroscopy

2D-IR spectroscopy is an equilibrium measurement, but one can make it a non-equilibrium experiment by using 2D-IR spectroscopy as a probe after some photo excitation of the system (in this work the isomerization of the photoswitch which is built in the peptide). This method can be seen as a combination of transient absorption and the 2D-IR spectroscopy (see Figure 2.4). Compared to the transient IR measurements one should be able to obtain more (detailed) information concerning the peptide dynamics. On one hand, the broad and partially overlapping IR bands can be excited selectively by the narrow IR-pump pulse and thus be separated, making the investigation of single-IR bands less complicated [23]. On the other hand one should be able to observe changes in coupling between different oscillators which happen during conformational changes [47].

Three pulses are used for the measurement (details of the setup are described in chapter 3): a UV pulse excites the photo switch and thus initiates the conformational change of the peptide, and a 2D-IR pulse pair probes structural properties like coupling between different vibrational oscillators during the conformational change. The resulting spectrum is the difference of the 2D-IR spectrum (which is also a difference spectrum) after a certain delay between the UV-pump pulse and the IR-pump pulse and the 2D-IR spectrum with no UV excitation. Usually, the time delay between the IR-pump and the IR-probe pulse is set constant (1.2 ps). Like in transient absorption, taking difference spectra has the advantage that the signal from molecules, which are not excited, cancel each other out.

The big advantage of this method compared to other transient structure determining method such as time-resolved multidimensional NMR is the much higher time-resolution. By using 100 fs pulses transient spectra in steps of approximately 1 ps after initialization of

the conformational change can be taken. Nevertheless, this method is not at all established for peptide dynamics investigations. Small thioxopeptides with well resolved IR bands in the amide I region constitute well defined model systems to investigate the capability of this method.

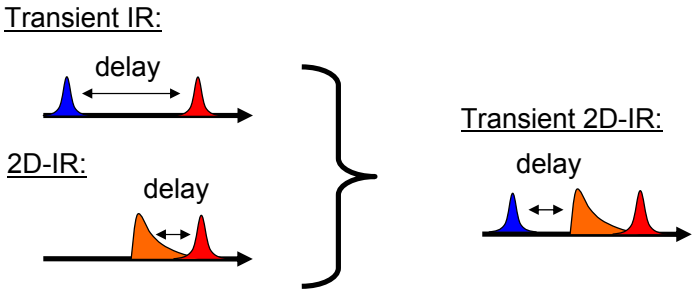

Figure 2.4: Pulse sequences of the transient IR, 2D-IR and transient 2D-IR methods.

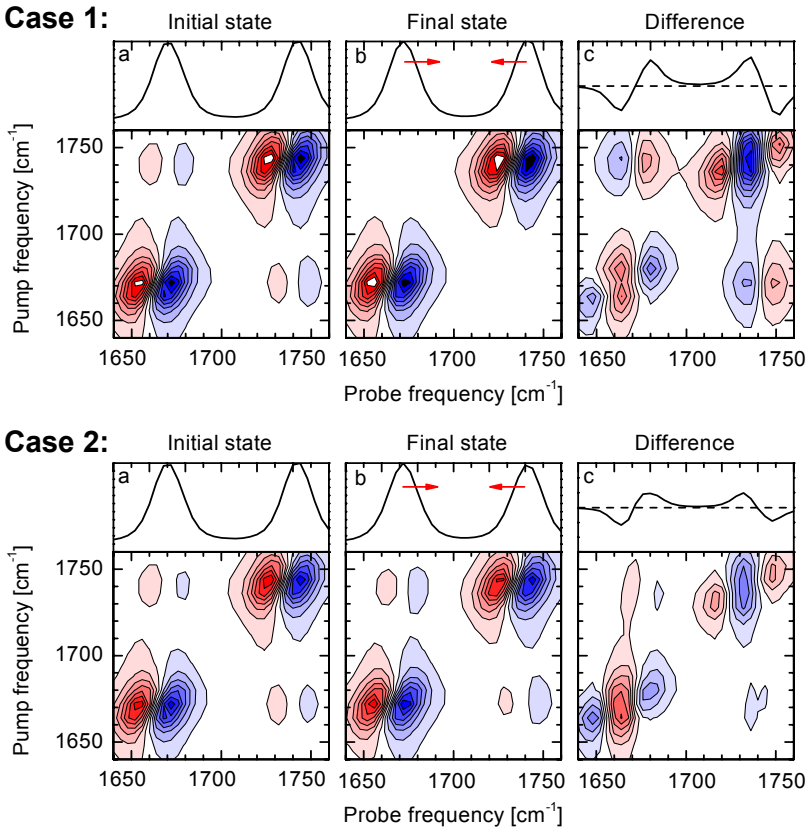

Figure 2.5: Examples for transient 2D-IR spectra. Initial parameters: $\varepsilon_1 = 1672$ cm^{-1}, $\varepsilon_2 = 1742$ cm^{-1}, $\beta_{12} = 10$ cm^{-1} (coupling). Change of parameters: (case 1, top) $\Delta\beta_{12}$: -10 cm^{-1}, (case 2, bottom) $\Delta\varepsilon_1$: +1.5 cm^{-1}, $\Delta\varepsilon_2$: -1.5 cm^{-1}.

An example where the coupling changes during e.g. a conformational change of a molecule is shown in Figure 2.5 (top) [23]. It contains two coupled (10 cm^{-1}) oscillators at spectrally well resolved positions (1672 cm^{-1} and 1742 cm^{-1}). Since the transient 2D-IR spectrum is a difference spectrum (final state minus initial state) a feature obtained in the final 2D-IR spectrum appears with the same sign in the transient 2D-IR difference spectrum while the one of the initial 2D-IR spectrum changes its sign. From the initial to the final state the coupling changes from 10 cm^{-1} to 0 cm^{-1}. Due this change, the bands also move in their spectral positions slightly (the left one shifts blue while the right one shifts red in this case). This shift leads to characteristic blue-red-blue resp. red-blue-red shape for the blue- resp red-shift of the bands. An evident change can also be seen in the off-diagonal region. The blue-red feature is caused by the disappearance of the initially cross peak.

Nevertheless, a similar spectrum can be obtained when the coupling does not change and only a blue- resp. red-shift of + 1.5 cm^{-1} resp. - 1.5 cm^{-1} of the absorption bands is induced (see Figure 2.5, bottom). On the diagonal the same shapes as in example 1 are seen. Thus, just looking at the diagonal does not give enough information about the origin of this spectral change. In the off-diagonal region the same shape as on the diagonal can be seen, but with much smaller intensity. Thus, if the coupling change in case 1 is big enough one should be able to distinguish between different origins which causes the spectral change. If the coupling change is relatively small, the off-diagonal spectral change will be dominated by the shift, so no difference between cases 1 and 2 would be apparent.

These examples indicate that one has to be very careful with the interpretation of transient 2D-IR spectra. Indeed, to draw the correct conclusions from these spectra can be quite challenging (see chapter 9).

Chapter 3

Material and Methods

3.1 Synthesis

The aim of the synthesis is to have an optimal model for the investigation with time-resolved infrared spectroscopy, especially for the transient 2D-IR measurements. Therefore, the amino acid sequence is chosen so that the thioxopeptide is as small as possible (minimize number of infrared bands and the complexity of interactions), have a defined secondary structure (β-turn) before photoswitching (encanced by incorporation of a -Pro-Aib- moiety), and well-resolved bands in the infrared amide I region. However, the synthesis of α-aminoisobutyric acid (Aib)-containing thioxopeptides has been a challenging research field for the last decades.

With a variation of the 'Azirine/Oxazolone method' [73,74], which has been developed by Heimgartner et al. in the 1980s and 1990s, it is possible to synthesize thioxopeptides without significant epimerization (see 1.4) and thus high quantum yields. Different reaction mechanisms have been conceived, of which the most probable is presented in the following section.

Additionally, the complete procedure for the synthesis of the thioxopeptides Boc-Ala-Pro-ψ(SC-NH)-Aib-Ala-OMe and Boc-Ala-ψ(O^{13}C-NH)-Pro-ψ(SC-NH)-Aib-Ala-OMe which have been synthesized during this work, are presented in this chapter.

The thioxopeptides Z-Gly-ψ(SC-NH)-Aib-Ile-OMe, Z-Ala-ψ(SC-NH)-Aib-Ile-OMe, Z-Ile-ψ(SC-NH)-Aib-Gly-OMe and Boc-Phe-Ile-ψ(SC-NH)-Aib-Phe-OMe have been synthesized and provided by the Heimgartner group [75–77].

3.1.1 Reaction mechanism

In this synthesis method an N-terminal protected amino thioacid (**1**) reacts with a 3-amino-2*H*-azirine [98] (**2** to **3**). The probable mechanism is shown in Figure 3.1 (a) [73,74]. The

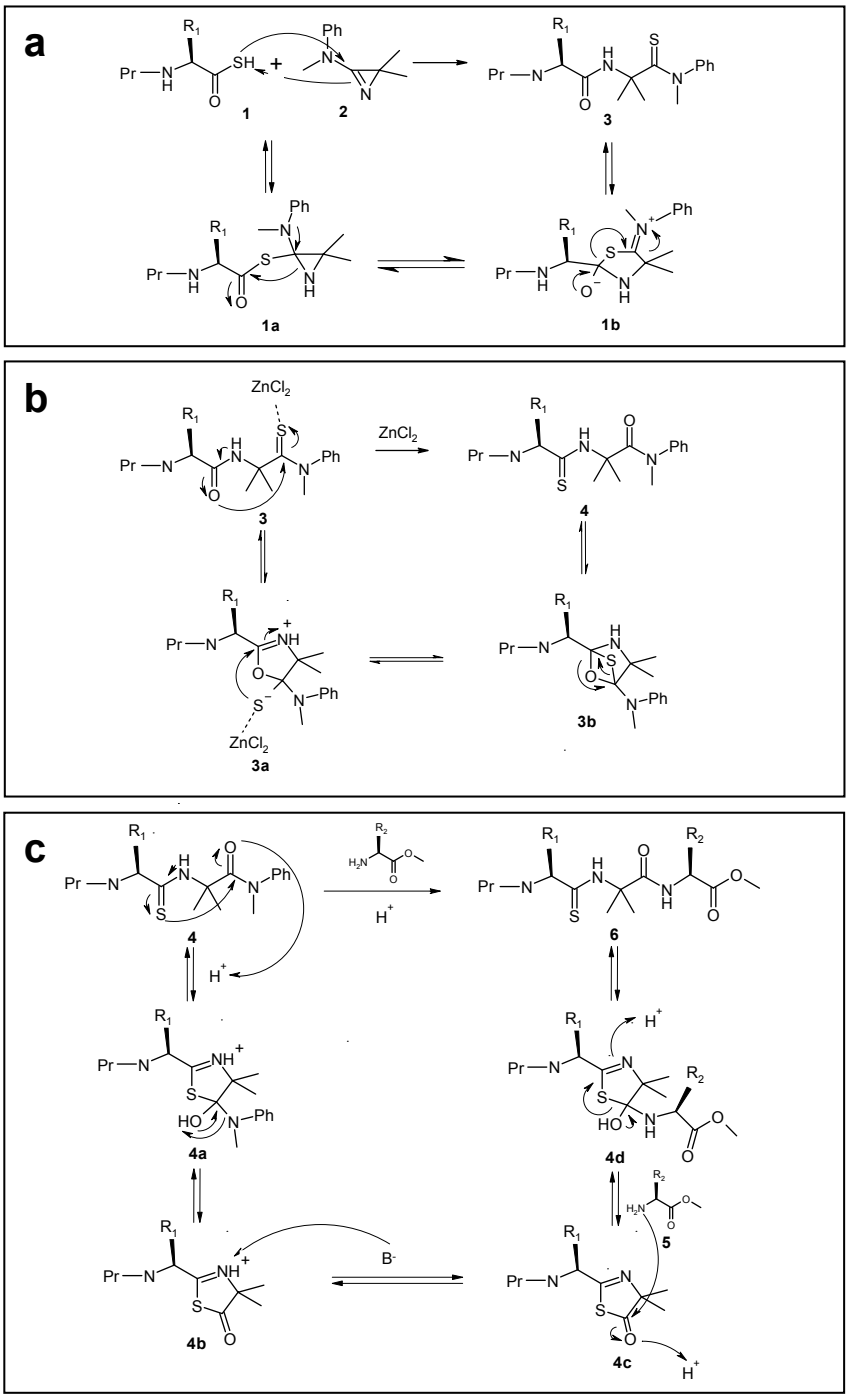

Figure 3.1: Schematic representation of probable reaction mechanisms to synthesize Aib-containing thioxopeptides via a variation of the 'Azirine/Oxazolone method' [73, 74].

difference to conventional coupling reactions is that not the carbon acid is activated but the amine because of the ring tension. When the C(2) atom of the 3-amino-2*H*-azirine (**2**)

is substituted with two methyl groups (as shown in the scheme), the dipeptide **3** ends with a sulfur containing Aib amino acid. The next step contains a shift of the sulfur atom to the N-terminal amino acid catalyzed by $ZnCl_2$ (see Figure 3.1 (b), **3** to **4**) [76]. This variation of the 'Azirine/Oxazolone method' can be compared to the normal 'Azirine/Oxazolone method' where the shift takes place only under acidic conditions. Racemization of the residue R_1 during the appearance of the intermediate product 1,3-thiazol-5(4*H*) (**3a**) can be suppressed by using $ZnCl_2$ because the reaction takes place on a much faster time scale. The last step includes the addition of a third amino acid (**5**) on the C-terminal side of **4** (see Figure 3.1 (c)) [73,74]. As it can be seen in the reaction mechanism the reaction has a 1,3-thiazol-5(*H*) intermediate product (**4a** and **4b**) again. The racemization is suppressed by the leaving group -NPhMe which makes the reaction from **4a** to **4b** fast. So after a short time ($\sim$ 1.5. min) **4b** can be neutralized with a base (**4b** to **4c**), its resulting product does not racemize anymore. The whole reaction ends with a Aib-containing trithioxopeptide **6**.

3.1.2 Boc-Ala-Pro-ψ(SC-NH)-Aib-Ala-OMe

The synthesis of Boc-Ala-Pro-ψ(SC-NH)-Aib-Ala-OMe has been carried out with a total yield of 8 % according the procedure described by Lehmann et al. [77], but using different amino acids. All synthesis steps are illustrated in the following Figure:

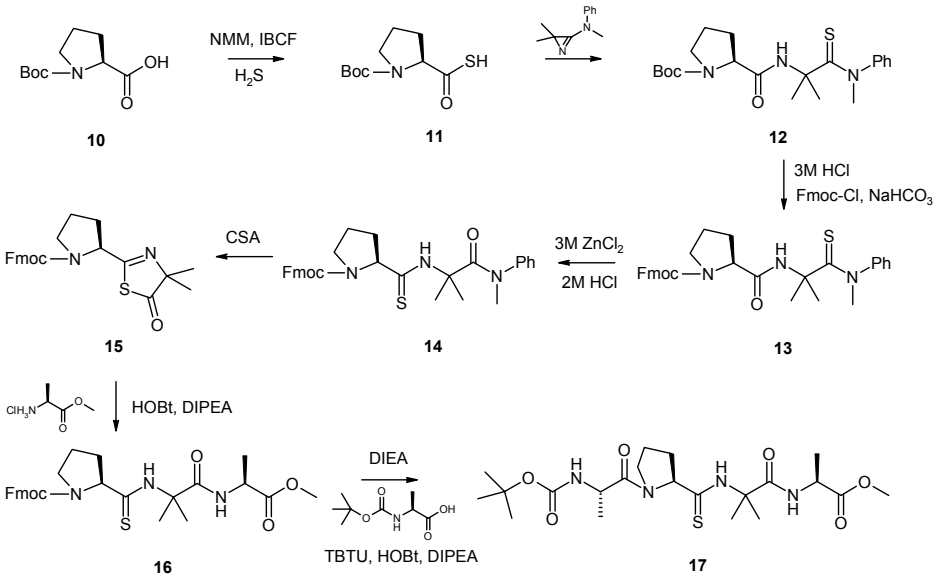

Figure 3.2: Synthesis of Boc-Ala-Pro-ψ(SC-NH)-Aib-Ala-OMe.

Abbveriatons: CSA= (±)-camphor-10-sulfonic acid, DIEA= Diethylamine, DIPEA=

N-Ethyldiisopropylamine, HOBt= 1-Hydroxybenzotriazole, IBCF= Isobutylchloroformate, NMM= *N*-Methylmorpholine, r.t.= room temperature, TBTU= *O*-(Benzotriazole-1-yloxy)-tripyrrolidinophosphonium-hexafluorphosphate, THF= Tetrahydrofurane.

Flash chromatography: MERCK Silica gel 60 (0.063 - 0.200 mm); IR: FT-IR spectrometer 175C, BIO-RAD, res.: 1 cm^{-1}; ^{1}H-NMR: Bruker ARX-300 spectrometer, chemical shifts δ_H are reported in ppm with respect to the internal solvent; MS: Bruker EsquireLC MS; Mp: Dr. Tottoli apparatus, BUECHI.

Boc-Pro-SH (11)

3.07 mL NMM (2.82 g, 27.9 mmol) and 1.83 mL IBCF (1.91 g, 14.0 mmol) were added to a solution of 3.00 g Boc-L-Pro-OH (**10**) (14.0 mmol) in 50 mL THF at -4 °C. *In situ* synthesized H_2S (33 % H_2SO_4 was dropped to 134.5 g $Na_2S{\cdot}H_2O$) was added slowly to the solution. After stirring for 2.5 h at -4 °C the reaction mixture was taken up in 40 mL Et_2O and extracted three times each with 40 mL 0.1 M H_3PO_4. The combined aqueous phases were washed three times each with 40 mL Et_2O. Drying over $NaSO_4$ and removal of the solvent yielded 2.73 g (11.8 mmol, 84 %) of a yellow liquid. The product was analyzed only by FT-IR spectroscopy and then directly subjected to the next reaction step, because the compound proved not to be very stable.

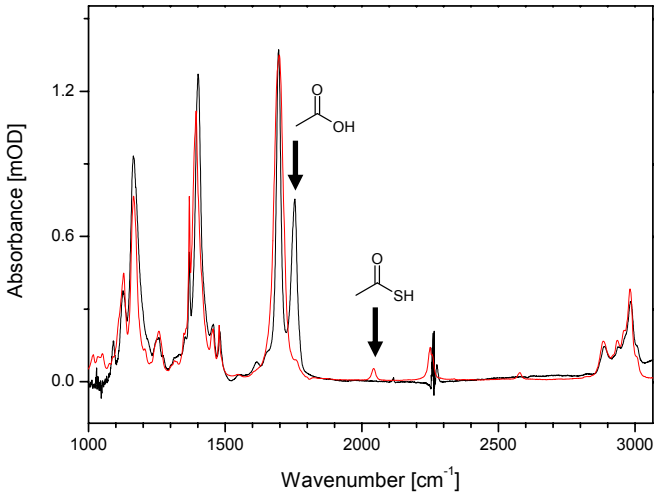

Figure 3.3: The FT-IR spectrum of Boc-Pro-OH (**10**) (black) and Boc-Pro-SH (**11**) (red) with the new COSH band at 2043 cm^{-1}.

Boc-Pro-Aib-ψ(SC-NH)-N(Me)Ph (12)

2.28 g 3-(N-Methylanilino)-2,2-dimethyl-2H-azirine (11.8 mmol) were added to a solution of 2.73 g Boc-Pro-SH (**11**) (11.8 mmol) in 50 mL CH_2Cl_2 at 0 °C. The solution was warmed up to r.t. After stirring for 115 min, the reaction mixture was extracted three times each with 40 mL 5% $NaHSO_4$. The combined aqueous phases were washed three times each with 40 mL CH_2Cl_2. Drying over $NaSO_4$ and removal of the solvent yielded 4.75 g (11.7 mmol, 99 %) of a light-yellow foam.

Analytical data: R_f: 0.35. ^{1}H-NMR (300 MHz, $CDCl_3$): 8.37, 7.78 (*s*, NH), 7.45-7.10 (*m*, 5 arom. H), 4.10-3.75 (*m*, Proα), 3.70 (*s*, NMe), 3.60-3.20 (*m*, Proδ), 2.05-1.70 (*m*, Proβ and Proγ), 1.64, 1.54 (*s*, AibCH_3)), 1.42 (*s*, BocCH_3).

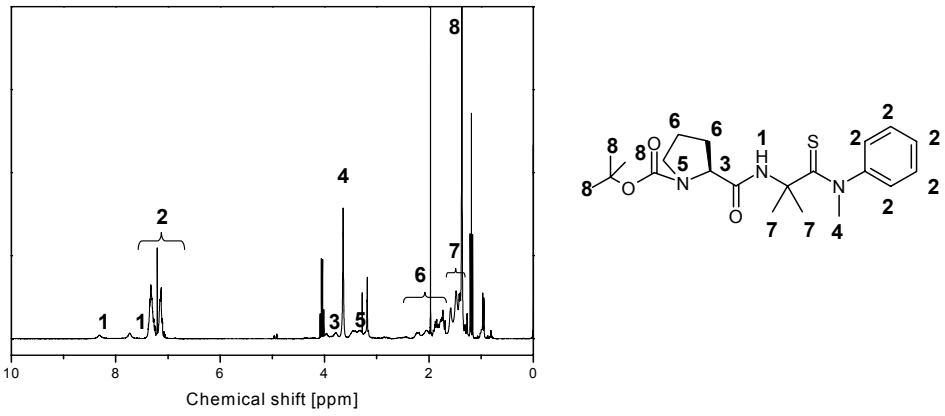

Figure 3.4: ^{1}H-NMR spectrum of Boc-Pro-Aib-ψ(SC-NH)-N(Me)Ph (**12**) in $CDCl_3$.

Fmoc-Pro-Aib-ψ(SC-NH)-N(Me)Ph (13)

4.75 g Boc-Pro-Aib-ψ(SC-NH)-N(Me)Ph (**12**) (11.7 mmol) was diluted in 192 mL 3 M HCl in THF:H_2O (1:1). After stirring for 18 h, the solution was cooled down to 0 °C, set alkaline with $NaHCO_3$ and mixed with 60 mL of H_2O and 70 mL of dioxane. 3.34 g Fmoc-Cl (12.9 mmol) were added to the solution. After stirring for 160 min at 0 °C, the reaction mixture was quenched by addition of 20 mL H_2O and subsequently extracted three times each with 40 mL Et_2O. The combined organic layers were dried over $NaSO_4$ and the solvent was evaporated. The residue was further purified by flash chromatography. Elution with AcOEt:n-Hexane (2:1) afforded 3.51 g (6.7 mmol, 57 %) of a yellow foam.

Analytical data: R_f: 0.35. ^{1}H-NMR (300 MHz, $CDCl_3$): 8.71, 7.85 (*s*, NH), 7.80-7.15 (*m*, 13 arom. H), 4.50-4.15 (*m*, $CHCH_2O$), 4.00-3.85 (*m*, Proα), 3.69 (*s*, NMe), 3.65-3.45 (*m*, Proδ), 2.10-1.75 (*m*, Proβ and Proγ), 1.62, 1.56 (*s*, AibCH_3).

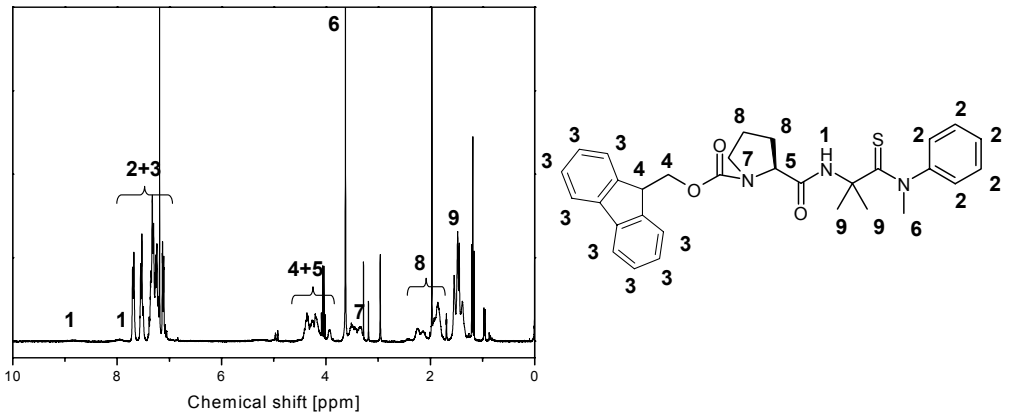

Figure 3.5: ^{1}H-NMR spectrum of Fmoc-Pro-Aib-ψ(SC-NH)-N(Me)Ph (**13**) in $CDCl_3$.

Fmoc-Pro-ψ(SC-NH)-Aib-N(Me)Ph (14)

16.73 g $ZnCl_2$ (122.7 mmol) were added to a solution of 1.57 g Fmoc-Pro-Aib-ψ(SC-NH)-N(Me)Ph (**13**) (2.98 mmol) in 40 mL AcOH. After stirring for 20 min at r.t., 4 mL of saturated HCl in AcOH (2.1 M) were added to the solution. Stirring was continued for 30 min at r.t., thereafter the reaction mixture was quenched by addition of 50 mL 5% $NaHCO_3$, extracted three times each with 40 ml CH_2Cl_2. The combined organic phases were dried over $NaSO_4$ and the solvent was evaporated. The residue was further purified by flash chromatography. Elution with AcOEt:n-Hexane (2:1) afforded 531 mg (1.01 mmol, 34 %) of a yellow foam.

Analytical data: R_f: 0.16. ^{1}H-NMR (300 MHz, $CDCl_3$): 9.24 (*s*, NH), 7.80-7.20 (*m*, 13 arom. H), 4.50-4.25 (*m*, $CHCH_2O$), 4.30-4.10 (*m*, Proα), 3.75-3.40 (*m*, Proδ), 3.24 (*s*, NMe), 2.20-1.80 (*m*, Proβ and Proγ), 1.65, 1.63 (*s*, AibCH_3).

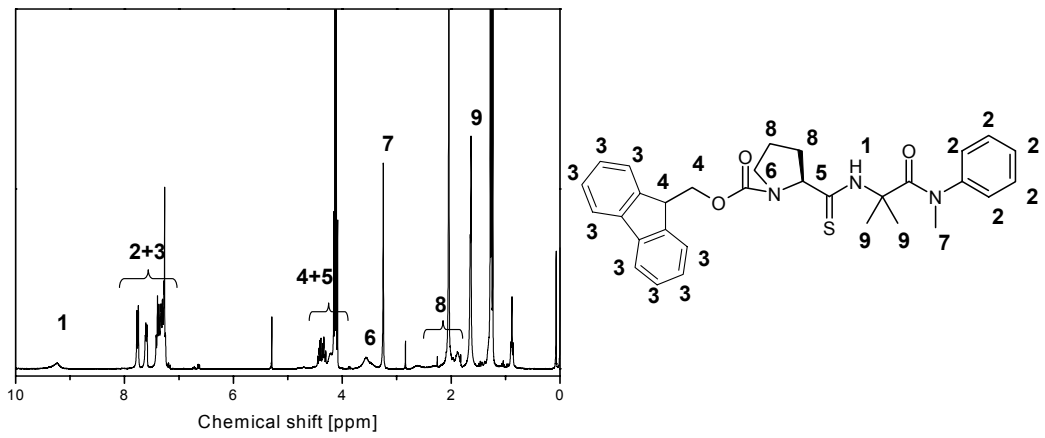

Figure 3.6: ^{1}H-NMR spectrum of Fmoc-Pro-ψ(SC-NH)-Aib-N(Me)Ph (**14** in $CDCl_3$.

Fmoc-Pro-1,3-thiazol-5(4*H*)-one (15)

258 mg CSA (1.11 mmol) were added to a solution of 531 mg Fmoc-Pro-ψ(SC-NH)-Aib-N(Me)Ph (**14**) (1.01 mmol) in 18 mL CH_2Cl_2. After stirring for 1.5 min at r.t., the reaction mixture was quenched by addition of 20 mL 5% $NaHCO_3$ and extracted three times each with 20 mL CH_2Cl_2. Drying over $NaSO_4$ and removal of the solvent yielded 415 mg (0.99 mmol, 98 %) of a white powder.

Analytical data: R_f: 0.38. ^{1}H-NMR (300 MHz, $CDCl_3$): 7.85-7.20 (m, 8 arom. H), 4.65-4.20 (m, $CHCH_2O$ and Proα), 3.70-3.45 (m, Proδ), 2.40-1.90 (m, Proβ and Proγ), 1.43, 1.39, 1.32 (s, CCH_3).

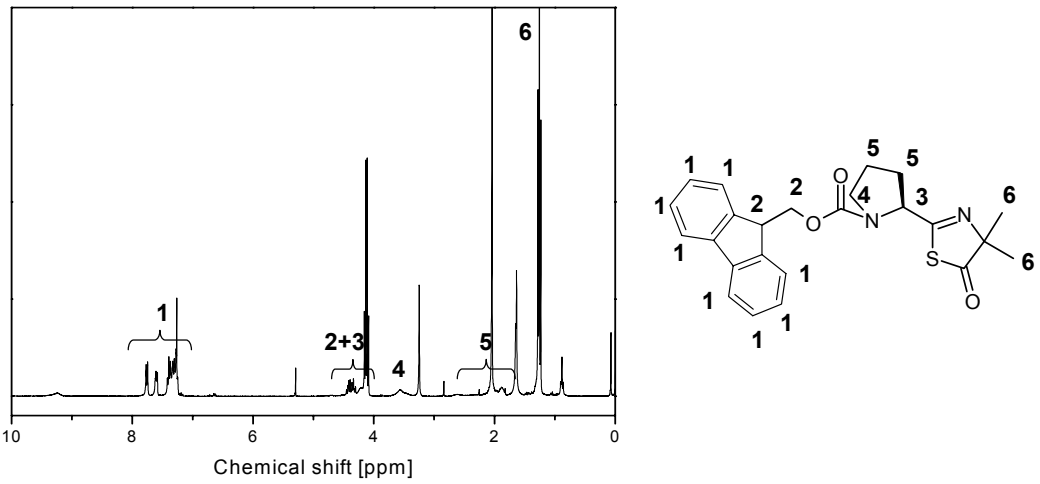

Figure 3.7: ^{1}H-NMR spectrum of Fmoc-Pro-1,3-thiazol-5(4*H*)-one (**15**) in $CDCl_3$.

Fmoc-Pro-ψ(SC-NH)-Aib-Ala-OMe (16)

337 μl DIPEA (255 mg, 1.98 mmol), 303 mg HOBt (1.98 mmol) and 152 mg L-HCl·Ala-OMe (1.09 mmol) were added to a solution of 415 mg Fmoc-Pro-1,3-thiazol-5(4*H*)-one (**15**) (0.99 mmol) in 10 mL CH_3CN. After stirring for 100 h at r.t., the reaction mixture was diluted in 15 mL CH_2Cl_2, and extracted three times each with 30 mL 5% $NaHCO_3$ and 30 mL 5% $KHSO_4$. The combined aqueous layers were washed three times each with 40 ml CH_2Cl_2. Drying over $NaSO_4$ of the combined organic layers and removal of the solvent yielded a compound, which was purified by flash chromatography. Elution with AcOEt afforded 320 mg (0.61 mmol, 62 %) of a white powder.

Analytical data: R_f: 0.30. IR (CD_3CN): $\widetilde{\nu}$ = 3343m, 3316m, 3071w, 3045w, 2989m, 2957m, 2889w, 1745s, 1705s, 1685s, 1675s, 1520s, 1479w, 1453s, 1420s, 1384w, 1356m, 1339m, 1213w, 1196m, 1173m, 1125m cm^{-1}. ^{1}H-NMR (300 MHz, CD_3CN): 9.68 (s, AibNH), 7.90-7.25 (m, 8 arom. H), 7.01 (s, AlaNH), 4.60-4.40 (m, Alaα), 4.50-4.15 (m,

$CHCH_2O$ and Proα), 3.61 (*s*, OMe), 3.65-3.45 (*m*, Proδ), 2.30-1.80 (*m*, Proβ and Proγ), 1.65, 1.56 (*s*, AibCH_3), 1.27 (*d*, AlaCH_3). MS (ESI): *m/z* 546 ($[M+Na]^+$). Mp.: 159-163 °C.

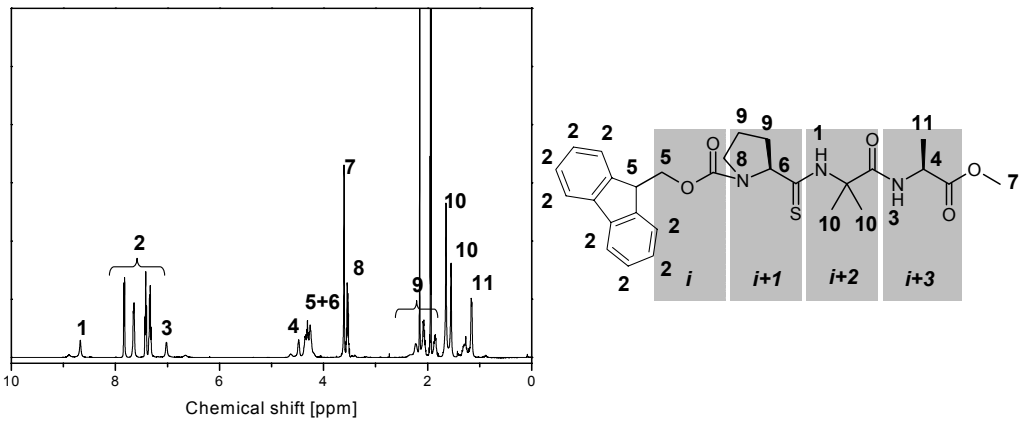

Figure 3.8: ^{1}H-NMR spectrum of Fmoc-Pro-ψ(SC-NH)-Aib-Ala-OMe (**16**) in CD_3CN.

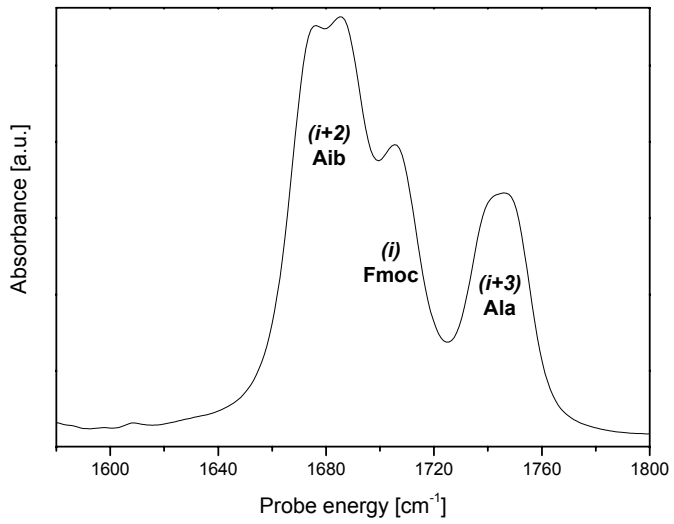

Figure 3.9: FT-IR spectrum of Fmoc-Pro-ψ(SC-NH)-Aib-Ala-OMe (**16**) in CD_3CN in the amide I region.

Boc-Ala-Pro-ψ(SC-NH)-Aib-Ala-OMe (17)

0.30 mL DIEA were added to a solution of 118 mg Fmoc-Pro-ψ(SC-NH)-Aib-Ala-OMe (**16**) (0.23 mmol) in 4 mL CH_3CN. After stirring for 3 h at r.t., the solution was concentrated in vacuo. The residue (HN-Pro-ψ(SC-NH)-Aib-Ala-OMe) was dissolved in 2 mL CH_3CN and added to a solution of 87 μl DIEA (65 mg, 0.51 mmol), 48 mg Boc-Ala-OH (0.25

mmol), 81 mg TBTU (0.25 mmol) and 39 mg HOBt (contains 12% H_2O, 0.25 mmol) in 2 mL CH_3CN. Stirring was continued for 20 h at r.t., after that the reaction mixture was mixed with 20 mL CH_2Cl_2 and extracted three times each with 15 mL 5% $NaHCO_3$ and 15 mL 5% $KHSO_4$. The combined aqueous layers were washed three times each with 15 mL Et_2O. Drying over $NaSO_4$ of the combined organic layers and removal of the solvent yielded a compound, which was purified by flash chromatography. Elution with AcOEt afforded 86 mg (0.18 mmol, 79 %) of a light-yellow powder.

Analytical data: R_f: 0.25. IR (CD_3CN): $\widetilde{\nu}$ = 3383*m*, 3348*m*, 3314*m*, 3045*w*, 2986*m*, 2958*w*, 2944*w*, 2881*w*, 1745*s*, 1711*s*, 1672*s*, 1641*s*, 1518*s*, 1448*s*, 1367*m*, 1284*w*, 1250*m*, 1172*s* cm^{-1}. ^{1}H-NMR (300 MHz, CD_3CN): 8.63, 8.43 (*s*, AibNH), 7.16 (*d*, Ala(4)NH), 5.73, 5.52, 5.12 (*d*, Ala(1)NH), 4.57 (*t*, Ala(1)α), 4.37 (*t*, Ala(4)α), 4.35-4.25 (*m*, Proα), 3.80-3.55 (*m*, Proδ), 3.66 (*s*, OMe), 2.25-1.85 (*m*, Proβ and Proγ), 1.65, 1.53 (*s*, AibCH$_3$), 1.39 (*s*, BocCH$_3$), 1.27 (*d*, Ala(4)CH$_3$), 1.20 (*d*, Ala(1)CH$_3$). MS (ESI): *m/z* 495 ([M+Na]$^+$). Mp.: 165-169 °C.

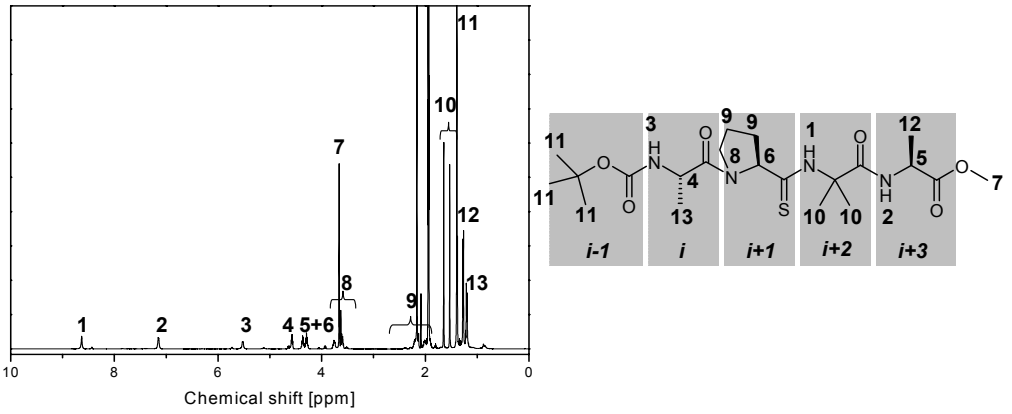

Figure 3.10: ^{1}H-NMR spectrum of Boc-Ala-Pro-ψ(SC-NH)-Aib-Ala-OMe (**17**) in CD_3CN.

3.1.3 Boc-Ala-ψ(O^{13}C-NH)-Pro-ψ(SC-NH)-Aib-Ala-OMe

The synthesis of Boc-Ala-ψ(O^{13}C-NH)-Pro-ψ(SC-NH)-Aib-Ala-OMe (yield: 86 %) has been made according the exact same procedure described in the section before except that in the final synthesis step it has been used Boc-Ala-ψ(O^{13}C-OH)-OH.

Analytical data: R_f: 0.25. IR (CD_3CN): $\widetilde{\nu}$ = 3390*m*, 3343*m*, 3311*m*, 3047*w*, 2985*m*, 2963*w*, 2939*w*, 2880*w*, 1745*s*, 1710*s*, 1672*s*, 1623*s*, 1600*s*, 1516*s*, 1453*s*, 1420*s*, 1368*m*, 1285*w*, 1248*m*, 1173*s* cm^{-1}. ^{1}H-NMR (300 MHz, CD_3CN): 8.64, 8.43 (*s*, AibNH), 7.13 (*d*, Ala(4)NH), 5.71, 5.51, 5.13 (*d*, Ala(1)NH), 4.59 (*t*, Ala(1)α), 4.37 (*t*, Ala(4)α), 4.35-4.25 (*m*, Proα), 3.80-3.55 (*m*, Proδ), 3.67 (*s*, OMe), 2.30-1.90 (*m*, Proβ and Proγ), 1.65, 1.54

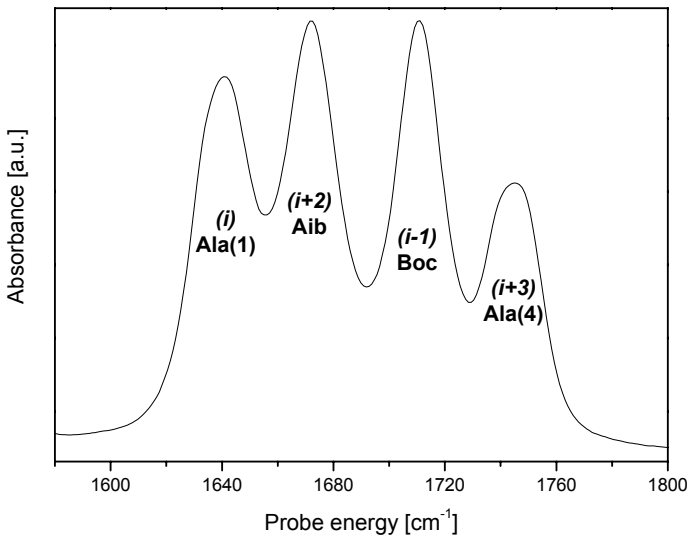

Figure 3.11: FT-IR spectrum of Boc-Ala-Pro-ψ(SC-NH)-Aib-Ala-OMe (**17** in CD_3CN in the amide I region.

(s, AibCH$_3$), 1.40 (s, BocCH$_3$), 1.28 (d, Ala(4)CH$_3$), 1.21 (d, Ala(1)CH$_3$). MS (ESI): m/z 496 ([M+Na]$^+$). Mp.: 181-185 °C.

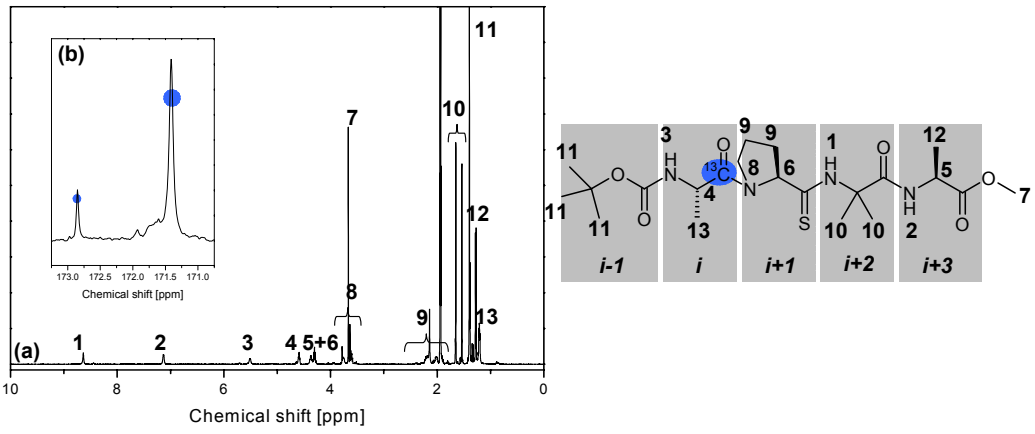

Figure 3.12: ^{1}H- (a) and ^{13}C-NMR (b) spectrum of Boc-Ala-ψ(O^{13}C-NH)-Pro-ψ(SC-NH)-Aib-Ala-OMe in CD_3CN.

3.2 Sample Preparation

For the measurements the thioxopeptides are dried in an rotation evaporator to vacuum and then dissolved in deuterated acetonitrile (ARMAR Chemicals, 99.5 Atom%D, CAS 2206-26-0). For FT-IR, UV/Vis, ^{1}H-NMR, 2D-IR and transient IR measurements the con-

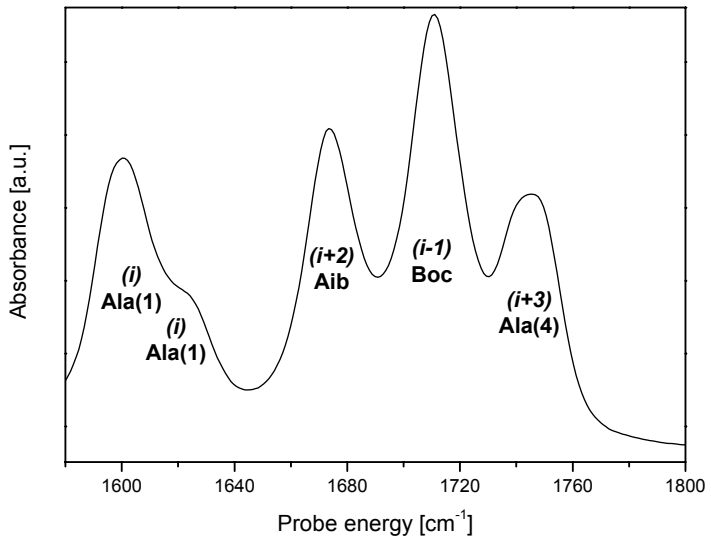

Figure 3.13: FT-IR spectrum of Boc-Ala-ψ(O^{13}C-NH)-Pro-ψ(SC-NH)-Aib-Ala-OMe in CD_3CN in the amide I region.

centration is chosen to be about 30 mM, for transient 2D-IR and ^{13}C-NMR measurements about 100 mM. For UV/Vis, FT-IR, NMR and 2D-IR measurements a conventional cell with two CaF_2 windows and a spacer thickness of 50 or 100 μm is used. The transient IR measurements, where the thioxopeptides are excited electronically, thus isomerize and after long irradiation also decompose, require a fast exchange of the volume in the measuring spot in between two subsequent laser pulses (1 kHz repetition rate) to avoid artifacts because of molecules still being in the excited state due to irradiation of the previous UV-pump pulse. For this purpose a flow cell is used which is described in detail in [99].

3.3 Linear Spectroscopy

UV/Vis spectroscopy

To measure UV/Vis spectra a CARY 219 spectrophotometer with a resolution of 1 nm is used.

FT-IR spectroscopy

IR spectra are recorded on a FTS 175C spectrometer. All data are recorded with a liquid nitrogen-cooled MCT detector with 1 cm^{-1} resolution.
For photoisomerization an KrF excimer laser (248 nm, Spectra Physik) is used. The UV light is directed onto the sample inside the FT-IR spectrometer, allowing to measure spectra without removing the sample.

NMR measurements

To record ^{1}H-NMR spectra an arx-300 or an av-600 spectrometer is used. The later one is also used to measure temperature-dependent spectra and also for ^{13}C-NMR measurements.

3.4 Time-Resolved IR Spectroscopy Setup

To perform time-resolved measurements, a Ti:sapphire laser system is used to produce 800 nm pulses. The light then is split into two parts, one part is used generate mid-infrared pulses between 3 and 8 μm in an optical parametric amplifier (OPA). The other part is used to produce UV pulses at 266 nm to trigger the isomerization of the thioamide unit. The mid-infrared and the UV beams are combined again in the pump/probe setup 3.14. These four stages are described in the following sections in detail.

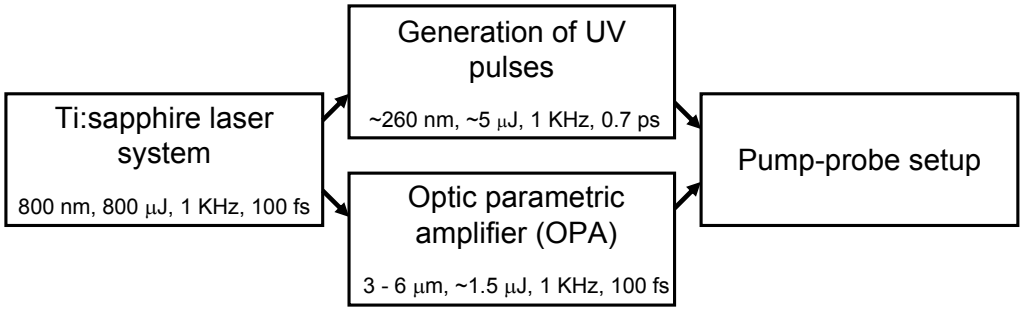

Figure 3.14: Schematic representation of the whole setup with the Ti:sapphire laser system, the optical parametric amplifier (OPA), the generation of the UV pulses and the pump/probe setup.

3.4.1 Laser system

A commercially available laser system (Spectra-Physics Lasers) is used to generate short, intense 800 nm pulses which then can be modified by nonlinear processes needed for the generation of the mid-infrared (OPA) and UV pulses (see Figure 3.15). The system consists of a Ti:sapphire laser oscillator ('Tsunami') which is based on a titanium-doped aluminum oxide (Ti:Al_2O_3, Ti:sapphire) as a gain medium, pumped by a frequency doubled Nd:YVO_4 continuous laser ('Millenia'). Short laser pulses are generated by mode locking and dispersion compensation [100, 101]. The oscillator produces pulses at 800 nm with a temporal duration of 80 fs, a repetition rate of 80 MHz and a pulse energy of about 6 nJ. The pulses are guided through a regenerative amplifier ('Spitfire'), using chirped

pulse amplification, to generate intense pulses. In the amplifier the pulse is first stretched, amplified in a Ti:sapphire cavity which is pumped by a frequency doubled Nd:YLF laser ('Evolution'), and then re-compressed to its original duration [102]. The system produces 800 nm pulses with a temporal duration of about 100 fs, a repetition rate of 1KHz and a pulse energy of nearly 800 μJ. After the laser system the beam is split into two parts of about 300 and 500 μJ. The first part is used for the generation of the mid-infrared pulses in the OPA and the second part for the the generation of the UV light.

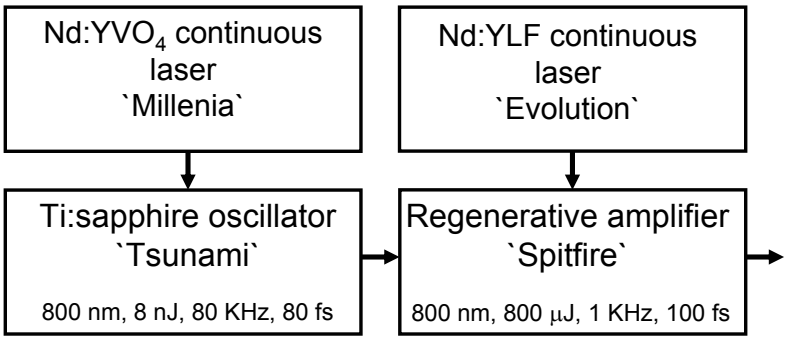

Figure 3.15: Schematic representation of the Ti:sapphire laser system with its single components.

3.4.2 Optical parametric amplifier (OPA)

A home-built two stage optical parametric amplifier (OPA), based on a β-barium borate (BBO) crystal, followed by difference frequency mixing in a $AgGaS_2$ crystal is used to generate intense and stable mid-infrared pulses, tunable between 3 and 8 μm (see Figure 3.16) [103–105]. With a fraction of the 800 nm light ($\sim$ 1 - 2 μJ) a white-light continuum is generated in a sapphire window which is then focused as a seed for the parametric amplification into a BBO crystal (type II, $\vartheta = 27°$, $\varphi = 30°$) in spatial overlap with another small fraction (15 μJ) of the 800 nm light (serving as pump pulse). The generated idler pulse is removed by a dichroic mirror (DM3), while the signal pulse is used as a seed for a second amplification stage in the same BBO crystal. A third fraction (200 μJ) of the 800 nm light serves as the pump light for the second stage. The combined energy of the generated signal and idler pulses is approximately 60 μJ per pulse. Signal and idler pulses are separated by another dichroic mirror (DM4) and the idler passes over a variable delay line to adjust the temporal delay between the two pulses. Both pulses are then focused into a $AgGaS_2$ crystal (type I, $\vartheta = 33°$, $\varphi = 45°$), where the difference frequency, with respect to the frequencies of signal and idler, is generated. Mid-infrared pulses are obtained which are tunable between 3 and 8 μm (1200-3500 cm^{-1}). The typical pulse energy is $\sim$ 1.5 μJ,

the temporal duration is about 100 fs and the spectral width 200 cm^{-1}.

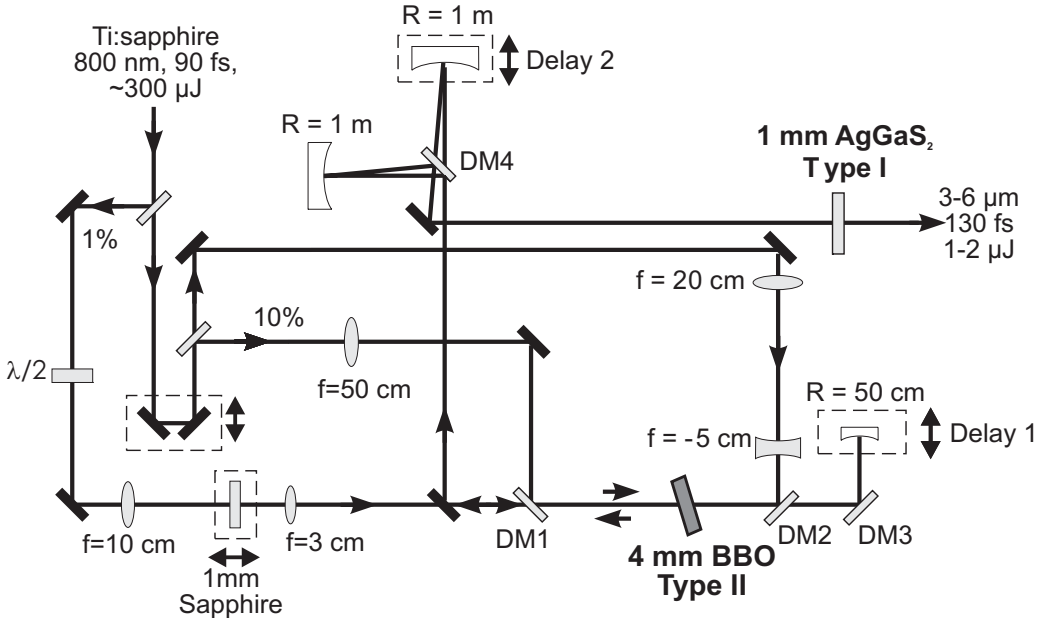

Figure 3.16: Schematic representation of the OPA (Figure taken from Stenger [104]).

3.4.3 Generation of 266 nm pulses

The UV-pump light at $\sim$ 266 nm is generated by frequency tripling the second fraction of the 800 nm output of the Ti:sapphire system in two BBO crystals (see Figure 3.17). The first BBO crystal (type I, $\vartheta = 30°$) is used to generate the second harmonic (2 x 800 nm $\rightarrow$ 400 nm, SHG). In the second BBO crystal (type II, $\vartheta = 58°$, $\varphi = 30°$) the generated second harmonic (400 nm) is mixed with the fundamental light (800 nm) to obtain 266 nm light, called third harmonic generation (THG). Because the fundamental and the second harmonic are temporally separated after the first BBO crystal, a third BBO crystal (type I, $\vartheta = 70°$) is used as a timeplate to compensate this delay. After the third harmonic generation the beam is guided through a 10 cm fused silica rod to stretch the 266 nm pulses temporally to 0.7 ps. The stretching avoids undesired nonlinear effects like white light generation and/or color center formation in the sample cell. The 266 nm light is isolated from the remaining undesired 400 and 800 nm light by dielectric mirrors. To restore a proper spacial beam profile the beam is focused on a pinhole which is then imaged onto the sample. The pulse energy at the sample is approximately 5 μJ.

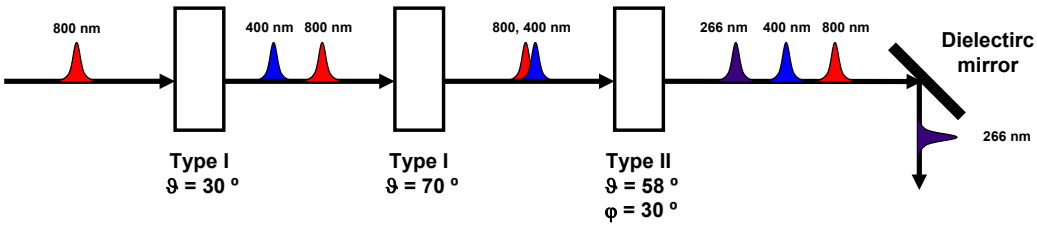

Figure 3.17: Schematic representation of the generation of the 266 nm pulses.

3.4.4 Pump/probe setup

In Figure 3.18 the pump/probe setup is shown which is used for the 2D-IR and transient IR measurements. The outcoming beam from the OPA is first filtered through a long pass filter to get rid of the signal and the idler. Two small parts of the mid-infrared beam are reflected off a wedged BaF_2 window, resulting in the IR-probe and reference beams. The transmitted part is used as IR-pump beam.

The IR-probe and reference beam pass a telescope which then focus them on two different regions in the cell in a way with a spot size of approximately 90 μm. After the sample cell the IR-probe and reference beams are spectrally dispersed in a grating spectrometer and focused onto a double array MCT (Mercury Cadmium Telluride, HgCdTe) detector (2×31). The typical spectral resolution at 6 μm is 4 cm^{-1} with a total IR-probe of window of 120 cm^{-1}.

The IR-pump beam is guided through a Fabry-Perot interferometer which consists of two parallel partial reflectors on a piezo-controlled mirror mount. In this way a tunable narrow band pump pulse ($\sim$ 10 cm^{-1}) can be cut out of the originally 200 cm^{-1} bandwidth, coming from the OPA. During the measurement the center frequency is controlled by the computer. The IR-pump beam is guided over a delay line to control the temporal delay with respect to the IR-probe and reference beam. In this way it is possible to record spectra at different time delays after the sample has been excited with the IR-pump pulse. It is then focused onto the sample cell with a spot size of about 120 μm and IR-pump and IR-probe beam are spatially completely overlapped. After the cell the IR-pump beam is blocked.

The UV-pump beam is guided over an independent delay stage to be able to vary the temporal delay of the pulses in relation to the IR pulses. The beam then is focused in the sample cell, having a sport size of approximately 140 μm and a complete overlap with the IR-probe resp. IR-pump beam. After the cell the UV-pump beam is blocked.

For transient IR measurements no IR-pump beam is used. the UV-pump beam passes

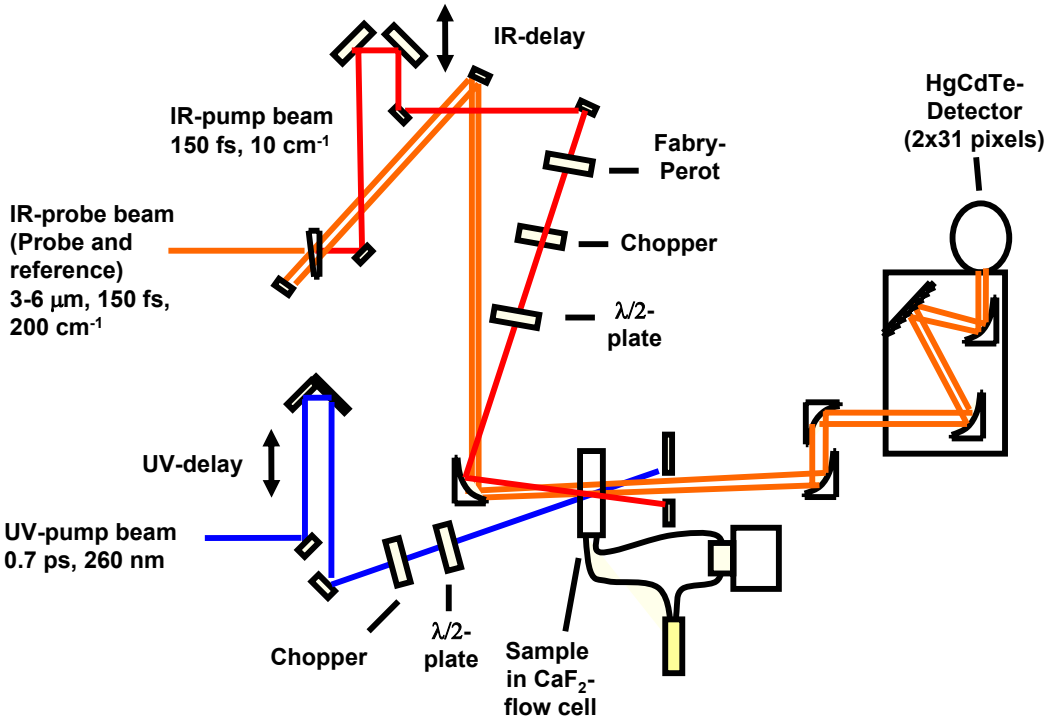

Figure 3.18: Schematic representation of the pump/probe setup.

a chopper, working at 500 Hz to block every second UV pulse. Thus only every second time a IR-probe beam interacts with the sample the sample is also electronically excited. The absorbance change signal, recorded with the computer, then shows the difference between two successively IR-probe pulses, probing with UV excitation ($I_{UV_{ON}}$) minus probing without excitation ($I_{UV_{OFF}}$):

$$\Delta A_{T1D} = -log\frac{I_{UV_{ON}} \cdot I_{Ref.,UV_{OFF}}}{I_{UV_{OFF}} \cdot I_{Ref.,UV_{ON}}}. \tag{3.1}$$

The reference IR-pulse ($I_{Ref.,UV_{ON}}$ and $I_{Ref.,UV_{OFF}}$) assures that the intensity fluctuations of the UV laser pulse are corrected to achieve low noise (averaging over 300 pulses results in a noise level of about 30 μOD). The typical transient IR spectrum show negative and positive features. The negative signal corresponds to absorption which is missing after UV excitation and the positive signals show absorptions newly created.

The 2D-IR measurements work in the same way as the transient IR measurements. The IR-pump pulse passes a 500 Hz chopper. The signal which is recorded finally is the difference between two successive IR-probe pulses, one with vibrational excitation with

the IR-pump pulse ($I_{IR_{ON}}$) and one without ($I_{IR_{OFF}}$):

$$\Delta A_{2D} = -log\frac{I_{IR_{ON}} \cdot I_{Ref.,IR_{OFF}}}{I_{IR_{OFF}} \cdot I_{Ref.,IR_{ON}}}. \quad (3.2)$$

2D-IR spectra typically are represented in a 2D plot with the vertical axis showing the central IR-pump pulse frequency and the horizontal axis the spectral range where the sample is probed. Red color represent positive and blue color negative absorption, which is due to newly created resp. missing 'species' after IR excitation.

The transient 2D-IR measurements are a combination of the two mentioned above. The IR-pump pulse is used with a 500 Hz chopper while the UV-pump pulse is passing a 250 Hz chopper. Thus, four sets of data are recorded: $I_{IR_{ON}UV_{ON}}$, $I_{IR_{ON}UV_{OFF}}$, $I_{IR_{OFF}UV_{ON}}$, $I_{IR_{OFF}UV_{OFF}}$. The calculated signal for the transient 2D-IR spectrum then is:

$$\Delta A_{T2D} = -log\frac{I_{IR_{ON}UV_{ON}} \cdot I_{IR_{OFF}UV_{OFF}} \cdot I_{Ref.,IR_{OFF}UV_{ON}} \cdot I_{Ref.,IR_{ON}UV_{OFF}}}{I_{IR_{OFF}UV_{ON}} \cdot I_{IR_{ON}UV_{OFF}} \cdot I_{Ref.,IR_{ON}UV_{ON}} \cdot I_{Ref.,IR_{OFF}UV_{OFF}}} \quad (3.3)$$

The relative polarizations (perpendicular and parallel) can be varied by two $\lambda/2$ plates placed in the beam paths of the UV- and IR-pump pulses.

Chapter 4

N-Methylthioacetamide as a Photoswitch

N-Methylthioacetamide (NMTAA) is the simplest photoswitchable thioamide and is almost 100 % in the trans conformation in its thermal equilibrium. Its ability to photoisomerize has already been investigated in earlier times with different steady state methods like UV-, IR-, Raman- and ^{1}H-NMR-spectroscopy [49, 64, 106, 107]. At the beginning of this thesis, NMTAA has been investigated with transient IR spectroscopy in Hamm's group (Zürich), with transient UV/Vis-spectroscopy in Wachtveitl's group (Frankfurt) and completed with *ab inito* calculations in Olivucci's group (Siena). In this chapter the most important results are summarized and discussed specifically with respect to probable photophysical pathways. In [108] and [109] a more detailed description can be found.

4.1 Steady State Absorption

The solid lines in Figure 4.1 (a) and (c) show the UV and infrared absorption spectra of *trans*-NMTAA in D_2O at room temperature. The S_2 state, which is due to a $\pi - \pi^*$ excitation (see below), gives rise to the main UV absorption band centered at 255 nm, while a much weaker shoulder at 305 nm is due to the S_1 state (n-π^* transition). In the infrared spectrum, three prominent bands were of main interest in the infrared study. They were assigned on the basis of a normal mode calculation on BLYP 6-31G(d) level (GAUSSIAN98), which was capable of reproducing approximate frequencies, relative intensities, and energy shifts upon isomerization. The band at 1545 cm^{-1} is the amide II band, which is strongly blue-shifted with respect to matrix isolation spectra of NMTAA [106] and broadened due to strong interaction with the D_2O solvent. The band at 1409 cm^{-1} and the weaker band at 1372 cm^{-1} can best be characterized as "symmetric" and "antisymmetric" stretch motion of the C-C-N-C backbone. Both modes also involve an

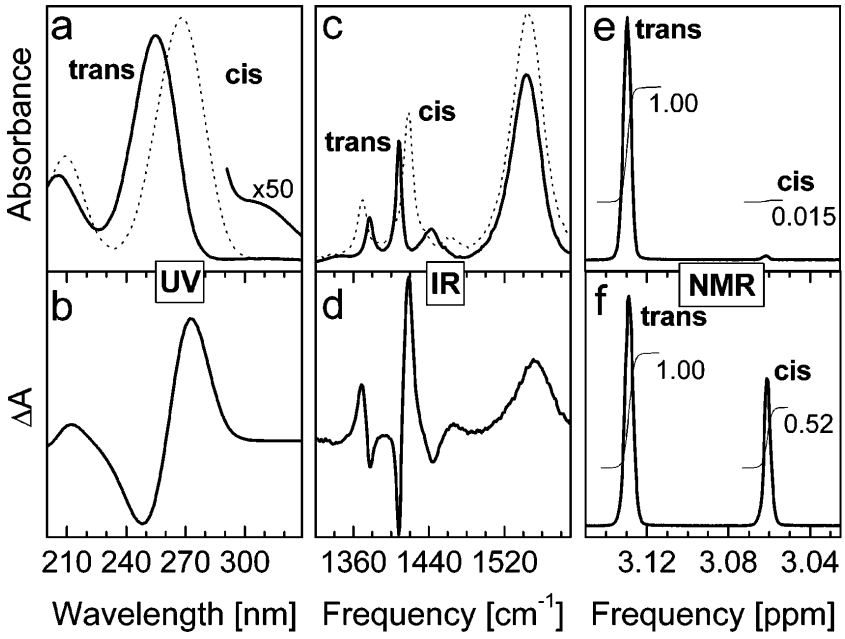

Figure 4.1: (a) Solid lines: UV-absorption spectrum of *trans*-NMTAA in deuterated water. (b) Difference absorption spectrum under UV-irradiation. (c) Solid line: FT-IR absorption spectrum of *trans*-NMTAA before irradiation. (d) FT-IR difference absorption spectrum under UV-irradiation. The dotted lines in (a) and (c) show the *cis*-NMTAA absorption spectra, which were constructed from the trans and the difference spectra. (e) NMR spectrum at room temperature before irradiation and (f) in photo equilibrium after 256 nm irradiation. The numbers indicate the normalized peak areas.

umbrella-like motion of the methyl groups (The extinction coefficients for *trans*-NMTAA are 12 400 L mol^{-1} cm^{-1} at 255 nm and 200 L mol^{-1} cm^{-1} at 1545 cm^{-1}). The changes in UV and infrared absorption due to UV irradiation are shown in Figure 4.1 (b) and (d). In the UV, a red-shift is observed for the $\pi - \pi^*$ absorption band, and this shift obscures any changes that may occur in the region of the n-π^* band. In the IR vibrational spectrum, the trans band at 1409 cm^{-1} undergoes a blue-shift and gains in oscillator strength upon photoisomerization, while a red shift is observed for the 1372 cm^{-1} band. The amide II band of the cis species is stronger and peaks at slightly larger energies than the trans band. Kinetic measurements, based on both UV and FT-IR absorption data, show an exponential decrease of the *trans*-NMTAA concentration and a simultaneous growth of the *cis*-NMTAA photoproduct. There are well-defined isosbestic points in the difference absorption spectra, which is an indication of simple two-state kinetics cis $\overset{h\nu}{\rightleftharpoons}$ trans. Indeed, due to the strongly overlapping UV-absorption bands of the two isomers, the photoreaction can take place in both directions, and a photoequilibrium between cis and trans species is eventually established. The *cis*-NMTAA concentration in the photostationary state

under 260 nm irradiation is 34%, compared to only 1.5% in thermal equilibrium before irradiation (Figure 4.1, e and f).

4.2 Time Resolved Infrared Measurements

Changes in the mid-infrared absorption at different pump/probe time delays after 260 nm excitation of *trans*-NMTAA are shown in Figure 4.2 (a). All data are magic angle signals and thus unaffected by rotational diffusion. Apart from a positive offset, the transient spectra at very early times after photoexcitation have the same shape as that of the FT-IR absorption spectrum of *trans*-NMTAA. Within the first 30 ps the initial bleaching signal is reduced to little more than half of its original size, and positive absorption bands grow in at the spectral positions of the *cis*-NMTAA vibrations. This dynamics subsequently continues on a much slower time scale. After 1 ns, the difference spectra fully reproduce the FT-IR difference spectrum, and no further changes are observed for longer time delays. These results were found to be independent of concentration in the range of 50-250 mM.

Figure 4.2 (b) shows the transient IR absorption changes at different pump/probe delays for 308 nm excitation of *trans*-NMTAA to the S_1 state, revealing very similar signals as seen for the 260 nm excitation of *trans*-NMTAA to the S_2 state. At time delays larger than 300 ps the signals match perfectly, whereas at intermediate delays (10 ps, 30 ps) the bleach of the trans bands appears to be smaller for S_2 excitation than for S_1-excitation. it is shown below (Figure 4.3), that this small difference is indeed significant and is due to more efficient fast relaxation to the electronic ground state, when the S_2 state is excited.

Figure 4.2 (c) shows the transient IR absorption changes at different pump/probe delays for 280 nm excitation of *cis*-NMTAA[1] to the S_2 state. The opposite shapes (cis bleach followed by the growth of the *trans*-NMTAA bands) is observed compared to the 260 nm excitation of *trans*-NMTAA to the S_2 state.

No vibrational bands could be identified that may be assigned to NMTAA in an electronically excited state. The most probable reason is that the IR absorption bands of these species may either have shifted out of the spectral window used for detection, as the bond order of the thioamide N-C bond is reduced, the nitrogen and carbon centers pyramidalize and the force constants are strongly changed, or their distribution may be so broad that their absorption remains hidden in the unstructured background signal [108]. The transient infrared measurements thus appear to be sensitive only to ground-state molecules that have dissipated most of the excitation energy. They monitor the arrival of

[1]Under continuous irradiation at 248 nm it can thus prepared a sample with a cis concentration of 45%. When this sample is then excited by a short laser pulse at 280 nm, where *cis*-NMTAA absorbs 10 times more than *trans*-NMTAA, more than 90% of the excited molecules are initially in the cis configuration.

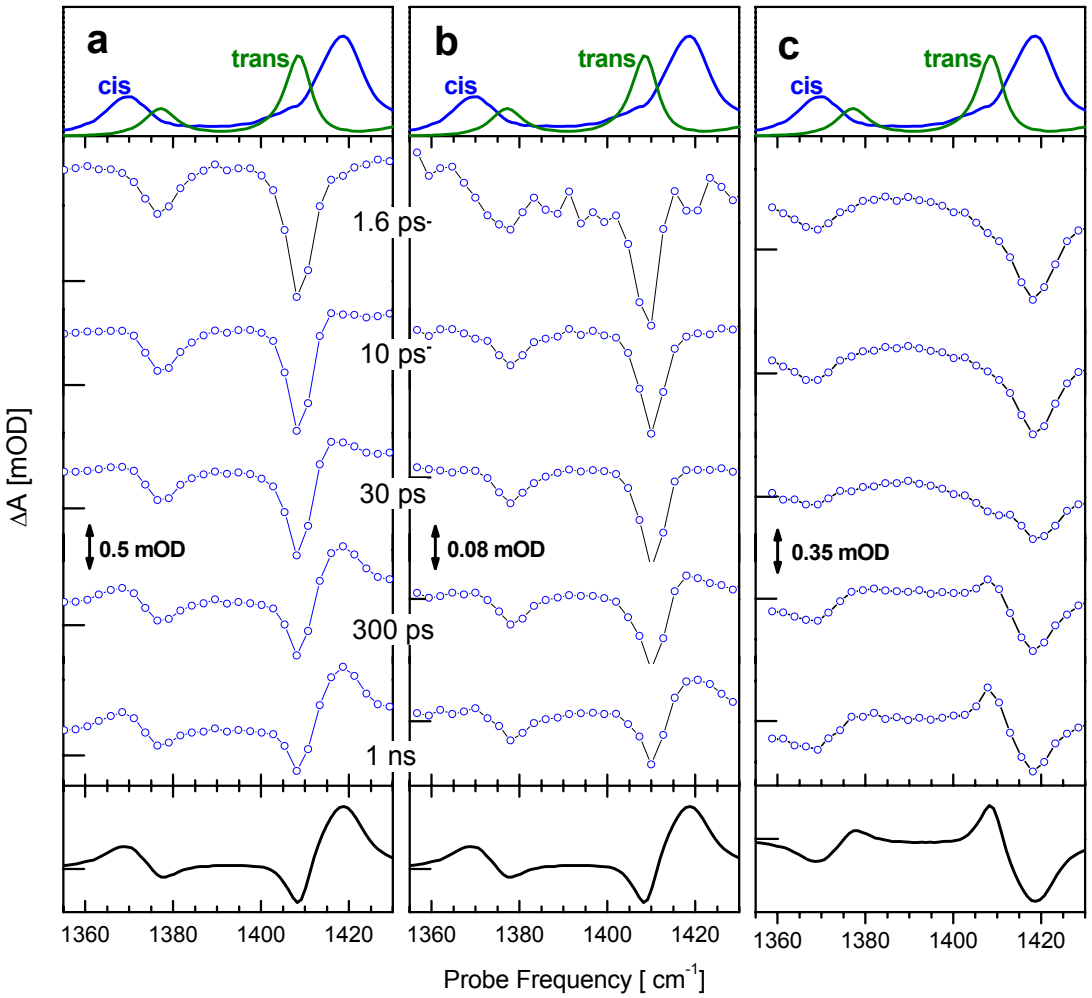

Figure 4.2: Top: FT-IR absorption spectra of (blue) *trans*- and (green) *cis*-NMTAA. Middle: Magic angle transient infrared difference absorption spectra of *trans*-NMTAA after (a) $\pi - pi^*$ (S_2, 260 nm) and (b) n-π^* (S_1, 308 nm) excitation and of (c) a sample containing 45 % *cis*-NMTAA after $\pi - pi^*$ (S_2, 280 nm) excitation with different delays between the UV-pump and IR-probe pulse. Bottom: FT-IR difference absorption spectra of (a, b) *trans*-NMTAA and (c) *cis*-NMTAA.

population in either the relaxed cis or trans conformation of NMTAA, and the observed dynamics is therefore due to the joint processes of electronic relaxation and vibrational cooling [110, 111].

Figure 4.3 (a) shows the contributions of cis and trans species to the transient spectra at different time delays after 260 nm excitation of *trans*-NMTAA to the S_2 state, extracted from the fits using their ground-state absorption spectra. It can be seen that both

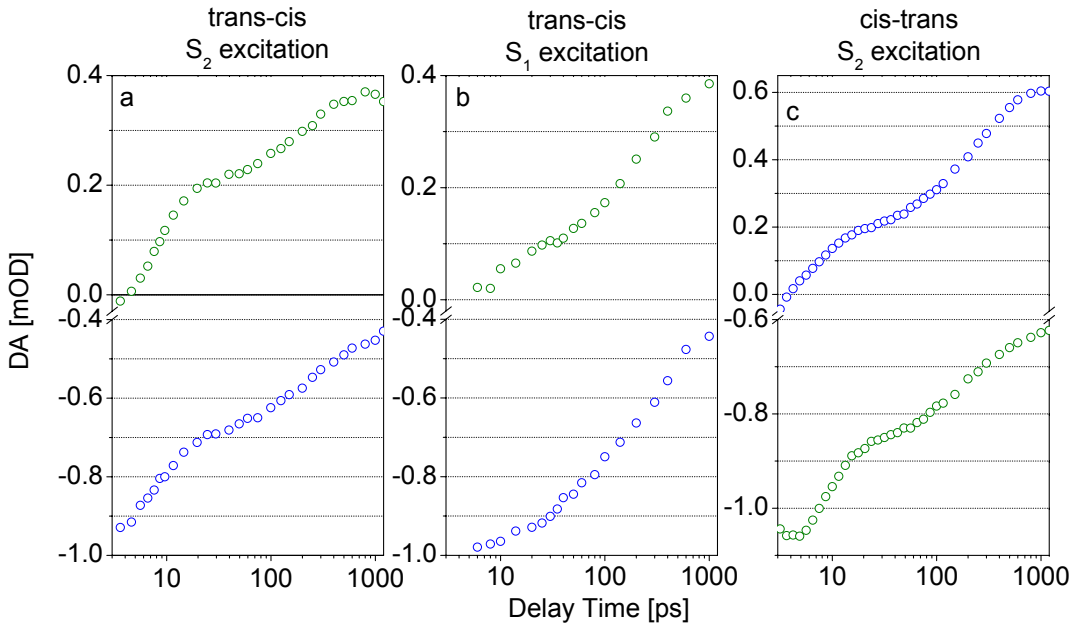

Figure 4.3: The temporal contribution of the trans (blue) and cis (green) bands after (a) $\pi - \pi^*$ (S_2) excitation of *trans*-NMTAA, (b) n-π^* (S_1) excitation of *trans*-NMTAA and $\pi - \pi^*$ (S_2) excitation of *cis*-NMTAA.

the recovery of the initial trans ground state and the formation of *cis*-NMTAA occur on two distinct time scales of 8-9 ps and 250 ps which are compatible with those obtained from SVD analysis [108]. The transient UV/Vis measurements yield complementary information on the dynamics in the electronically excited states, revealing that the 250-ps time constant represents the lifetime of an electronically excited state with an absorption band near 500 nm [108]. About 30% of the initially excited trans population returns to the (cold) trans ground state within the first 20-30 ps following the 260 nm pump pulse. At the same time, another 15-20% is converted into ground state *cis*-NMTAA (in total about 50 % of the initially excited molecules). This early recovery of the IR absorption bands of cold ground-state species indicates fast electronic decay and very efficient excess energy dissipation from the thioamide to the solvent. A strong interaction of NMTAA with D_2O is already apparent from the broad amide II absorption band that is strongly blue-shifted compared to the matrix-isolated molecule [106] and efficient energy dissipation could take place, for example, via dipolar coupling to the D_2O molecules of the first hydration shell, as is the case of NMA in water [112] and more directly through intermolecular hydrogen-bonds. As a result, the 8-9 ps time constant very probably reflects the cooling of photoexcited NMTAA in deuterated water. This value only puts an upper limit to the time constant of fast electronic decay.

Further reduction of the initial *trans*-NMTAA bleach and the growth of the *cis*-

NMTAA absorption bands take place on a much slower time scale which is comparable to the time of excited-state decay in the visible measurements [55, 108]. Just as on the fast time scale, roughly 2 times more trans species than cis species are formed in the slow process. Overall, 35-40% of the excited NMTAA molecules are converted into cis, and the remaining molecules return to the ground state in the trans conformation.

While the contributions of cis and trans species to the transient spectra at different time delays after 280 nm excitation of *cis*-NMTAA to the S_2 state show the same bi-phasic time scale, a very different situation is encountered upon 308 nm excitation of the *trans*-NMTAA to the S_1 state where the new absorption features appear to form later (see Figure 4.3, b and c). In contrast to the two distinct timescales for the ground state recovery after S_2 excitation, a continuous, slow growth of the photoproduct bands is observed. In the transient spectra of Figure 4.2 this difference, which is also confirmed by a singular value decomposition analysis, is reflected by the slightly larger bleaching signal at intermediate delays for S_1 excitation.

In the top row of Figure 4.4 the photoproduct spectra in deuterated water for a delay of 1 ns is shown[2]. At the end of the photoreaction the well separated peaks of ground state *trans*- and *cis*-NMTAA directly report on the quantum yields for isomerization. Without isomerization, the spectra in the top row would have exactly the same amplitude and shape as the initial bleach signal at early times. However, the amplitude of the trans bands in Figure 4.4 (a) and (b) only amounts to 60% of the corresponding bleach signals in Figure 4.4 (d) and (e), indicating a isomerization quantum efficiency of about 40%. Likewise, the cis bands in Figure 4.4 (c) contain only 40% of the initial cis bleach intensity (Figure 4.4, f) as a result of a 60% quantum efficiency for cis $\rightarrow$ trans isomerization. This simple argument can be used as long as only one species (cis or trans) is excited by the pump beam. The bleach signal in the first column of Figure 4.4 contains contributions from 5% of *trans*-NMTAA, which must be taken into account when calculating isomerization quantum efficiency. The isomerization quantum yield are determined to be 30-40% in the trans$\rightarrow$cis direction and 60-70% in the cis$\rightarrow$trans direction. The error in the quantum efficiency determination is mainly due to uncertainties in the fits with overlapping (Lorenzian) line shapes. Thermal cis $\rightarrow$ trans relaxation on the ground state surface is too slow to influence either of the measurements significantly. Independent of the comparison with the initial bleach signals, the similarity of the photoproduct signals for S_2 and S_1 excitation of *trans*-NMTAA and S_2-excitation of *cis*-NMTAA clearly show, that similar ratios of both isomers are formed independently of the initial configuration and excitation wavelength.

Transient infrared measurements of *trans*-NMTAA in CD_3CN upon S_2-excitation have

[2]The spectra are obtained by subtracting from the pump/probe data the negative contribution, i.e. the pump/probe spectrum at early delays, which is shown in the bottom row

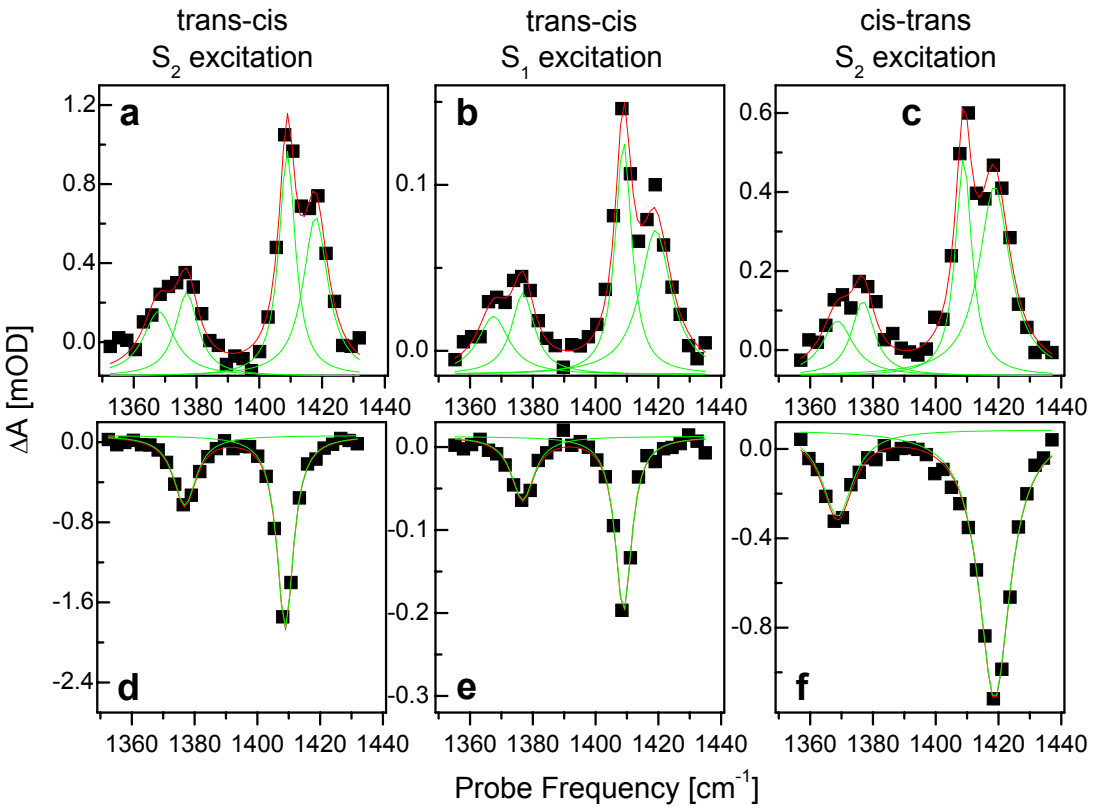

Figure 4.4: (a-c) Photoinduced vibrational bands of NMTAA in D_2O at long time delays for different excitation conditions and initial conformations. The spectra were obtained by subtracting the pure bleaching signal at a pump/probe delay of 2 ps from the original pump/probe data. Vertical scales are chosen to yield the same height of the trans peak in all spectra. (d-f) Short time pump/probe spectra (2 ps) that were subtracted from the 1 ns data to produce the top graphs. The relative scales are the same as in the top graphs. Key: (a, d) $\pi - \pi^*$ (S_2) excitation of *trans*-NMTAA; (b, e) n-π^* (S_1) excitation of *trans*-NMTAA; (c, f) $\pi - \pi^*$ (S_2) excitation of *cis*-NMTAA.

been performed as well [109]. Very similar dynamics has been found with a bi-phasic isomerization mechanism with time constants of 10 and 350 picoseconds.

4.3 Excited-State Relaxation Mechanism

Although the transient IR spectra of NMTAA are not sensitive directly to the electronically excited state(s), our observation of different ground state recovery following $^1n - \pi^*$ (S_1) and $\pi - \pi^*$ (S_2) excitation can nevertheless be critically related to the excited state relaxation mechanism and thioxopeptide isomerization. In addition, the transient UV/Vis measurements by Huber et al. and *ab initio* calculations of the minimum energy path (MEP) achieved by De Vico et al. [108] reveal important information to the mechanism.

The proposed mechanism is shown schematically in Figure 4.5. The *ab initio* calcula-

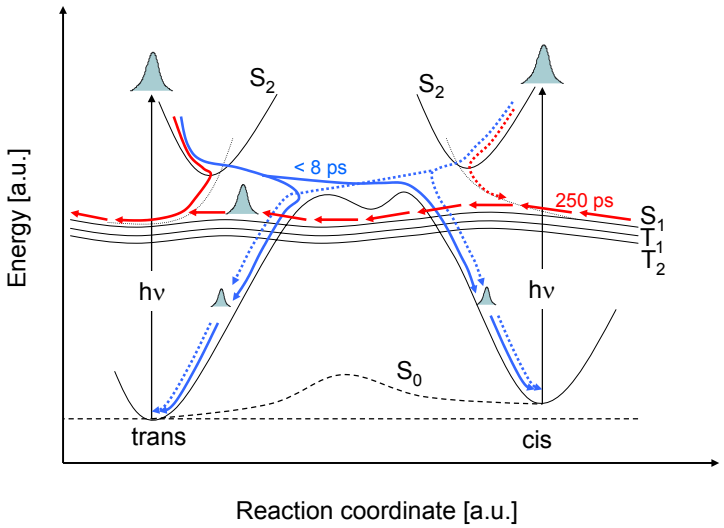

Figure 4.5: Schematic representation of the of the photoisomerization of *trans*- and *cis*-NMTAA. The multiple intersections between the S_1,T_1,T_2 and the S_0 energy profiles represent the conical intersections and the intersystem crossings.

tions [108] suggest that after S_2 excitation the system relaxes on a very fast timescale to S_1 (or lower lying triplet) state via a conical intersection point. This initial relaxation is dominated by the C-N and C-S expansion which is consistent with the resonance Raman spectra recorded on N-Metyhlacetamide, where torsional modes are not enhanced [113]. This fast relaxation to S_1 is also consistent with the observation that the time scales and the quantum efficiency of isomerization (60 - 70 % trans and 30 - 40 % cis) is not dependent on the irradiation wavelength (irradiation of *trans*-NMTAA with 260 nm or irradiation of accumulated *cis*-NMTAA with 280 nm), which indicates that the initial kinetic energy (or the S_2 state) plays no role in the trans→cis photoisomerization mechanism, but a common intermediate state (the S_1 or the lowest triplet state) does. The common state is populated from either the trans (260 nm excitation) or the cis (280 nm excitation) conformer and then decays via the same pathways.

The *ab initio* calculations [108] show very flat S_1 and triplet states along the torsional coordinate with four conical intersection (CI) resp. intersystem crossing (ISC) points to the ground state S_0, lying energetically above the minima of the respective excited electronic states. One CI resp. ICS leads to the cis conformation of NMTAA while the other three to the trans conformation, which would be consistent with the isomerization quantum efficiency of 60 - 70 % *trans*-NMTAA and 30 - 40 % *cis*-NMTAA. The flat potential energy surface suggests a diffusive search of the molecules for the conical intersection resp. intersystem crossing points along the C-N torsional coordinate.

The theoretical prediction that the conical intersection resp. intersystem crossing points lie energetically above the minima of the respective excited electronic states indicates that fast relaxation to the electronic ground state may be limited upon direct S_1 excitation because the molecules do not have enough excess energy to directly access conical intersection or intersystem crossing points. In contrast, molecules that are initially prepared in the S_2 state (260 and 280 nm excitation) can give rise to a highly thermally excited S_1 or triplet population with enough excess energy to follow directly into the S_1/S_0 conical intersections or T_1/S_0 intersystem crossing points. The remaining population in the excited state may get trapped either in the S_1 or the lowest lying triplet state. This situation is indeed consistent with the time-resolved infrared measurements: After 260 and 280 nm excitation to the S_2 state two time scales are found for the relaxation to the ground state (8 - 9 ps for the direct relaxation and 250 ps for the temporary trapping on the S_1 or the lowest lying triplet state), while after 308 nm excitation to the S_1 state only the slower relaxation time is found.

Within this scenario, which of these excited states is finally populated or the ordering of the triplet states is not critical to explain the presence of fast and slow electronic relaxation to the electronic ground state. Satzger et al. [55] proposed that the bi-phasic relaxation time scale after S_2 excitation arises from the population of the $^3n-\pi^*$ (fast relaxation) and the $^3\pi-\pi^*$ (slow relaxation) triplet state, while, according the El-Sayed rule [114], the lower lying $^3\pi-\pi^*$ triplet state (slow relaxation) would be preferentially populated after S_1 ($^1n-\pi^*$) excitation. To establish the exact role of the excited states in the fast isomerization dynamics, additional experimental information would be required.

4.4 Conclusion

In summary, the time-resolved IR-study of NMTAA shows that its isomerization is completed within 1 ns. The trans (30 - 40 %) and cis (60 - 70 %) quantum yields in the photoisomerization of NMTAA do not depend on the initial conformation (cis or trans) of the molecule or the solvent and are very similar for S_2 and S_1 excitation. This strongly suggests a common intermediate state, S_1 or, more likely, the lowest-lying triplet state, on which the outcome of the photoreaction is determined. According to *ab initio* calculations [108] S_1, T_1, and T_2 are essentially flat along the isomerization coordinate and energy is required to reach the conical intersections or intersystem crossing points to the electronic ground state. Thus, once the excess energy from photoexcitation is dissipated, relaxation back to the ground state should be essentially diffusion-controlled. In line with this interpretation is our second observation that a well-defined fast component in the ground state relaxation of NMTAA is only present for S_2 but not for S_1 excitation. On

the fast time scale, the ground state could be accessed with the excess energy available from S_2 decay. However, a fast intersystem crossing pathway via the $^3n-\pi^*$ state, which is bypassed upon S_1 excitation cannot be excluded. The proposed isomerization mechanism implies that larger secondary thioxopeptides can undergo photoisomerization as long as there are little constraints to the diffusion about the thioamide (essentially single) bond in the electronically excited state due to neighboring residues. For the same reason one may expect expect more rigid secondary structure elements to be broken less efficiently by UV-excitation of a thioxopeptide unit.

Chapter 5

Equilibrium Conformations of the Model Thioxopeptide

It is known that small Pro-Aib-containing peptides tend to form β-turns whose most specific property is a $i \rightarrow i+3$ hydrogen-bond (Pro being the amino acid *i+1*, Aib the amino acid *i+2*) [77]. In this chapter the investigations of the conformations of Boc-Ala-Pro-ψ(SC-NH)-Aib-Ala-OMe are shown, with the aim to identify molecules folded in the β-turn conformation. For this purpose, (2D-)IR,^{13}C- and temperature-dependent ^{1}H-NMR measurements are used.

5.1 Infrared absorption

The FT-IR absorption spectrum of thioxopeptide Boc-Ala-Pro-ψ(SC-NH)-Aib-Ala-OMe (**1a**) in Figure 5.1 shows four bands in the 1700 cm^{-1} region, which can be assigned to the four C=O stretch modes of the molecule: amino acid *i* at 1641 cm^{-1} (Ala(1)), amino acid *i+2* at 1672 cm^{-1} (Aib), urethane protection group *i-1* at 1711 cm^{-1} (Boc) and amino acid *i+3* at 1745 cm^{-1} (Ala(4)). In the spectrum of the isotope labelled thioxopeptide Boc-Ala-ψ(O^{13}C-NH)-Pro-ψ(SC-NH)-Aib-Ala-OMe (**1b**) the ^{13}C=O stretch band Ala(1) is red-shifted to 1600 cm^{-1} and a fifth, three times weaker band is visible at 1625 cm^{-1} which is hidden in the spectrum of **1a**. It is argued that these two bands are due to Ala(1) in $i \rightarrow i+3$ hydrogen-bonded (lower frequency) and non hydrogen-bonded (higher frequency) conformations of the thioxopeptide.

Assuming, based on the results of the pump-probe measurements in chapter 6, a 1.5 times larger oscillator strength for hydrogen-bonded Ala(1) band with respect to the 1625 cm^{-1} absorption, it is estimated that approximately 60-70% of all molecules adopt the β-turn conformation in acetonitrile solution at room temperature. In a very similar oxopeptide Boc-Cys-Pro-Aib-Cys-OMe this β-turn structure has been stabilized by a disul-

fide bridge between the two cysteine sidechains [45]. Opening of a part of these turn structures after light-cleavage of the disulfide bond led to a new equilibrium between hydrogen-bonded and non hydrogen-bonded conformations on a 200 ps timescale [47]. The final conformational distribution in that experiment may be regarded as similar to the starting distribution of thioxopeptide **1** before the photoisomerization of the thioamide bond, which perturbs this equilibrium.

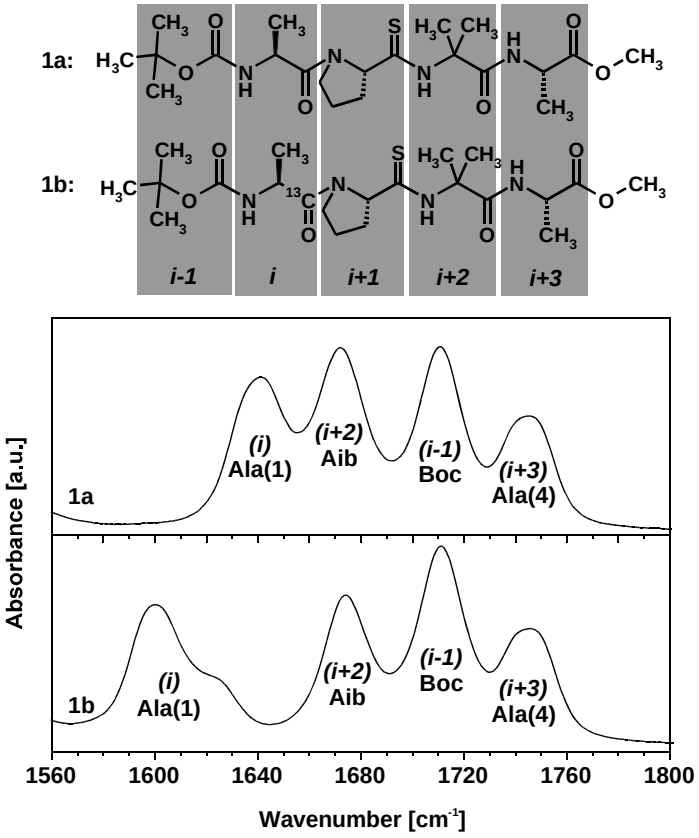

Figure 5.1: FT-IR absorption spectra of the thioxopeptides **1a** and **1b** at 293 K.

The propensity of different thioxopeptides to form intramolecular hydrogen-bonds has, in the past, been inferred from infrared absorption spectra in acetonitrile and CH_2Cl_2 solution [115]. In the non-polar solvent distinct NH-stretch bands arise for hydrogen-bonded amide and thioamide units and a dominant β-turn conformation was identified for the protected thioxopeptide Boc-Pro-Gly-ψ(SC-NH)-$NHCH_3$ (see Figure 5.2 a). In Boc-Pro-ψ(SC-NH)-Gly-$NHCH_3$, on the other hand, the thioamide proton was found to take part in a hydrogen-bond with the neighboring carbonyl group, forming a competing C_5 ring structure (see Figure 5.2 b) [115]. A similar situation is found in the crystal structures of Boc-Gly-Ala-Aib-OMe, Boc-Gly-Ala-ψ(SC-NH)-Aib-OMe where β-turns are

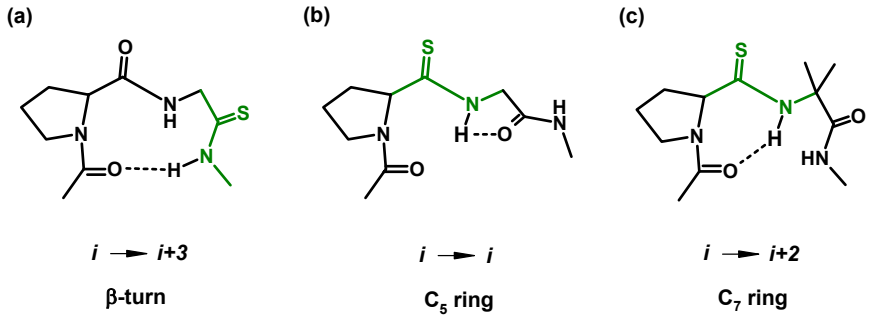

Figure 5.2: Hydrogen-bonding found in different thioxopeptides.

formed while in Boc-Gly-ψ(SC-NH)-Ala-Aib-OMe it does not [116, 117]. Since thioamide protons are stronger hydrogen-bond donors than amide protons, a perturbation of the β-turn conformation of **1a**/ **1b** should be considered. Shaw et al. have shown that detailed information on intramolecular hydrogen-bonding of thioxopeptides can sometimes be gained from an analysis of the NH-stretch region in apolar solvents [115]. Non hydrogen-bonded and hydrogen-bonded amide (CONH)- and thioamide (CSNH)-protons give rise to signals in four distinct spectral windows (see color shading in Figure 5.3). Clearly, the FT-IR spectrum of Fmoc-Pro-ψ(SC-NH)-Aib-Ala-OMe (precursor molecule of **1a** and **1b**) exhibits, in chloroform, a band due to an hydrogen-bonded thioamide proton at 3260 cm^{-1} indicating the presence of a C_7 ring structure (see Figure 5.2 c) most likely with the Fmoc carbonyl group acting as the hydrogen-bond acceptor (red-shifted C=O stretch band of Fmoc). This NH-stretch band, however, transforms into a weak tail in the absorption spectrum of **1a** and **1b**. At the same time, in chloroform the same double band for the ^{13}C=O stretch vibration (isotope-labelled Ala(1)) as in acetonitrile is observed (compare Figure 5.3 and 5.1), being consistent with the presence of a $i \rightarrow i+3$ hydrogen-bonded conformation mentioned above.

Figure 5.4 shows the temperature dependent FT-IR spectra of thioxopeptide **1b** between 3 and 40 °C. By increasing the temperature the Ala(1) band of the non hydrogen-bonded species increases. *Ab initio* calculations on NMA (*N*-Methylacetamide) dimers suggest that only hydrogen-bond lengths smaller than 3.5 $\AA$ can induce a red shift of the stretching of the accepting C=O group by as much as 25 cm^{-1} [94]. In addition, a smaller red shift is expected for the amide I mode of the peptide unit acting as hydrogen-bond donor. Indeed, Figure 5.4 shows a slight red-shift of the Aib band maximum when increasing the temperatures, which strengthens the statement above to have a $i \rightarrow i+3$ hydrogen-bond between the H-atom of Aib and the carbonyl group of Ala(1).

This assignment is consistent with temperature-dependent ^{1}H-NMR and 2D-IR data.

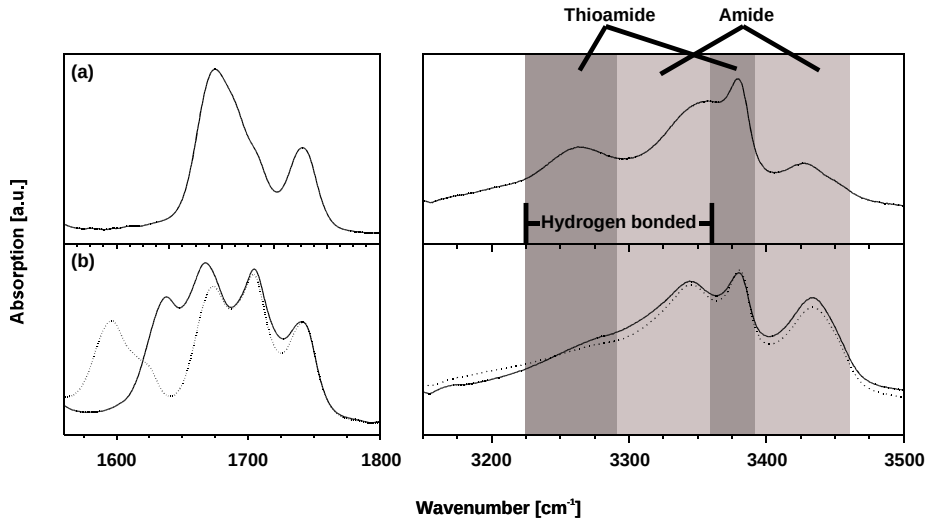

Figure 5.3: FT-IR absorption spectra in chloroform of thioxopeptide Fmoc-Pro-ψ(SC-NH)-Aib-Ala-OMe (a, precursor of **1a** and **1b**) and **1a** (b, solid lines) and **1b** (b, dashed lines). For Fmoc-Pro-ψ(SC-NH)-Aib-Ala-OMe, the red-shifted thioamide N-H stretch band indicates the presence of a C_7 ring structure with a hydrogen-bond between the carbonyl group of Fmoc and the thioamide proton. This conformation is strongly reduced in thioxopeptide **1a** and the fraction of hydrogen-bonded amide protons is enhanced.

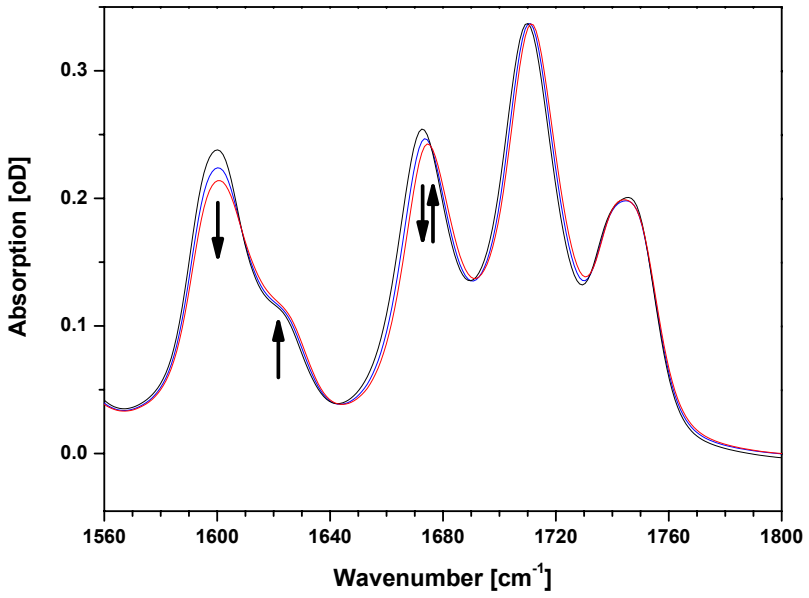

Figure 5.4: FT-IR spectra of thioxopeptide **1b** at temperatures of 3 (black), 21 (blue) and 40 (red) °C. Arrows indicate changes with increasing temperature.

5.2 ^{1}H-NMR spectra

Figure 5.5(a) shows the ^{1}H-NMR spectra of thioxopeptide **1a** in the 7 ppm region for temperatures between 253 to 313 K. The signal at 8.5 ppm is due the NH-proton of Aib (next to C=S), the peak at 7.0 ppm is due to Ala(4) and the one at 5.5 ppm is the amide proton signal of Ala(1). The amide protons of Aib and Ala(1) give rise to multiple peaks, which do, however, not reflect the splitting of the Ala(1) band in the FT-IR spectrum. The integral intensity ratio of the two peaks of Aib is 9:1 which is reproduced in the ^{13}C-NMR spectrum of **1b** (Figure 5.5 b, ^{13}C atom of Ala(1)). The two amide proton peaks of Aib can therefore be assigned to the trans (90%) and cis (10%) conformations of the Ala(1)-Pro peptide bond. The Ala(1) signal may be additionally split due to trans and cis forms of urethane [118,119], and the ratio of these three amide proton signals is 1:8:1, indicating that the main peak and one small peak are due to the trans proline conformation.
In Figure 5.5(c) the chemical shifts for the NH-protons are plotted as a function of the temperature T. The main NH-protons peaks of Ala(1) and Ala(4) shift with 2.5 and 2.4 ppb/K (ppb = parts per billion), which is significantly less than *N*-Methylacetamide ($H_3CCONHCH_3$, 8.0 ppb/K) in the same solvent (*N*-Methylthioacetamide $H_3CCSNHCH_3$ in acetonitrile shows a ^{1}H-NMR-temperature dependence of 3.8 ppb/K. Therefore, the value for the SC-NH proton should not be compared to the OC-NH protons). Since the chemical shift of protons, which participate in an intramolecular hydrogen-bond, changes less as a function of temperature than that of protons which are fully exposed to the solvent [119], this observation is consistent with the amide proton of Ala(4) acting as donor in a $i \rightarrow i{+}3$ hydrogen-bond with the carbonyl oxygen of Ala(1) and can explain the double peak in the IR spectrum of the isotope-labelled molecule. In addition, partial $i{+}3 \rightarrow i$ hydrogen-bonding with Ala(1) as a proton donor is indicated by the NMR data. Indeed, in the FT-IR spectrum the stretch band of the C=O group at 1745 cm^{-1} (Ala(4)) is broadened, which could be due to it acting as an hydrogen-bond acceptor. However, the very small spectral changes observed for the C=O stretch bands of Boc and Ala(4) upon photo isomerization of the thioamide bond (see below) do no support this hypothesis.

5.3 2D-IR Measurements

In Figure 5.6 (left) the 2D-IR spectrum of **1b** with a time delay of 1.2 ps between the IR-pump and IR-probe pulse is shown. The cross peak (encircled in Figure 5.6) between the modes of Ala(1) and Aib indicates spatial proximity of these two residues, in line with the presence of a $i \rightarrow i{+}3$ hydrogen-bonded conformation.

For longer time-delays between the IR-pump and IR-probe pulse excitation transfer between different modes takes place and cross peaks grow at the cost of the diagonal

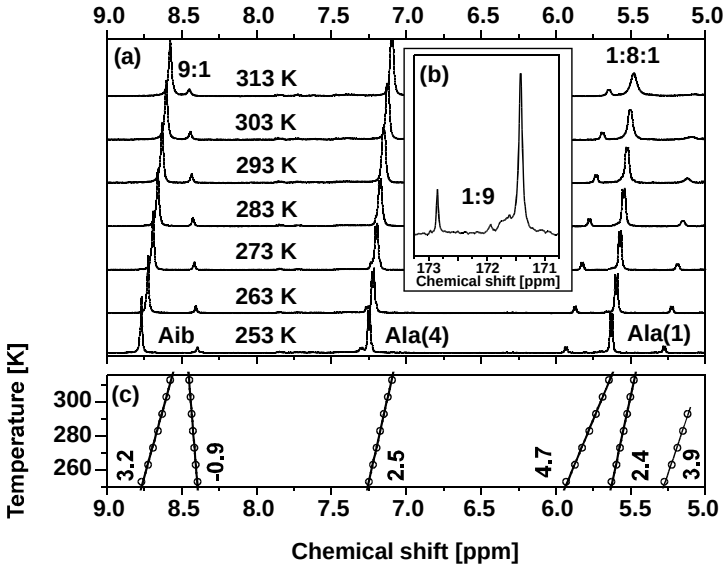

Figure 5.5: (a): ^{1}H-NMR spectrum of thioxopeptide **1a** in the NH-region at temperatures between 253 and 313 K. (b): The ^{13}C-NMR peaks of the ^{13}C=O carbon (Ala(1)) of thioxopeptide **1b**. (c): Temperature dependent chemical shift gradients (given in ppb/K) of the O=C-NH- resp. S=C-NH-protons.

peaks (this experiment is the analogue of spin transfer in a NOESY experiment in NMR). After a few picoseconds the energy should be allocated to all modes[1]. On the right hand side of Figure 5.6, horizontal cuts through the 2D-IR spectrum for time delays between pump and probe pulses of 1.2 ps (grey) and 4 ps (red) are observed, which were normalized to the diagonal signal. The upper cut on the right hand side of Figure 5.6 clearly shows that population transfer takes place to Ala(1) when the band of Aib (1672 cm^{-1}) is excited initially (two negative bands are growing in at 1600 and 1625 cm^{-1}, with corresponding positive excited state absorption signals). The reverse is observed when the bands at 1600 cm^{-1} or at 1625 cm^{-1} are excited. However, there is no sign for population transfer between the modes underlying the bands at 1600 and 1625 cm^{-1}. This is a strong indication that these two bands are due to molecules in different conformations which do not interconvert on a picosecond timescale.

For longer time-delays between the IR-pump and IR-probe pulse excitation transfer between different modes takes place and cross peaks grow at the cost of the diagonal peaks (this can be viewed as the analogue of an NMR-NOESY experiment). However, after a few picoseconds the energy should be allocated to all C=O modes in a peptide with only four residues[2]. In addition, low frequency modes are populated by the decay of the C=O

[1]In comparison to a NOESY experiment a cross peak not only appears due to direct population transfer, but also due to coupling to lower frequency modes [120]

[2]In comparison to a NOESY experiment a cross peak not only appears due to direct population transfer,

stretch excitations. This too can give rise to apparent cross peaks, whose intensity thus becomes less sensitive to molecular structure. On the right hand side of Figure 5.6 we compare horizontal cuts through the 2D-IR spectrum for time delays between pump and probe pulses of 1.2 ps (grey) and 4 ps (red), which were normalized to the diagonal signal. The upper cut on the right hand side of Figure 5.6 clearly shows that population transfer takes place to Ala(1) when the band of Aib (1672 cm^{-1}) is excited initially (two negative bands are growing in at 1600 and 1625 cm^{-1}, with corresponding positive excited state absorption signals). The reverse is observed when the bands at 1600 cm^{-1} or at 1625 cm^{-1} are excited. However, there is no sign for population transfer between the modes underlying the bands at 1600 and 1625 cm^{-1}. This is a strong indication that these two bands are due to molecules in different conformations which do not interconvert on a picosecond timescale.

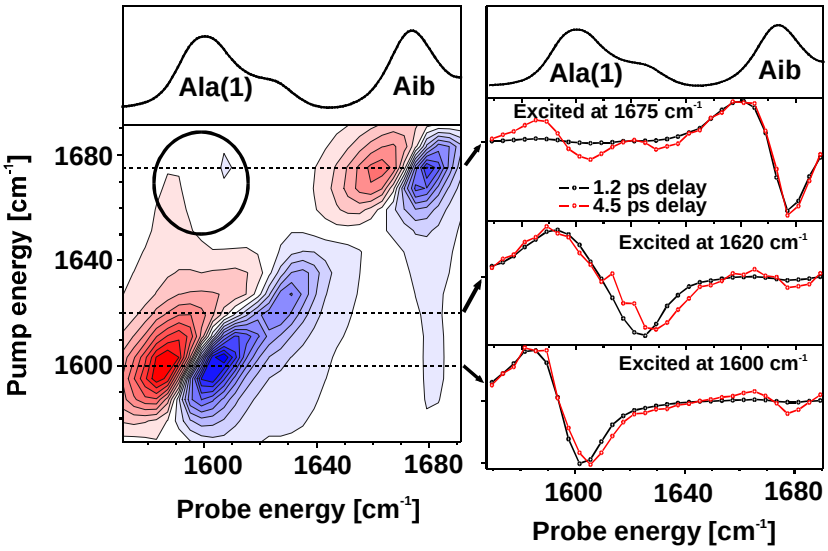

Figure 5.6: Left: 2D-IR spectrum of thioxopeptide **1b** at 293 K for a 1.2 ps time delay between pump and probe pulses with perpendicular polarization. Red corresponds to positive signals ($1 \rightarrow 2$ transition, excited state absorption), blue to negative ($0 \rightarrow 1$ transition, bleach and stimulated emission). The difference between two contour lines is 0.14 mOD. Right: Cuts at 1600, 1620 and 1675 cm^{-1} for 1.2 (black) and 4.5 ps (red) time delays.

but also due to coupling to lower frequency modes [120].

5.4 Conclusion

In this chapter, the conformations of the small thioxopeptide Boc-Ala-Pro-ψ(SC-NH)-Aib-Ala-OMe has been analyzed by linear and two-dimensional IR spectroscopy, as well as by NMR methods. It has been shown that in acetonitrile solution at room temperature a hydrogen-bonded structure, in which the amide proton of Aib forms a hydrogen-bond with the C=O carbonyl of the Ala(1) moiety, is present in coexistence with more non hydrogen-bonded conformations, which remain unresolved. At higher temperatures the equilibrium is shifted away from the hydrogen-bonded conformation. β-turn opening and -closing happens on a timescale much slower than 4 ps, and can therefore not be detected by 2D-IR exchange spectroscopy.

Chapter 6

Photoisomerization of the Model Thioxopeptide

The isomerized conformation of the photoswitch (cis form) hinders the peptide to form a β-turn, which is the dominant conformation of -Pro-Aib-containing thioxopeptides with a trans thioamide bond (see previous chapter). In this chapter the results of the time-resolved infrared measurements on the conformational change ($i \rightarrow i{+}3$ hydrogen-bond breaking) of Boc-Ala-Pro-ψ(SC-NH)-Aib-Ala-OMe, initiated by the isomerization of the built-in photoswitch, are presented.

6.1 Results

Changes in the mid-infrared spectrum of thioxopeptide Boc-Ala-Pro-ψ(SC-NH)-Aib-Ala-OMe (**1a**) and Boc-Ala-ψ(O^{13}C-NH)-Pro-ψ(SC-NH)-Aib-Ala-OMe (**1b**) after $\pi \rightarrow \pi^*$ excitation are shown for different time delays between the UV-pump and the IR-probe pulse in Figure 6.1 and 6.2. At early delay times, negative absorption is visible at the spectral positions of the vibrations of the initial trans species with positive absorption appearing red-shifted from these negative signals. Both negative and positive signals decrease for longer delays, however, the time-dependence is different at different spectral positions (see Figure 6.3, spectral positions are indicated in Figure 6.1 and 6.2 with arrows). As observed in previous studies [56], the red-shift of all bands in the amide I region at early delays is in part due to anharmonic coupling to low frequency modes, excited by the excess laser energy (released upon fast relaxation from S_2 to lower-lying electronic states, see chapter 4). As a result of energy dissipation from the low frequency modes to the solvent this red-shift almost completely decays on a 10-15 ps timescale for peptide units further away from the photoexcited moiety. On the other hand, the C=O oscillators (i and $i{+}2$), which are nearest neighbors of the thioxopeptide unit and are sensitive to

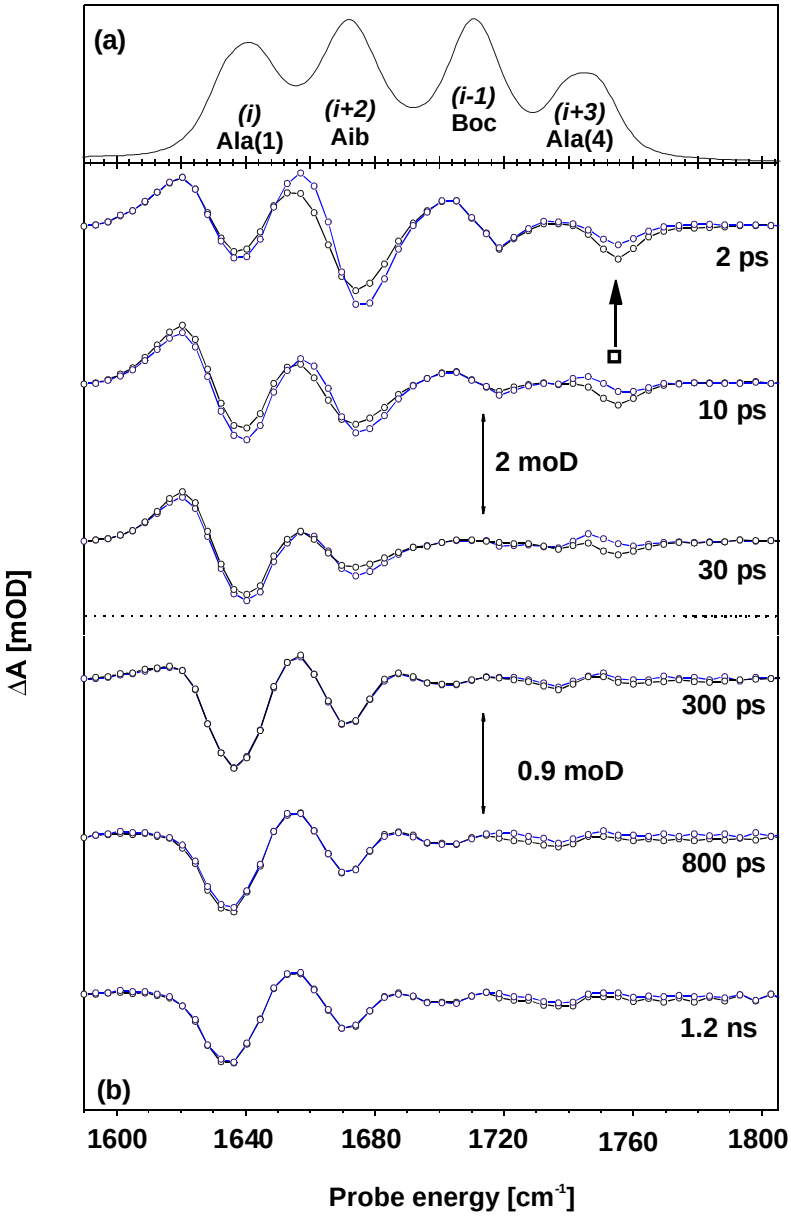

Figure 6.1: (a): FT-IR absorption spectrum of thioxopeptides **1a**. (b): Transient infrared difference absorption spectra of thioxopeptide **1a** after $\pi \rightarrow \pi^*$ excitation at different delays and parallel (black) and perpendicular (blue) between the UV-pump and IR-probe pulse.

the different charge distribution in the electronically excited state, continue to be shifted at longer time delays. Indeed, after a non-exponential initial decay, the Aib (*i+2*) signal decreases exponentially on a longer time scale of 240 ps. This decay is associated with relaxation into the electronic ground state, after the molecules have been trapped on the

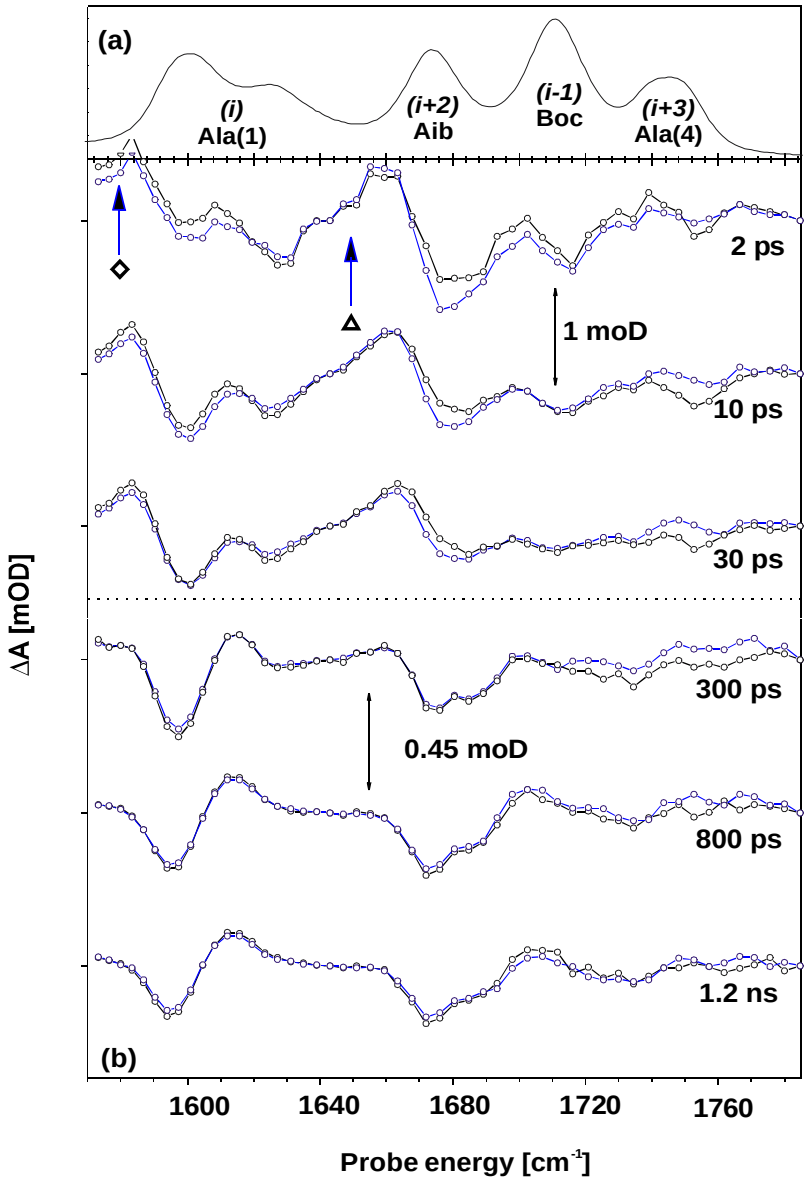

Figure 6.2: (a): FT-IR absorption spectrum of thioxopeptides **1b**. (b): Transient infrared difference absorption spectra of thioxopeptide **1b** after $\pi \rightarrow \pi^*$ excitation at different delays and parallel (black) and perpendicular (blue) between the UV-pump and IR-probe pulse.

lowest-lying electronic excited state (see chapter 4 and [55]). After one nanosecond the transient spectra no longer change. At this stage positive absorption is due to molecules, which have isomerized into the cis conformation in the electronic ground state, while negative absorption is due to the loss of molecules in the trans conformation. The data for

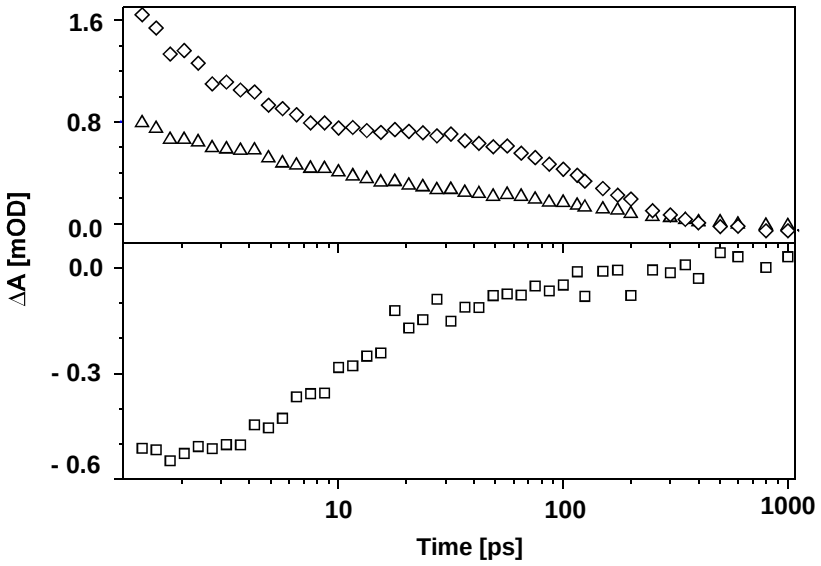

Figure 6.3: Time evolution of the C=O-stretch mode absorption of Ala(1) (*i*, **1b**, diamonds), Aib (*i+2*, **1a** , triangles) and of Ala(4) (*i+3*, **1a**, squares) mode absorption after $\pi \rightarrow \pi^*$ excitation. The spectral positions are indicated in Figure 6.1 and 6.2 with arrows. The signal shows the difference absorption signal at 1580 cm^{-1} for the C=O-stretch mode absorption of Ala(1), at 1651 cm^{-1} for the C=O-stretch mode absorption of Aib and at 1755 cm^{-1} for the C=O-stretch mode absorption of Ala(4).

1b shows an decrease of the C=O-stretch band of Ala(1) (amino acid *i*) at 1600 cm^{-1} and an approximately 50% smaller positive band at 1620 cm^{-1}. This is consistent with a $i \rightarrow i+3$ hydrogen-bond, which is broken after the isomerization of the thioamide bond (see Figure 6.4). Both the red-shift and the oscillator strength of the initially hydrogen-bonded carbonyl stretch vibration are thereby reduced. Additionally, a blue-shift and apparent loss of oscillator strength can be seen for the C=O-stretch absorption of Aib (amino acid at position *i+2*), which belongs to the proton donating peptide unit of the $i \rightarrow i+3$ hydrogen-bond. Only a very small blue-shift is observed for the C=O-stretch band of Boc and Ala(4), indicating that the terminal peptide units cannot be involved in strong intramolecular hydrogen-bonds in the initial trans-state of the thioxopeptide.

In addition of isomerization studies, changes in sample temperature have to be considered which can have a strong effect on the infrared absorption spectrum of (thi)oxopeptides, in particular in the presence of hydrogen-bonds. Temperature jumps (increase of up to 1 K in the excited volume [56]) always accompany pump/probe measurements because of the dissipation of excess laser energy upon electronic and vibrational energy relaxation.

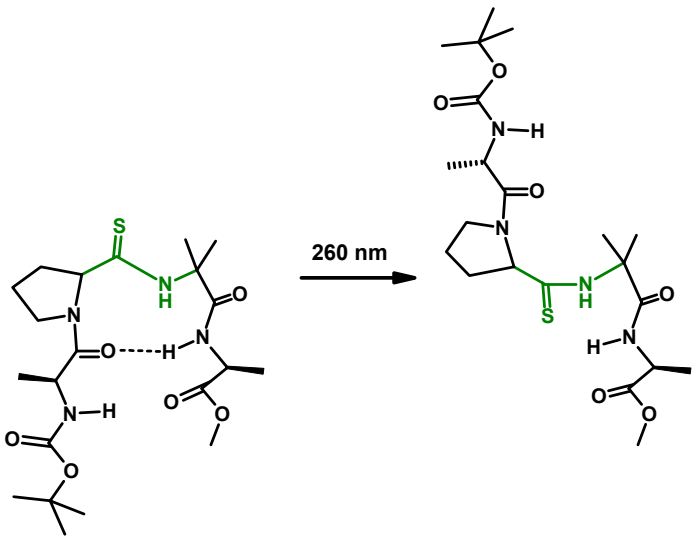

Figure 6.4: Schematic representation of the structural change of thioxopeptide **1a** after -Pro-ψ(SC-NH)-Aib- isomerization upon $\pi \rightarrow \pi^*$ excitation.

However, the temperature-induced changes in the FT-IR spectrum of **1a** in Figure 6.5 are very different from the pump/probe signals at a delay of 1 ns. The transient spectra of **1** must therefore be almost entirely caused by photoisomerization.

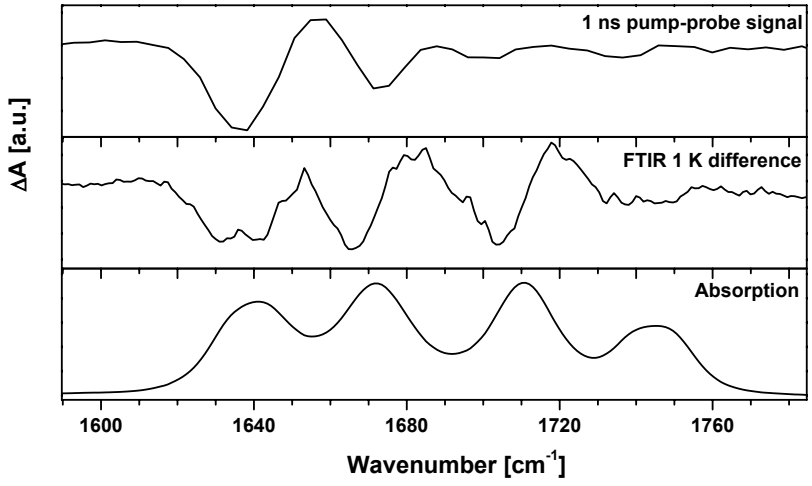

Figure 6.5: Comparison of absorption changes 1 ns after UV-excitation (top) and those induced by increasing the sample temperature from 21 to 22 °C in the FT-IR spectrometer (center) of thioxopeptide **1a**.

6.2 Conclusion

Transient infrared spectroscopy could be used to follow the $i \rightarrow i{+}3$ hydrogen-bond breaking. The whole process is completed within 1 ns. The hydrogen-bond breaking results in a strong blue-shift of the Ala(1) amide I band and a corresponding smaller blue-shift of the Aib amide I band. The spectral changes observed upon photoisomerization of the thioxopeptide are much more specific for identifying the intramolecular hydrogen-bond in the dominant equilibrium trans-conformation than the steady state absorption and temperature-dependent NMR data. The additional $i{+}3 \rightarrow i$ hydrogen-bond between Ala(1) (acting as proton donor) and Ala(4) (acting as proton acceptor) suggested by ^{1}H-NMR data in chapter 5 could nod be identified with this method. Thus, it is concluded that this hydrogen-band is not existing or very weak.

Chapter 7

Comparison with other -Aib-containing Thioxopeptides

In this chapter the conformations and isomerization properties of Boc-Ala-Pro-ψ(SC-NH)-Aib-Ala-OMe are compared to other potentially β-turn forming Aib-containing thioxopeptides, namely Z-Gly-ψ(SC-NH)-Aib-Ile-OMe, Z-Ala-ψ(SC-NH)-Aib-Ile-OMe, Z-Ile-ψ(SC-NH)-Aib-Gly-OMe and Boc-Phe-Ile-ψ(SC-NH)-Aib-Phe-OMe. Additionally, results on the backreaction on the electronic ground state after isomerization are shown. Theses thioxopeptides have been synthesized in Heimgartner's group (OCI, Zürich) [75–77] and were kindly provided.

7.1 Trithioxopeptides

7.1.1 Equilibrium conformations

In Figure 7.1 the structures and FT-IR absorption spectra (solid lines) of the three thioxopeptides Z-Gly-ψ(SC-NH)-Aib-Ile-OMe (**2a**), Z-Ala-ψ(SC-NH)-Aib-Ile-OMe (**2b**) and Z-Ile-ψ(SC-NH)-Aib-Gly-OMe (**2c**) are shown. The spectra of thioxopeptide **2a** and **2b** contain three bands in the amide I region, which have been assigned to the three C=O-stretch modes using the same numbering of residues with respect to the thio substituted amino acid as for Boc-Ala-Pro-ψ(SC-NH)-Aib-Ala-OMe (**1a**) and Boc-Ala-ψ(O^{13}C-NH)-Pro-ψ(SC-NH)-Aib-Ala-OMe (**1b**). The spectrum of thioxopeptide **2c** shows two additional bands. The two bands at 1740 cm^{-1} and 1756 cm^{-1} of thioxopeptide **2c** are assigned to different conformations of the C-terminal glycine due to the structural flexibility of this residue. On the other hand, the bands at 1707 cm^{-1} and 1722 cm $^{-1}$ are most probably both due to the C=O-stretch mode of the Z-protection group (i) in different open and hydrogen-bonded conformations. It is very likely that the extended wings near 1700

cm^{-1} in the absorption spectra of the thioxopeptides **2a** and **2b** are also due to hydrogen-bonded Z-groups. This assignment is supported by the spectral changes observed upon isomerization of the thioxopeptide bond (see below).

Figure 7.2(a) shows the ^{1}H-NMR spectra of thioxopeptide **2c** in the 7 ppm region for temperatures between 243 to 303 K. The signal at 8.5 ppm is due the NH-proton of Aib (next to C=S), the peak at 7.0 ppm is due to Gly and the one at 6.0 ppm is the amide proton signal of Ile. In Figure 5.5(b) the chemical shifts for the NH-protons are plotted as a function of the temperature T. The NH-proton peaks of Gly and Ile shift with 3.9 and 5.6 ppb/K (ppb = parts per billion). The shift of the Gly proton is significantly lower than the the one of the Ile proton and the *N*-Methylacetamide NH-proton ($H_3CCONHCH_3$, 8.0 ppb/K) in the same solvent[1]. Since the chemical shift of protons, which participate in an intramolecular hydrogen-bond, changes less as a function of temperature than that of protons which are fully exposed to the solvent [119], this observation is consistent with the amide proton of Gly acting as donor in a $i \rightarrow i{+}3$ hydrogen-bond with the carbonyl oxygen of Ala(1).

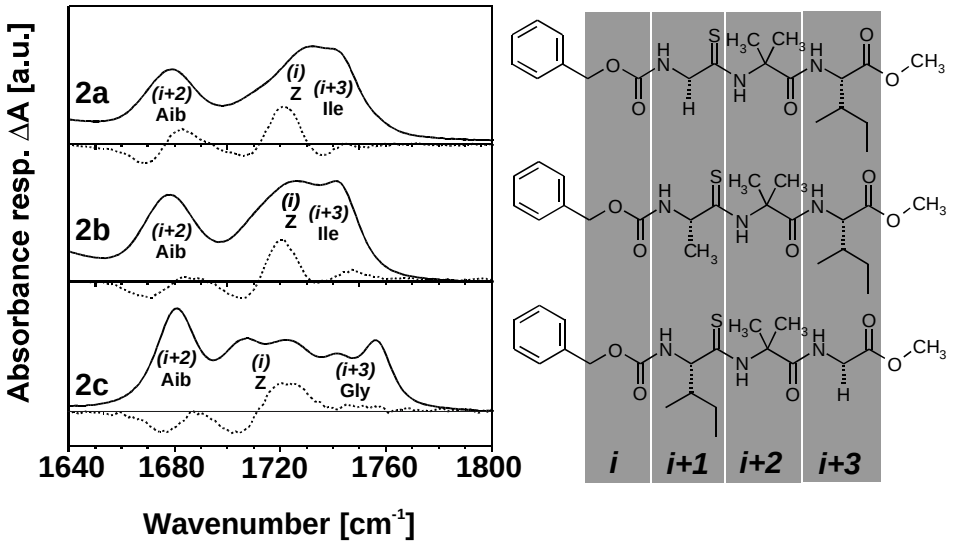

Figure 7.1: FT-IR absorption spectra (solid lines) and FT-IR difference absorption spectra (dashed lines) due to UV irradiation of the thioxopeptides **2a** - **2c** at 278 K.

7.1.2 Photoisomerization

FT-IR difference absorption spectra of the thioxopeptides **2a** to **2c** due to 248 nm irradiation ($\pi \rightarrow \pi^*$ excitation) are shown as dashed lines in Figure 7.1. The thioxopeptides are

[1] *N*-Methylthioacetamide $H_3CCSNHCH_3$ in acetonitrile shows a ^{1}H-NMR-temperature dependence of 3.8 ppb/K. Therefore, the value for the SC-NH proton should not be compared to the OC-NH protons

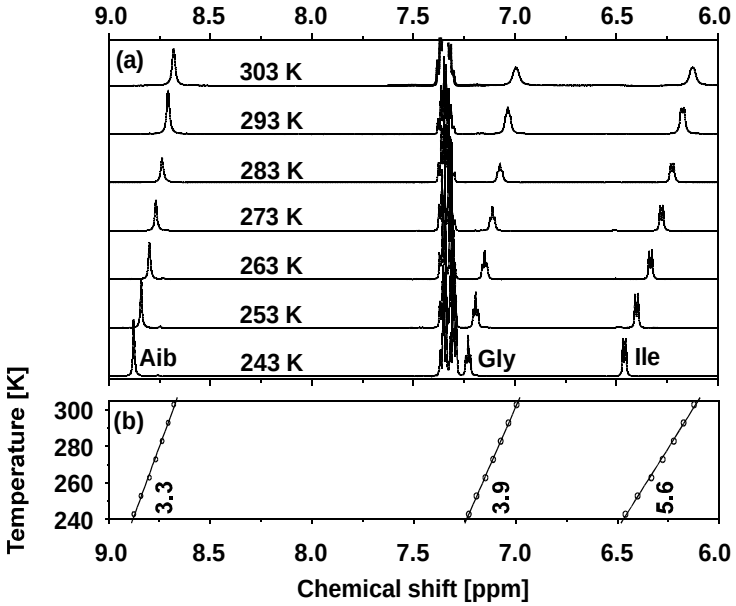

Figure 7.2: (a): ^{1}H-NMR spectrum of thioxopeptide **2c** in the NH-region at temperatures between 243 and 303 K. (b): Temperature dependent chemical shift gradients (given in ppb/K) of the O=C-NH- resp- S=C-NH-protons.

almost exclusively in the trans conformation in thermal equilibrium, so positive absorption in the difference absorption spectra is due to the cis conformation of the thioxopeptides (isomerized species), while negative absorption is due to a loss of molecules in the trans conformation. Despite the distinct absorption spectra of **2a** to **2c** the absorption changes due to irradiation are very similar. All three molecules show a blue-shift of the Aib band near 1680 cm^{-1}, less absorption around 1705 cm^{-1} and a strong positive signal near 1720 cm^{-1}. Only minor changes are observed in the spectral region of the ester group. The shape of the difference spectra near 1680 cm^{-1} corresponds to the negative derivative of the C=O-stretch band of Aib. This indicates a blue-shift of the cis band with respect to the trans band that is small compared to the width of the absorption band. This small blue-shift is in line with the ones obtained for the Aib band in thioxopeptide **1a/b**. On the other hand, in the C=O-stretch mode region of the Z-protection group (i) of **2c** there is a clear bleach of the 1707 cm^{-1} band at the cost of the 1722 cm^{-1} peak. This can be understood as a decrease in population of molecules with a hydrogen-bonded Z-protection group. The similar difference signals for **2a** and **2b** then indicate that these molecules, too, can exist in the trans-form in conformations with hydrogen-bonded C=O groups of the urethane, which give rise to the low frequency shoulder of the 1720 cm^{-1} absorption bands. Indeed, it has been noted previously [121], that the signals arising from the break-

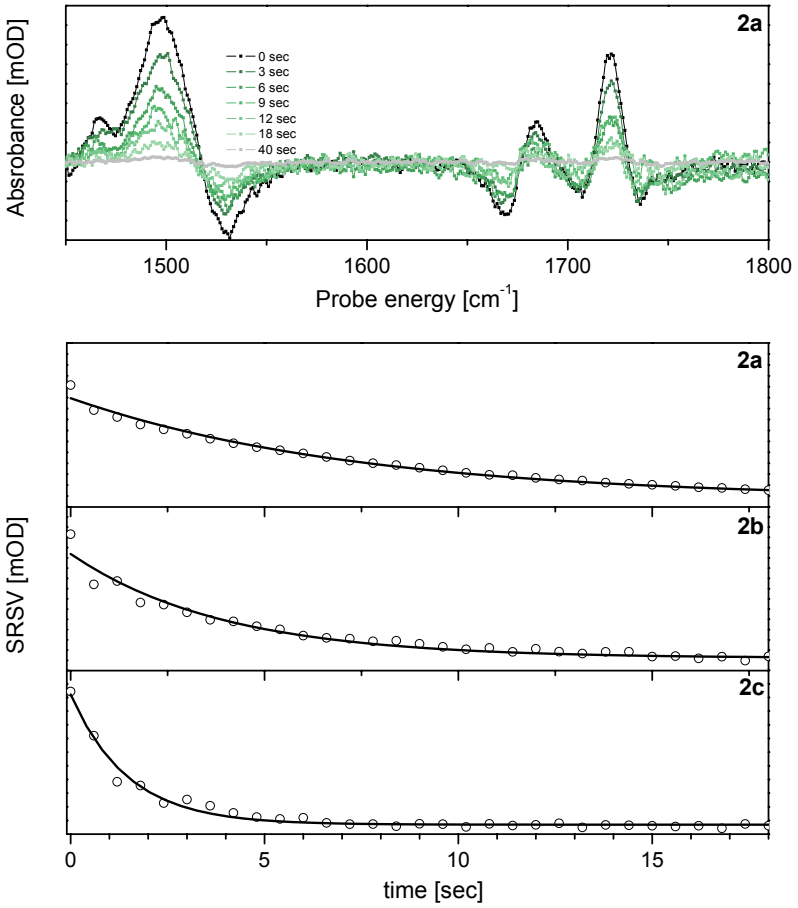

Figure 7.3: Top: Thermal backreaction at 5 °C after $\pi \rightarrow \pi^*$ excitation of the thioxopeptide **2a**. Bottom: Time trace of the thermal backreaction at 5 °C after $\pi \rightarrow \pi^3$ excitation of the thioxopeptides **2a** to **2c**. The datapoints are calculated by subtracting the absorption value at 1530 cm^{-1} from the one at 1570 cm^{-1}.

ing of intramolecular hydrogen-bonds are indeed dominant in the amide I IR difference spectra of thioxopeptides.

After irradiation at 248 nm is stopped, the system is out of equilibrium and thermally activated cis → trans relaxation in the electronic ground state takes place. The kinetics of this process have been measured by monitoring the decay of the irradiation-induced FT-IR difference signal at 278 K (dashed lines in Figure 7.1)[2]. Single-exponential decay with time constants of 4.7, 2.7 and 0.9 seconds was observed for **2a**, **2b** and **2c**, respectively (see Table 7.1). The back-reaction in the electronic ground state was thus rate-determining for the formation of the photoequilibrium, which made it impossible to determine reliably the photoisomerization quantum yields via kinetic measurements. For thioxopeptides **1a** and

[2]The relaxation times at room temperature of all four thioxopeptides lie below the time-resolution of our conventional FT-IR-spectrometer

1b the back-reaction was so fast that even at 278 K it could not be accumulated sufficient amount of photoproduct in order to record a FT-IR difference spectrum under irradiation conditions that did not damage the sample.

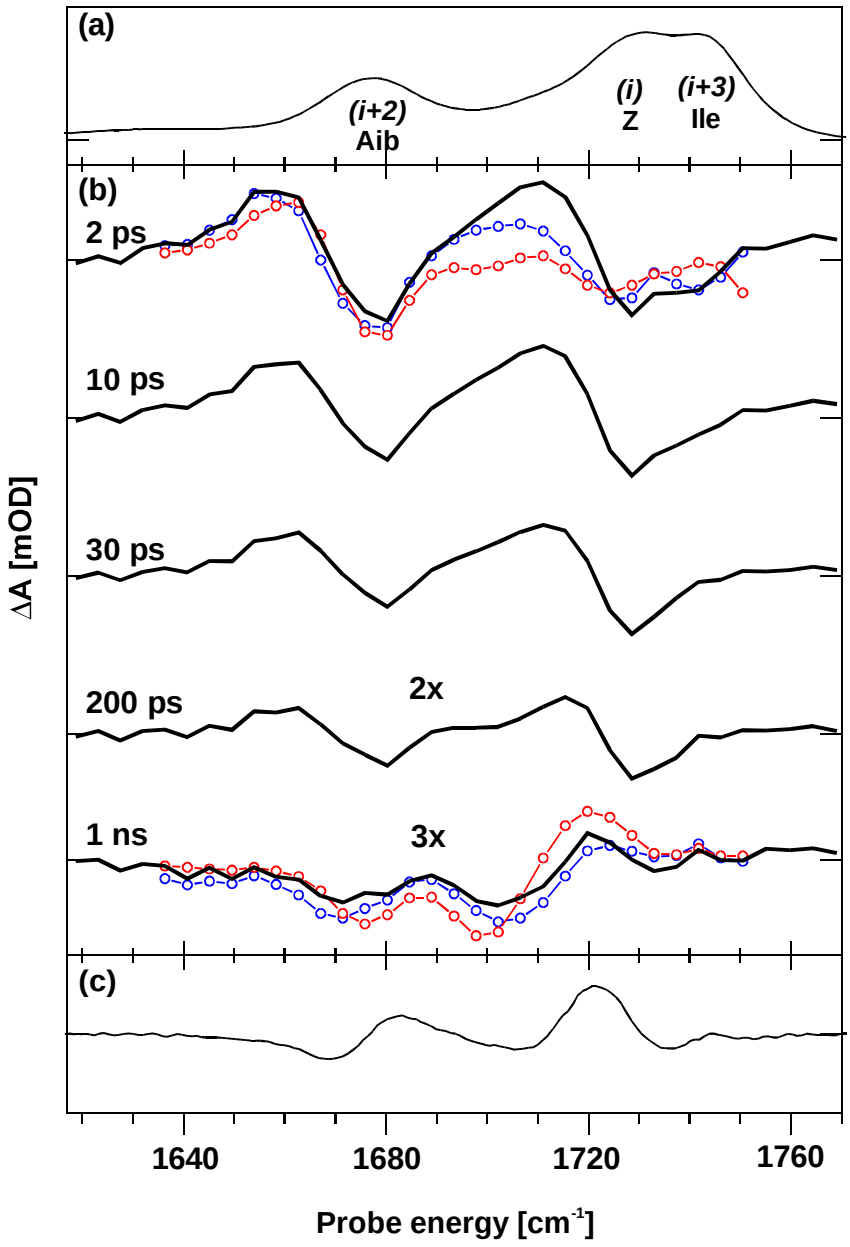

Figure 7.4: (a): FT-IR absorption spectrum of thioxopeptide **2a**. (b): Magic angle transient infrared difference absorption spectra of thioxopeptide **2a** (black), **2b** (blue) and **2c** (red) after $\pi \rightarrow \pi^*$ excitation with different time delays between the UV-pump and IR-probe pulse. (c): FT-IR difference absorption spectrum of thioxopeptide **2a**.

Transient spectra for the thioxopeptides **2b** (blue) and **2c** (red) are compared to those

of **2a** in Figure 7.4(b) for time delays of 2 ps and 1 ns. The 2 ps spectra have been scaled to superimpose the spectrally well-isolated Aib signals, in order to correct for different excitation densities, and the spectra after one nanosecond delay have been multiplied by the same factors. Since the C=O stretch band of Aib has a similar line shape in all three thioxopeptides the similar amplitudes of the 1 ns signals indicate comparable quantum yields of isomerization for **2a** - **2c**.

Thioxopeptide	**2a**	**2b**	**2c**	**1a**
$\pi \rightarrow \pi^*$ ex., abs. in *i+3* region [ps]	∼11	∼12	∼8	∼14
$\pi \rightarrow \pi^*$ ex., abs. in *i+2* region [ps]	150	130	160	240
Thermally activated relaxation [sec]	7.4	3.9	1.5	$\leq 0.5^a$

Table 7.1: Time constants observed in UV-pump/IR-probe measurements of the photo isomerization reaction after $\pi \rightarrow \pi^*$ excitation (top) and for thermally activated cis → trans relaxation in the electronic ground state at 278 K. *a*: Below time resolution of FT-IR spectrometer.

In addition to isomerization, the femtosecond pump laser also causes small changes in sample temperature (increase of $\approx 0.5K$ in the excited volume) which can also affect the infrared absorption spectrum [56]. For **1a,b** temperature-induced changes in the FT-IR spectra were found to be very different from the nanosecond pump/probe signal (see Figure 6.5), however, for **2a-2c** a temperature contribution to the transient spectra cannot be excluded (see Figure 7.6).

See Figure 7.5 and Table 7.1 for the time evolution of the thioxopeptides **2b** (black) and **2c** (red).

7.2 Tetrathioxopeptide without Hydrogen-Bond

7.2.1 Equilibrium conformations

Figure 7.7 (bottom) shows the FT-IR absorption spectrum of the thioxopeptide sequence Boc-Phe-Ile(=S)-Aib- Phe-OMe. The molecule has the four C=O oscillators, but only three bands are resolved. The redmost band contains the two amide I modes of Phe(1) and Aib, the 1740 cm^{-1} band is due to the ester C=O stretch, and only one band of the Boc protection group is seen at 1713 cm^{-1}. Multiple bands which could indicate the co-existence of open and hydrogen-bonded species are not resolved.

7.2.2 Photoisomerization

The dashed lines in Figure 7.7 show the FT-IR difference spectra of Z-Ile-ψ(SC-NH)-Aib-Gly-OMe **2c** (top) and Boc-Phe-Ile(=S)-Aib-Phe-OMe (bottom) after $\pi \rightarrow \pi^*$ excitation.

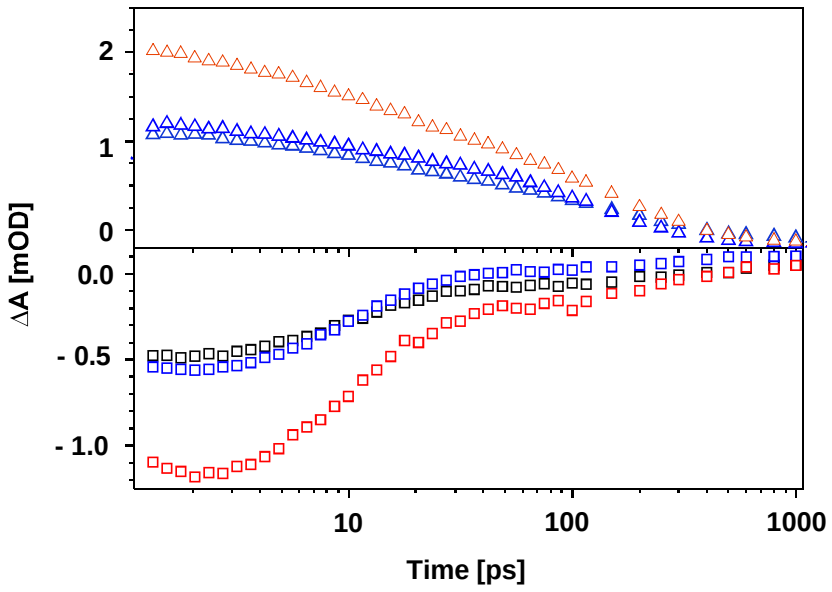

Figure 7.5: Time evolution of the C=O-stretch mode absorption of Aib (*i+2*, triangles) and of the amino acid at position *i+3* (squares) mode absorption after $\pi \rightarrow \pi^*$ excitation. The signal shows the difference absorption signal at 1658 cm^{-1} for the C=O-stretch mode absorption of Aib and at 1742 cm^{-1} resp. 1751 cm^{-1} for the C=O-stretch mode absorption of the amino acid at position *i+3* of thioxopeptide **2a** (black) and **2b** (blue) resp. **2c** (red).

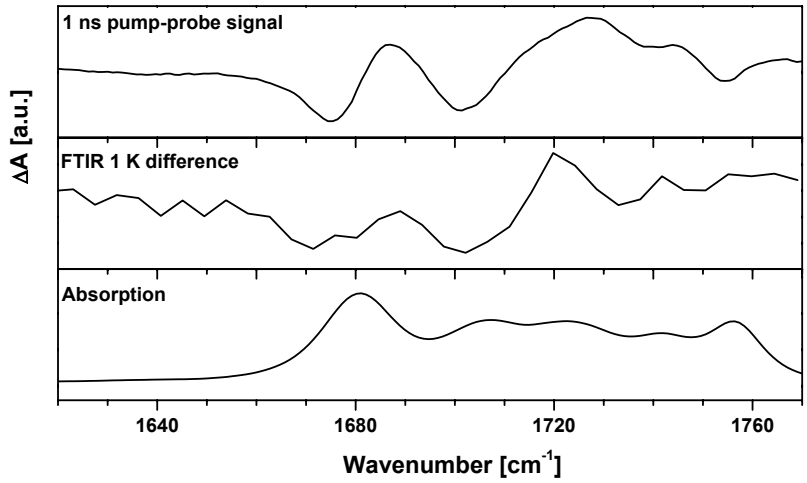

Figure 7.6: Comparison of absorption changes 1 ns after UV-excitation (top) and those induced by increasing the sample temperature from 21 to 22 °C in the FT-IR spectrometer (center) of thioxopeptide **2c**.

Despite the presence of a similar signal in the amide II region at 1520 cm^{-1}, which is evidence of successful isomerization, 248 nm irradiation of this peptide leads only to very weak absorption changes in the C=O stretch region.

Two $i \rightarrow i+3$ hydrogen-bonds between C=O of Boc and NH of Aib (the thioamide proton) and C=O of Phe(1) and NH of Phe(4) have been identified in the crystal structure of Boc-Phe-Ile(=S)- Aib-Phe-OMe [77]. In CD_3CN solution, however, no evidence is found for this 3_{10}-helical structure nor of any other hydrogen-bond for the latter molecule, given that the amide I FT-IR spectrum of the molecule is only weakly perturbed by the isomerization of the thioxopeptide bond. Thus, even in the presence of Aib and of a more strongly hydrogen-bond donating thioamide unit, the conformational preferences of these small peptides are very different and governed by their different sidechain interactions.

Another reason for the differences between the two tetrapeptides, in addition to that between crystal and solution structures, may be the conformation of the peptide bond between the Boc protection group and the first amino acid, which can adopt both the Z and the E forms. Crystalline Boc-l-phenylalanine, for example, is found in the E form, while the Z form typical of a regular peptide bond seems to dominate in solution [122,123].

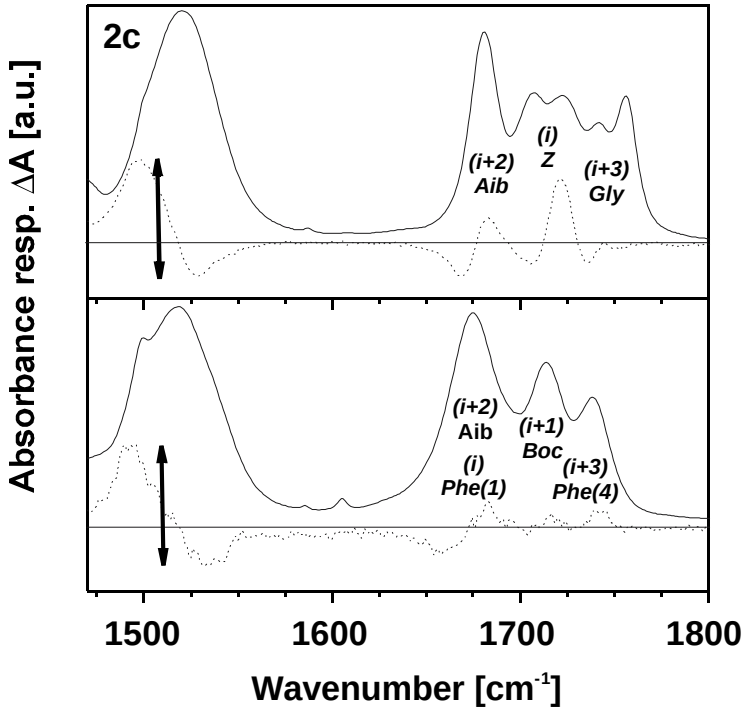

Figure 7.7: Solid lines: FT-IR spectra of thioxopeptide **2c** (top) and Boc-Phe-Ile-ψ(SC-NH)-Aib-Phe-OMe (bottom). Dashed lines: Difference FT-IR signal after $\pi \rightarrow \pi^*$ excitation of **2c** (top) and Boc-Phe-Ile-ψ(SC-NH)-Aib-Phe-OMe (bottom). The signal are scaled to have the same intensity in the amide II region (1500 - 1550 cm^{-1}).

7.3 Probable Relaxation Pathway after Excitation

The generalized reaction scheme in Figure 7.8 illustrates the different steps in the photoisomerization process common to all thioxopeptides. In the electronic ground state, where there is a significant barrier to (thermally activated) cis → trans isomerization, the thermodynamically stable trans conformation is re-established significantly faster (sub-second at room-temperature) in the molecules studied here than in non-Aib-containing thioxopeptides (several minutes [54]). Furthermore the isomerization times strongly decrease with the size of the residue of the thio-substituted amino acid at position *i+1* (with the rigid proline residue showing even shorter times than isoleucine). The conformational preference induced by the Aib residue and steric interaction between the side chain of the thio-substituted residue *i+1* and Aib thus seems to strongly destabilize the molecules in the cis conformation of the thioamide bond. The cis → trans relaxation times as a function of temperature, which have been reported for a series of thioxopeptides in ref. [54] suggest that entropic contributions to the barrier height, rather than enthalpic differences are primarily responsible for this destabilization. The cis → trans relaxation times also decrease with the thermodynamic stability of hydrogen-bonded conformations in the ground state of thioxopeptide **2a** - **2c**.

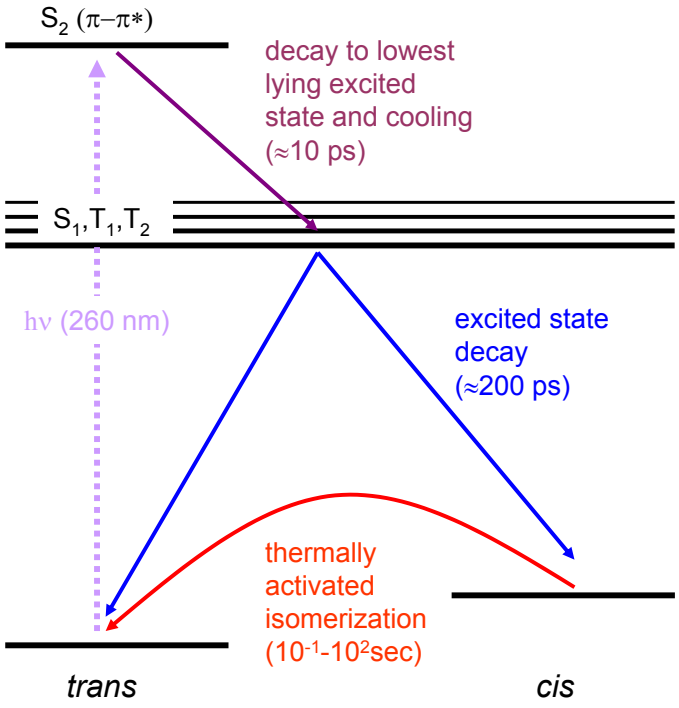

Figure 7.8: Schematic representation of the isomerization mechanism after $\pi \rightarrow \pi^*$ excitation and relaxation mechanism after isomerization in the thermal ground state of -Aib-containing thioxopeptides.

On the other hand very similar time constants for the photoisomerization reaction of the thioxopeptides containing the -(SC-NH)-Aib- moiety have been measured. The photoisomerization times are also in agreement with the excited state lifetimes of a variety of other thioxopeptides of different sizes and different amino acid residues next to the thioxopeptide unit [55]. In addition, in all thioxopeptides investigated so far quantum efficiencies of photoisomerization are significant (10-40%) and differ much less than the ground state isomerization time constants (although an accurate determination of quantum efficiencies is difficult, where the ground state relaxation is very fast). These observations call for some force driving trans $\rightarrow$ cis photoisomerization in apparent contradiction with *ab initio* excited state energy surfaces which are essentially flat along the torsional coordinate [108]. However, at the moment when a molecule relaxes back to the electronic ground state a strong driving force is predicted. The region in conformational space where the ground state is reached and from which the cis state can be formed via a driven motion [108] is apparently accessible via diffusive motion along a thioamide single bond in the excited state, without strong interference from side chains or the rest of the peptide backbone. The absence of a strong driving force in the excited state is also consistent with our observation of a relatively long-lived red-shift of the initially hydrogen-bonded Ala(1) C=O-stretch band. Its persistence indicates a relatively long lifetime of the $i \rightarrow i+3$ hydrogen-bond after photoexcitation, which would be highly unlikely in the case of a forced isomerization of the thioxopeptide unit on the excited state surface.

7.4 Conclusion

Transient infrared and difference FT-IR spectroscopy could be used to compare the $i \rightarrow i{+}3$ hydrogen-bond breaking of different -Aib-containing thioxopeptides. They show very similar isomerization dynamics, whereas the relaxation in the thermal ground state after isomerization differs significantly, strongly depending on the steric interaction of the side chain of the thio-substituted residue *i+1* and Aib.

Furthermore, it has been shown that Aib-containing peptides and thioxopeptides, which have increased hydrogen-bonding abilities because of the -SCNH- proton, do not automatically adopt a hydrogen-bonded conformation. The structure of these small peptides is most probably governed by their different sidechain interactions.

The current picture of the mechanism by which efficient photoisomerization is possible in a large number of monosubstituted thioxopeptides, involves a diffusive torsional motion about a thioamide single bond during the $\approx$ 200 ps lifetime of the lowest lying electronically excited state, followed by strongly driven motion in the electronic ground state. Further theoretical work is now needed in order to establish if a sufficiently large

region of conformational space can be sampled by the photo-excited peptides within 200 ps to reach the favorable conical intersections or intersystem crossing points, which, in the gas phase, have been predicted to lead to the cis photoproduct.

Chapter 8

Structural Information from Anisotropy Measurements

It is possible to obtain direct structural information from time-resolved pump/probe measurements, namely angles between transition dipole moments. Regarding the assumed structural rigidity caused by the Aib amino acid and the $i \rightarrow i{+}3$ hydrogen-bond, the structural parameters of the different thioxopeptides, obtained from the time-resolved measurements, are compared among each other and to the crystal structure of thioxopeptide Z-Ile-ψ(SC-NH)-Aib-Gly-OMe (**2c**).

8.1 Results

The angles between the transition dipole moments (between UV and IR and between different IR transition dipole moments) can be extracted from the anisotropy of the pump/probe data extrapolated to zero time delay, which is given by equation 2.6:

$$r(t) = \frac{\Delta A_{2D,\parallel,t} - \Delta A_{2D,\perp,t}}{\Delta A_{2D,\parallel,t} + 2\Delta A_{2D,\perp,t}},$$

where $\Delta A_{\parallel}$(t) stands for the signal recorded with parallel, $\Delta A_{\perp}$(t) for perpendicular polarization of the UV/IR-pump and IR-probe light. With equation 2.7:

$$\theta = \arccos\sqrt{\frac{5r(0)+1}{3}},$$

the corresponding angle can be calculated. In this chapter, measured anisotropies for the thioxopeptides Boc-Ala-Pro-ψ(SC-NH)-Aib-Ala-OMe (**1a**), Boc-Ala-ψ(O^{13}C-NH)-Pro-ψ(SC-NH)-Aib-Ala-OMe (**1b**), Z-Gly-ψ(SC-NH)-Aib-Ile-OMe (**2a**), Z-Ala-ψ(SC-NH)-Aib-Ile-OMe (**2c**) and Z-Ile-ψ(SC-NH)-Aib-Gly-OMe (**2c**) are shown and compared.

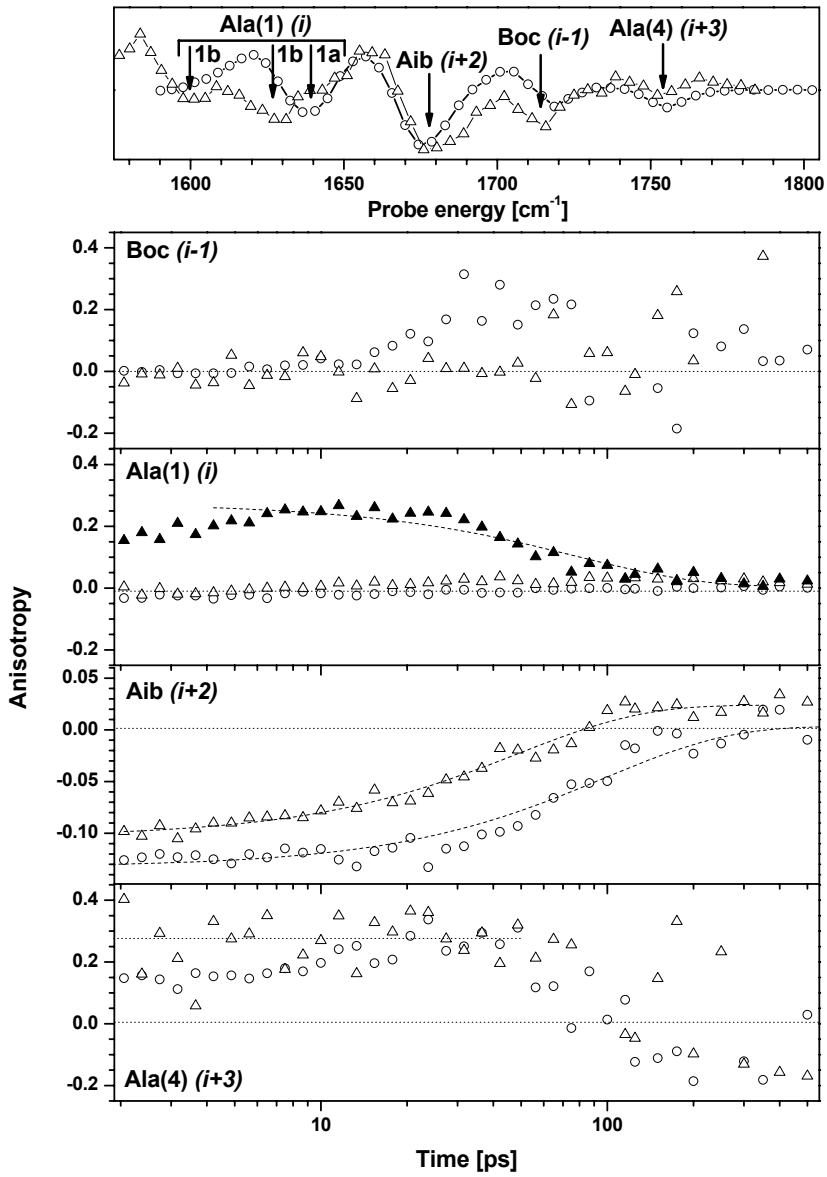

Figure 8.1: Top: Magic angle transient infrared difference absorption spectra of thioxopeptide **1a**(circles) and **1b** (triangles) after $\pi \rightarrow \pi^*$ excitation with 2 ps time delay between the UV-pump and IR-probe pulse. Bottom: Time evolution of the anisotropy for the different amide I bands between 2 and 500 ps of thioxopeptide **1a** (circles) and **1b** (triangles), revealed from the UV-pump/IR-probe measurements. The filled triangles are due to the non hydrogen-bonded Ala(1) band of thioxopeptide **1b** which is hidden under the Aib band in thioxopeptide **1a**. The corresponding anisotropy values are shown in Table 8.1.

The transition absorption changes of the thioxopeptides **1a** and **1b** recorded with parallel (black) and perpendicular (blue) polarization between the UV-pump and the IR-probe pulse are shown in Figure 6.1 and 6.2. It can be seen that at spectral positions of

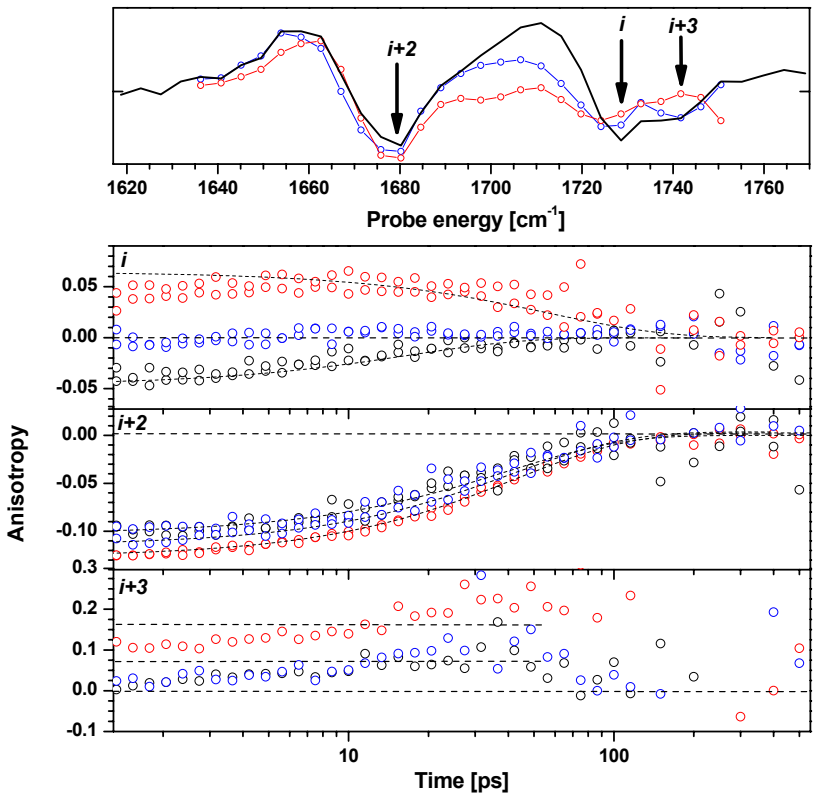

Figure 8.2: Top: Magic angle transient infrared difference absorption spectra of thioxopeptide **2a** (black), **2b** (blue) and **2c** (red) after $\pi \rightarrow \pi^*$ excitation with 2 ps time delay between the UV-pump and IR-probe pulse. Bottom: Time evolution of the anisotropy for the different amide I bands between 1 and 500 ps of thioxopeptide **2a** (black), **2b** (blue) and **2c** (red), revealed from the UV-pump/IR-probe measurements. The corresponding anisotropy values are shown in Table 8.1.

the amide I bands the intensities of the negative and positive bands differ with different polarizations. They vanish when increasing the time delay between the UV-pump and IR-probe pulse (see Figure 6.1 and 6.2). The time evolution of this anisotropy is illustrated in Figure 8.1 for the different vibrational bands (**1a**: circles, **1b**: triangles). Looking at one specific band (Aib of thioxopeptide **1a**, the anisotropy is at $\sim$ -0.13 for short time delays and then decays exponentially with a time constant of 60 - 70 ps to zero due to rotational diffusion. In thioxopeptide **1b** the non hydrogen-bonded Ala(1) band (*i*, filled triangles in Figure 2.6) is resolved which is not the case in thioxopeptide **1a** (hidden under the Aib band). The anisotropy offset of the Aib band in **1a** compared to the anisotropy time trace of **1b** is most probably due to this overlapping. The values which can be determined by extrapolating to time delay zero are summarized in Table 8.1.

Figure 8.2 shows the time evolution of the anisotropy of the thioxopeptides **2a** to **2c** for the different vibrational bands (**2a**: black, **2b**: blue, **2c**: red). The values are

calculated according the same way as for the thioxopeptides **1a/b**. The values which can be determined by extrapolating to time delay zero are summarized in Table 8.1.

Thioxopeptide		**1a**[a]	**1b**[a]	**2a**[a]	**2b**[a]	**2c**[a]	**2c**[b]
Anisotropy	*i-1*	0.00	0.00	n/a	n/a	n/a	n/a
	i	-0.02	-0.02,0.25[c]	-0.04	0.00	0.06	-0.06
	i+2 (Aib)	-0.14	-0.13	-0.10	-0.12	-0.13	-0.12
	i+3	0.27	0.27	0.08	0.08	0.16[d]	0.35
Angle	*i-1*	55/125	55/125	n/a	n/a	n/a	n/a
	i	123	123,30/150[c]	121	125	131	119
	i+2 (Aib)	71	70	66	69	70	68
	i+3	28/152	28/152	47/133	47/133	39/141[d]	163

Table 8.1: Anisotropy and angle between UV- and IR-transition dipole moments of the thioxopeptide **1a**, **1b** and **2a** - **2c**. n/a: Does not exist. *a*: Determined by time-resolved measurements. *b*: Calculated from crystal structure [77]. *c*: Hydrogen-bonded (at 1600 cm^{-1}) and non hydrogen-bonded (at 1623 cm^{-1}) band. *d*: Band at 1756 cm^{-1}.

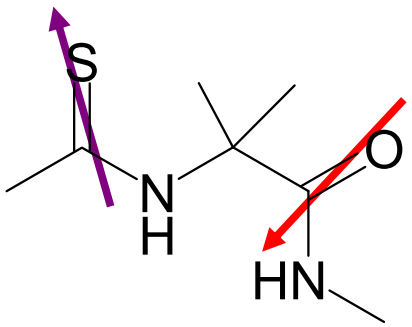

Figure 8.3: Schematic representation of the -ψ(SC-NH)-Aib- moiety common to all four thioxopeptides. Arrows indicate the orientation of the electronic $\pi - \pi^*$ and vibrational amide I transition dipole moments.

The measured anisotropies for Aib (*i+2*) are very similar (-0.10 to -0.14) for the different thioxopeptides, whereas the ones for the amino acid at position *i+3* scatter more strongly (0.08 to 0.27). The distribution of the anisotropies for amino acid *i* is between -0.04 to 0.06. This could indicate that the structure of all four thioxopeptides is at least partially restricted due to $i \rightarrow i+3$ hydrogen-bonding between amino acid *i* and *i+3*. Amide I transition dipole moments are known to be well localized, and can be approximated by a point dipole in the plane of a peptide unit forming an angle of 20° with respect to the C=O bond [93, 124]. The UV transition dipole moment of the

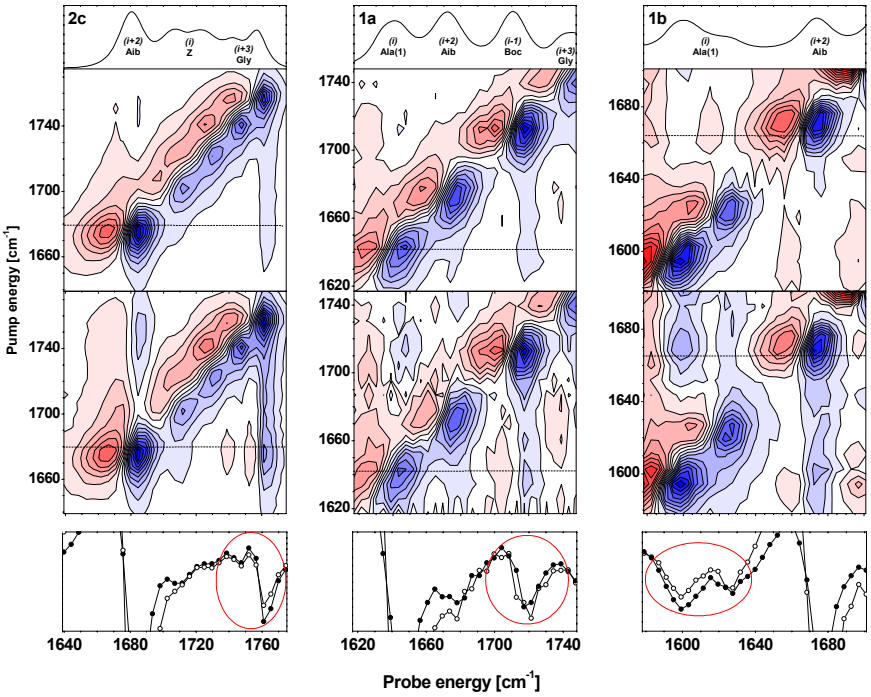

Figure 8.4: 2D-IR spectra with parallel (top) and perpendicular (middle) polarization and 4 ps time delay between the IR-pump and IR-probe pulse for thioxopeptide **2c**, **1a** and **1b**. Bottom: Cuts taken at IR-pump energies of 1665, 1640 and 1680 cm^{-1} for thioxopeptide **2c**, **1a** and **1b** respectively (indicated dashed lines in the 2D-IR spectra. The corresponding anisotropy values are shown in Table 8.2.

Thioxopeptide		**1a**[a]	**1b**[a]	**2c**[a]	**2c**[b]
Anisotropy	*i-1/i*	0.10	–	n/a	n/a
	i/i+2 (Aib)	–	-0.09,0.06[c]	–	-0.20
	i/i+3	-0.08	–	–	-0.16
	i+2 (Aib)*/i+3*	–	0.07	-0.02,-0.11[d]	-0.16
Angle	*i-1/i*	45/135	–	n/a	n/a
	i/i+2 (Aib)	–	65,48/132[c]	–	85
	i/i+3	63/117	–	–	75
	i+2 (Aib)*/i+3*	–	48/132	57/123,67/113[d]	105

Table 8.2: Anisotropy and angle values between IR transition dipole moments of the thioxopeptides **1a**, **1b** and **2a** - **2c**. n/a: Does not exist. –: Could not be determined because of spectral overlap. *a*: Determined by the time-resolved measurements. *b*: Calculated from crystal structure [77]. *c*: Hydrogen-bonded (at 1600 cm^{-1}) and non hydrogen-bonded (at 1623 cm^{-1}) band. *d*: Left (1740 cm^{-1}) and right (1756 cm^{-1}) band.

thioxopeptide unit can be approximated by the one determined for NMTAA in connection with the *ab initio* calculations reported in ref. [108]. This transition dipole, too, lies in the

(thio-)peptide plane at an angle of 16° with respect to the C=S bond (≈ 40° with respect to the N-C bond [125], see Figure 8.3). The measured anisotropies for thioxopeptide **2c** in solution are similar to those expected from the crystal structure [77] (last column in Table 8.1). The good agreement for Aib suggests a conserved and very rigid -(SC-NH)-Aib- core structure. The differences for the amino acid at position *i+3* point to greater flexibility of the terminal group or to a poor representation of the ester transition dipole moment by the amide I mode of a peptide unit. Nevertheless, it is apparent from the comparison of the anisotropy data for the four molecules that the tails of the thioxopeptides are more flexible than their inner part.

Anisotropy and corresponding angles between pairs of IR transition dipole moments can be obtained in the same way. Figure 8.4 (top) shows the 2D-IR spectra of the thioxopeptides **1a**, **1b** and **2c** with parallel and perpendicular polarization between the IR-pump and IR-probe pulse with a time delay of 4 ps between them. To show the difference of the signal intensities more clearly, cuts at at the pump energy of 1640 cm^{-1}, 1665 cm^{-1} and 1680 cm^{-1} are shown at the bottom in Figure 8.4 for thioxopeptide **1a**, **1b** and **2c** respectively. The corresponding anisotropy values are shown in Table 8.2. Most angles can not be determined because of strong overlap of different infrared bands.

Angles, which were determined, typically include a transition dipole moment of a moiety which is in the flexible part of the thioxopeptide (*i* and *i+3*), as shown by the UV-pump/IR-probe measurements. The only exception is the angle between the Ala(1) (*i*) and the Aib (*i+2*) residues in thioxopeptide **1b**. An angle of 65° was observed consistent with a β-turn structure [126].

8.2 Conclusion

Angles between transitions dipole moments can be measured by using polarization-dependent time-resolve pump/probe spectroscopy. The most rigid structure is found between moieties adjacent to the Aib amino acid, which is known to define peptide geometry with little margin. Additionally, the structural flexibility could be restricted to a certain extent due to $i \rightarrow i+3$ hydrogen-bonding, while the tails of the thioxopeptides are very flexible.

Chapter 9

Extension to Transient 2D-IR Measurements

Boc-Ala-Pro-ψ(SC-NH)-Aib-Ala-OMe is small, forming a secondary structure and has well-resolved bands in the infrared amide I region. Thus it is an ideal 'model' molecule to test the capability of transient 2D-IR spectroscopy to investigate peptide dynamics respectively to determine structural parameters during a conformational change. The measurements and following computer simulations only treat the Ala(1) and Aib amide I bands whose amide moieties are involved in the $i \rightarrow i{+}3$ hydrogen-bond in the β-turn and are therefore sensitive to its breaking (simulations are performed with Gaussian '03 calculations on a MeCO-Pro-ψ(SC-NH)-Aib-NHMe moiety).

9.1 2D-IR Spectra

Figure 9.1 (left) shows the measured 2D-IR spectra of Boc-Ala-Pro-ψ(SC-NH)-Aib-Ala-OMe (**1a**) with perpendicular ($\perp$) and parallel ($\parallel$) polarization and 1.2 ps time delay between the IR-pump and IR-probe pulse. Because the diagonal and cross-peak intensities depend differently on polarization, the weighted difference[1] between these two spectra in Figure 9.1 (right) suppresses the diagonal peaks and, ideally, the spectrum only shows the cross peaks [18]. A pair of cross-peaks is found for the hydrogen-bonded Ala(1) band and the Aib band (circled in Figure 9.1). This coupling indicates a spatial proximity which is in line with the presence of a $i \rightarrow i{+}3$ hydrogen-bonded conformation.

The same shape can be seen for Boc-Ala-ψ(O^{13}C-NH)-Pro-ψ(SC-NH)-Aib-Ala-OMe (**1b**) in Figure 9.2 (the difference spectrum is again obtained by subtracting the parallel from the perpendicular spectrum, multiplied by 2.75).

[1] Theoretically: 3$\times$ $\perp$ - $\parallel$, but here: 2.75$\times$ $\perp$ - $\parallel$ due to experimental inaccuracy.

This coupling is expected to change when the $i \rightarrow i{+}3$ hydrogen-bond is broken in the thioxopeptide. Transient 2D-IR spectroscopy should show a signal in the off-diagonal peak area (the spectrum is a difference spectrum between the 2D-IR spectrum after triggering the photoswitch and the one without triggering) after the photoswitch is triggered and the isomerization has taken place. Because the amide I bands are well resolved for this thioxopeptide, overlap of different signals are minimized.

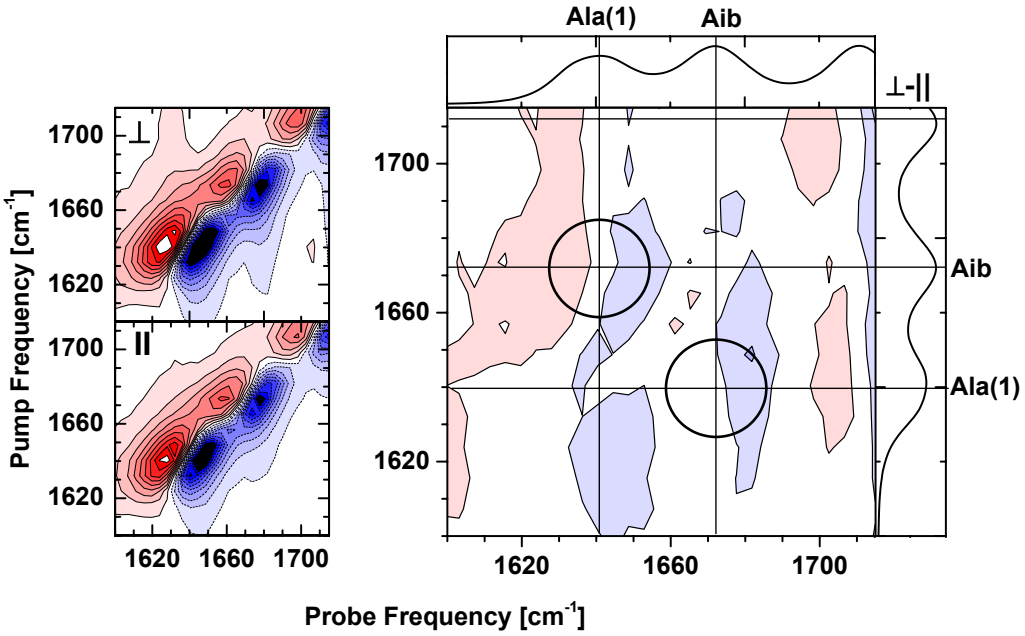

Figure 9.1: 2D-IR spectra with perpendicular (top left) and parallel (bottom left) polarization and 1.2 ps time delay between the IR-pump and IR-probe pulse of thioxopeptide **1a**. Right: Difference spectrum of the 2D-IR spectra with perpendicular and parallel polarization (3× ⊥ - ‖) to eliminate diagonal peaks. Coupling between the hydrogen-bonded Ala(1) and Aib band is circled.

9.2 Transient 2D-IR Spectra

In Figure 9.3 (c) and (d) transient 2D-IR spectra with 3 ps and 1 ns time delay respectively between the UV-pump pulse and the IR-pump pulse and 1.2 ps delay time between the IR-pump pulse and the IR-pump are shown. The polarization between the two IR-pulses is parallel[2]. The bands are better resolved the longer the time delay between the UV-pump

[2]The polarization between the UV-pump and the IR-pulses has no influence on the spectra with delay times bigger than 100 ps due to rotational diffusion which happens on a timescale of 60 to 70 ps.

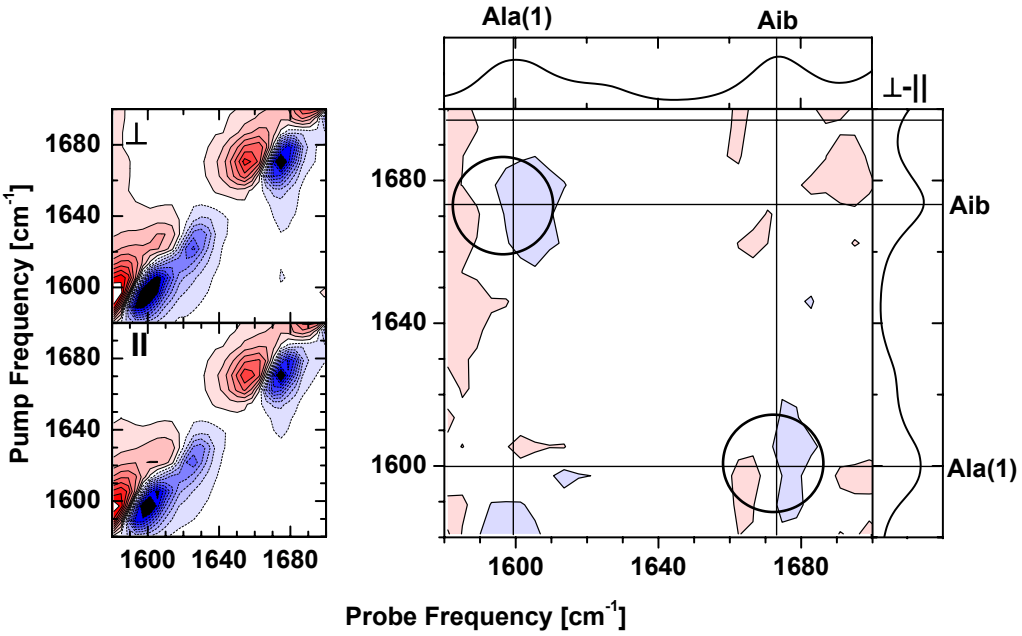

Figure 9.2: 2D-IR spectra with perpendicular (top left) and parallel (bottom left) polarization and 1.2 ps time delay between the IR-pump and IR-probe pulse of thioxopeptide **1b**. Right: Difference spectrum of the 2D-IR spectra with perpendicular and parallel polarization (3× ⊥ - ‖) to eliminate diagonal peaks. Coupling between the hydrogen-bonded Ala(1) and Aib band is circled.

and the IR pulses.

To look at the spectra in more detail, cuts are taken at different IR-pump frequencies. The cuts can be seen in Figure 9.4 (d) and (f) for the 1 ns time delay between the UV-pump and IR-pump pulse. The corresponding cuts for the equilibrium 2D-IR spectrum are shown in Figure 9.4 (c) and (e).

Figure 9.4 (f), which correspond to excitation of the Aib band, indicate a change in cross peak intensity at 1640 cm^{-1} (position of the hydrogen-bonded Ala(1) band, indicated with an arrow). This is expected to happen when the $i \rightarrow i{+}3$ hydrogen-bond of the thioxopeptide breaks upon photoisomerization. However, the cross peak should be the most intense at the IR-pump pulse position where the diagonal peak (the pumped peak) is strongest, namely at the pump energy = 1674.2 cm^{-1} (green curve in Figure 9.4 f). This is not the case, moreover, the most evident change of cross peak intensity seems to appear when pumping at 1657.5 cm^{-1}, which is closer to the spectral position of the hydrogen-bonded Ala(1) band. Thus, it is not clear if there is a change in cross peak intensity associated with $i \rightarrow i{+}3$ hydrogen-bond breaking or simply from direct excitation of the

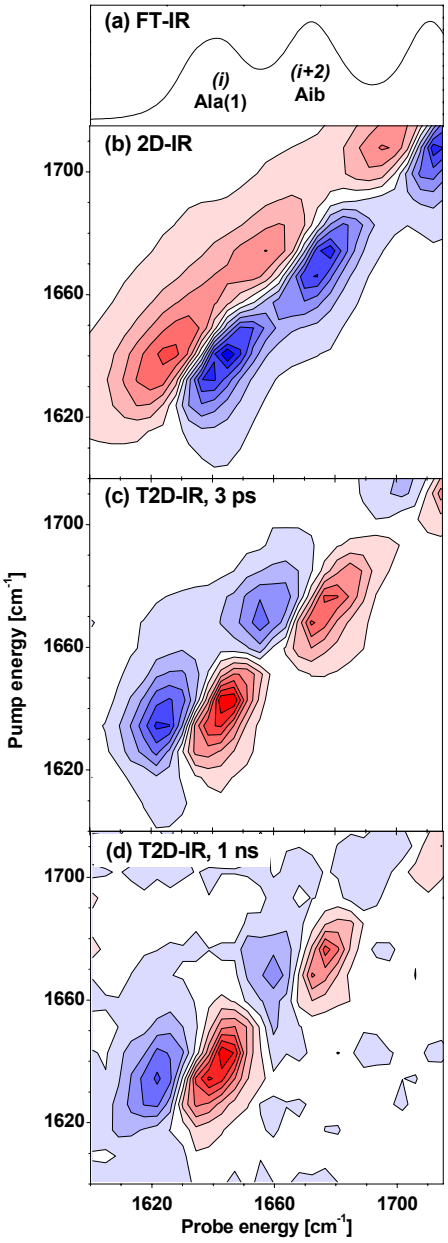

Figure 9.3: (a): FT-IR absorption spectrum at 293 K. (b): 2D-IR spectrum with 1.2 ps time delay and parallel polarization between the IR-pump and the IR-probe pulse. Contour intervals are 0.48 mOD. (c): Transient 2D-IR spectrum with 3 ps time delay and perpendicular polarization between the UV-pump and the IR-pump pulse and 1.2 ps time delay and parallel polarization between the IR-pump and the IR-probe pulse. Contour intervals are 17 μOD. (c): Transient 2D-IR spectrum with 1 ns time delay and perpendicular polarization between the UV-pump and the IR-pump pulse and 1.2 ps time delay and parallel polarization between the IR-pump and the IR-probe pulse. Contour intervals are 6 μOD.

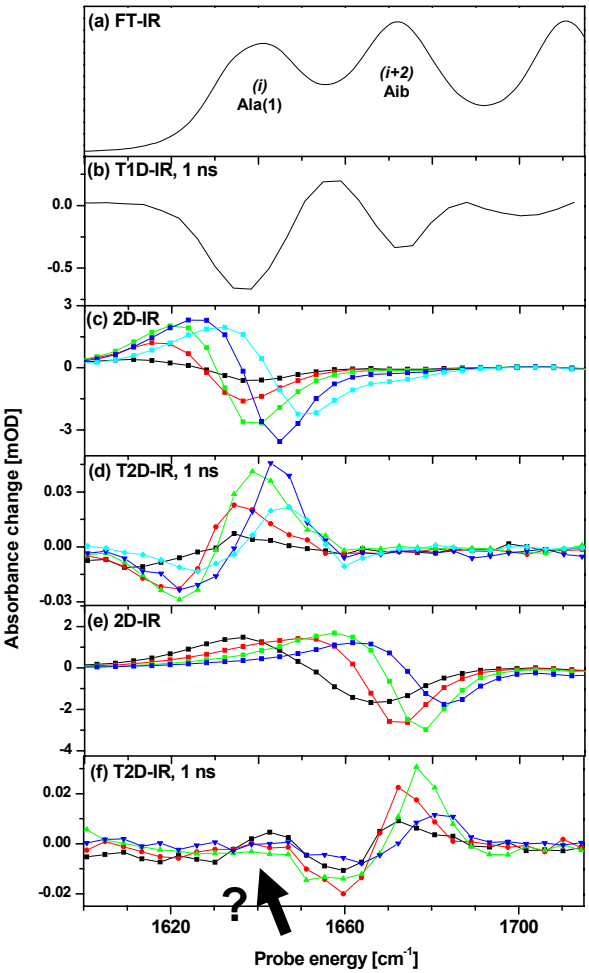

Figure 9.4: (a): FT-IR absorption spectrum at 293 K. (b): T1D-IR spectrum at 1 ns time delay between the UV-pump and the IR-pump pulse. (c): 2D-IR cuts at 1617.6 (black), 1626.0 (red), 1634.4 (green), 1642.8 (dark blue), 1651.2 (light blue) cm^{-1} with 1.2 ps time delay and parallel polarization between the IR-pump and IR-probe pulse. (d): Transient 2D-IR cuts at 1617.6 (black), 1626.0 (red), 1634.4 (green), 1642.8 (dark blue), 1651.2 (light blue) cm^{-1} with 1ns time delay and perpendicular polarization between the UV-pump and the IR-pump pulse and 1.2 ps time delay and parallel polarization between the IR-pump and the IR-probe pulse. (e): 2D-IR cuts at 1657.5 (black), 1665.9 (red), 1674.2 (green) and 1682.6 (dark blue) cm^{-1} with 1.2 ps time delay and parallel polarization between the IR-pump and the IR-probe pulse. (f): Transient 2D-IR cuts at 1657.5 (black), 1665.9 (red), 1674.2 (green) and 1682.6 (dark blue) cm^{-1} with 1 ns time delay and perpendicular polarization between the UV-pump and the IR-pump pulse and 1.2 ps time delay and parallel polarization between the IR-pump and the IR-probe pulse.

hydrogen-bonded Ala(1) band by the tail of the IR-pump pulse. For this reason, computer simulations of these two bands and their coupling before and after photoisomerization are performed.

9.3 Computer Simulations

Computer simulations of 2D-IR and transient 2D-IR spectra of the thioxopeptides **1a** and **1b** are performed by using the exciton model as described in chapter 2 (equation 2.2) [127]. The localized C=O stretch vibrators of Ala(1) and Aib are used as abscise, yielding the Hamiltonian:

$$H = \begin{pmatrix} 0 & & & & & \\ & \varepsilon_1 & \beta_{12} & & & \\ & \beta_{12} & \varepsilon_2 & & & \\ & & & 2\varepsilon_1 - \Delta & 0 & \sqrt{2}\beta_{12} \\ & & & 0 & 2\varepsilon_2 - \Delta & \sqrt{2}\beta_{12} \\ & & & \sqrt{2}\beta_{12} & \sqrt{2}\beta_{12} & \varepsilon_1 + \varepsilon_2 \end{pmatrix}.$$

Site energies ε_i are chosen randomly from a Gaussian distribution, representing the inhomogeneous width of the transitions (inhomogeneous and homogeneous broadening are treated separately because distinct timescales are assumed). The diagonalized matrix yields the energies E_i in the exciton basis. The transition dipole matrix in the site basis ($\overrightarrow{\mu}_i$ represent the localized transition dipole moments oriented 20 ° with respect to the C=O bond, see Figure 8.3):

$$H = \begin{pmatrix} 0 & \overrightarrow{\mu}_1 & \overrightarrow{\mu}_2 & 0 & 0 & 0 \\ \overrightarrow{\mu}_1 & 0 & 0 & \sqrt{2}\overrightarrow{\mu}_1 & 0 & \overrightarrow{\mu}_2 \\ \overrightarrow{\mu}_2 & 0 & 0 & 0 & \sqrt{2}\overrightarrow{\mu}_2 & \overrightarrow{\mu}_1 \\ 0 & \sqrt{2}\overrightarrow{\mu}_1 & 0 & 0 & 0 & 0 \\ 0 & 0 & \sqrt{2}\overrightarrow{\mu}_2 & 0 & 0 & 0 \\ 0 & \overrightarrow{\mu}_2 & \overrightarrow{\mu}_1 & 0 & 0 & 0 \end{pmatrix} \tag{9.1}$$

is equally transformed to the exciton basis, yielding the strength of bleach, stimulated emission and excited state absorption in the 2D-IR spectrum. The width of each transition is given by the homogeneous width along the probe axis and by the convolution of the homogeneous and the IR-pump width along the pump axis [128]. The single homogeneously broadened 2D-IR spectra then are added to get the full 2D-IR spectrum of the inhomogeneous distribution.

The simulations consider only the Ala(1) and Aib amide I bands, because they are the two acting as the proton acceptor and proton donor in the $i \rightarrow i{+}3$ hydrogen-bond respectively.

To simulate the (transient) 2D-IR spectra different parameters have to be determined: the IR-pump pulse width ω_{pump}, the homogeneous width ω_{hom}, the spectral positions of the bands E_i, their inhomogeneous widths ω_i, the relative transitions dipole strengths

$|\ \vec{\mu}_i\ |$, the ratio τ of the hydrogen-bonded and non hydrogen-bonded species in the thermal ground state, the coupling strength β and the angle θ between the two transition dipole moments of the two amide I bands. These parameters are approximately defined by FT-IR absorption spectra, UV-pump/IR-probe and anisotropy measurements, *ab initio* calculations and refined by fitting the 2D-IR spectrum of thioxopeptide **1b**(determined iteratively)[3]. The final parameters are summarized in Table 9.1 (for detailed information about the parameter determination see appendix A).

	1b	**1a**
IR-pump pulse width (ω_{pump}) [cm^{-1}]	10	
Homogeneous width (ω_{hom}) [cm^{-1}]	10	
Spectral position, Ala(1), bonded ($E_{Ala,bonded}$) [cm^{-1}]	1602	1642
Spectral position, Ala(1), non bonded ($E_{Ala,nonbonded}$) [cm^{-1}]	1626	1666^a
Spectral position, Aib (E_{Aib}) [cm^{-1}]	1675	
Inhomogeneous width, Ala(1), bonded ($\omega_{Ala,bonded}$) [cm^{-1}]	24.0	
Inhomogeneous width, Ala(1), non bonded ($\omega_{Ala,nonbonded}$) [cm^{-1}]	26.0	
Inhomogeneous width, Aib (ω_{Aib}) [cm^{-1}]	16.5	
Transition dipole strength ($\mu_{Ala,nonbonded}$; $\mu_{Aib,bonded}$; $\mu_{Aib,nonbonded}$) [D]	1.0^a	
Transition dipole strength ($\mu_{Ala,bonded}$) [D]	1.24^a	
Coupling (β) [cm^{-1}]	-6	
Coupling (β_{nb}) [cm^{-1}]	0	
Angle between transition dipole moments (θ) [°]	70	
Ratio hydrogen-bonded:non hydrogen-bonded (τ)	5:4	

Table 9.1: Parameters determined for the simulation of the (transient) 2D-IR spectra. ^{a}: $E_{Ala,bonded,\mathbf{1a}}$+($E_{Ala,nonbonded,\mathbf{1b}}$-$E_{Ala,bonded,\mathbf{1b}}$). ^{b}: Normalized to 1.

9.3.1 Simulated 2D-IR spectra

To achieve the full 2D-IR spectrum, the 2D-IR spectra of the non hydrogen- and hydrogen-bonded species have to be simulated separately and then added with a weighting factor (relative amount of the two different species before isomerization). Spectra for the non hydrogen-bonded species are simulated with the Ala(1) band at 1626 cm^{-1} (**1b**) and 1666 cm^{-1} (**1a**), assuming that the coupling β_{nb} is 0 (see appendix A for details), while for the spectra with hydrogen-bonded species the Ala(1) band at 1602 cm^{-1} (**1b**) and 1642 cm^{-1} (**1a**) is used. In both spectra, the same Aib band position is used as the second amide I band (proton donor).

Figure 9.5 shows the experimental (a) and simulated (b) 2D-IR spectrum of thioxopeptide **1b** with the parameters of Table 9.1. For comparison, cuts are taken at different IR-pump positions (see Figure 9.5, c and d).

[3]Thioxopeptide **1b** is chosen because the Ala(1) and Aib bands are well resolved.

The same parameters (except the spectral positions of the bands) are used to simulate the 2D-IR spectrum of thioxopeptide **1a**. The same spectral difference between the non hydrogen-bonded and the hydrogen-bonded Ala(1) band is used as found in thioxopeptide **1b** (24 cm^{-1}) and both are shifted by 40 cm^{-1} (isotope shift). The simulated (a) and experimental (b) 2D-IR spectrum of thioxopeptide **1a** is shown in Figure 9.6. For comparison, cuts are taken at different IR-pump positions (see Figure 9.6 c).

In both cases good agreement between the simulated and experimental 2D-IR spectra is found. Therefore, the determined parameters are adopted for the simulations of the transient 2D-IR spectra.

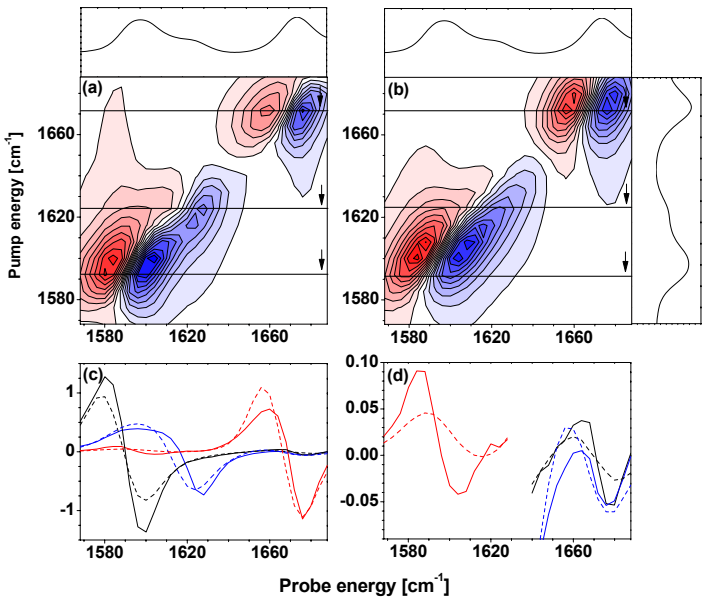

Figure 9.5: Top: Experimental (a) and simulated (b) 2D-IR spectrum with perpendicular polarization and 1.2 ps time delay between the IR-pump and IR-probe pulse of thioxopeptide **1b**. Bottom: Cuts taken at IR-pump pulse frequencies of 1593 (black), 1624 (blue) and 1672 cm^{-1} (red) in the experimental (solid lines) and simulated (dashed lines) 2D-IR spectrum. Graph (d) is scaled up to resolve the cross peaks.

9.3.2 Simulated long-time transient 2D-IR spectra

Long-time transient 2D-IR spectra (1 ns time delay, isomerization and $i \rightarrow i+3$ hydrogen-bond breaking is completed) are difference spectra obtained by subtracting the unperturbed 2D-IR spectrum from the 2D-IR spectrum taken after a certain time delay after triggering the photoswitch. Thus, molecules which have the same spectrum before and after the trigger (i.e. the non hydrogen-bonded molecules) do not contribute. Therefore, the 2D-IR spectrum of the hydrogen-bonded species (state before isomerization) are subtracted from the 2D-IR spectrum of the non hydrogen-bonded species (state after

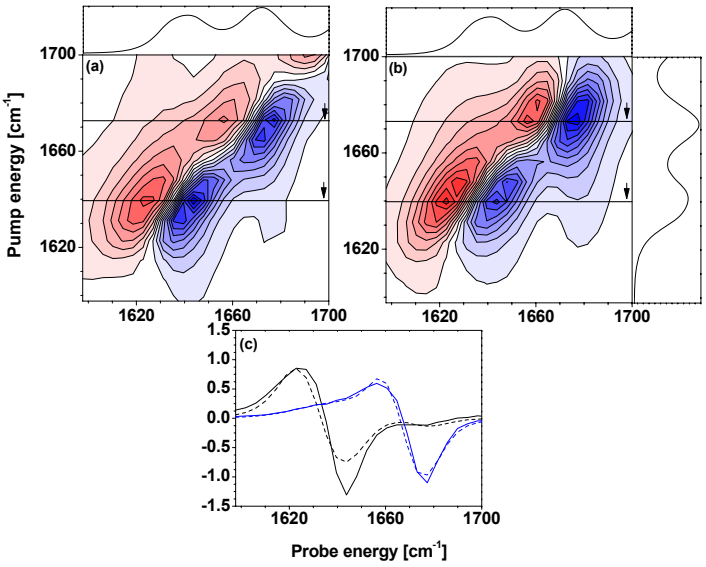

Figure 9.6: Top: Experimental (a) and simulated (b) 2D-IR spectrum with perpendicular polarization and 1.2 ps time delay between the IR-pump and IR-probe pulse of thioxopeptide **1a**. (c): Cuts taken at IR-pump pulse frequencies of 1640 (black) and 1673 cm^{-1} (blue) in the experimental (solid lines) and simulated (dashed lines) 2D-IR spectrum.

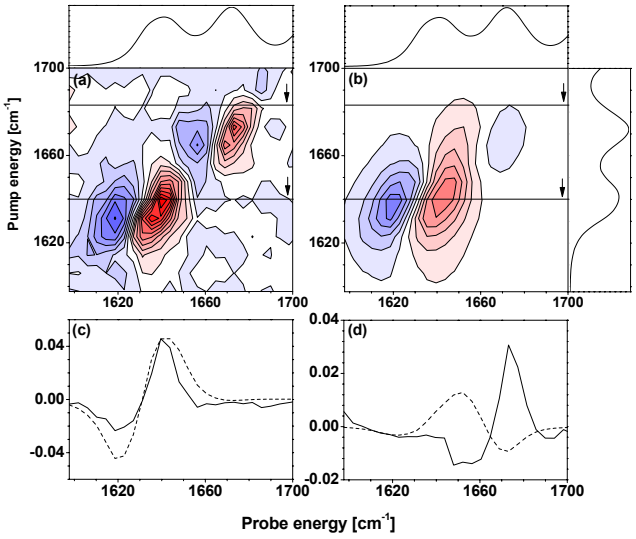

Figure 9.7: Top: Experimental (a) and simulated (b) transient 2D-IR spectrum with parallel polarization and 1.2 ps time delay between the IR-pump and IR-probe pulse and with perpendicular polarization and 1 ns time delay between the UV-pump and IR-pump pulse of thioxopeptide **1a**. Bottom: Cuts taken at IR-pump pulse frequencies of 1640 (c) and 1673 cm^{-1} (d) in the experimental (solid lines) and simulated (dashed lines) transient 2D-IR spectrum.

isomerization).

The simulated transient 2D-IR spectrum of thioxopeptide **1a** (assuming equal weight of the initial and final state) is shown in Figure 9.7 (b). The simulated and experimental spectra fit well in the spectral area of the Ala(1) band, while they differ significantly in the Aib region (see Figure 9.7, c and d). This could imply that the relative transition dipole strengths of the hydrogen-bonded and non hydrogen-bonded Aib bands (which overlap strongly) differ significantly (until now the parameters are set as $\mu_{Aib,bonded} = \mu_{Aib,nonbonded}$). Therefore, the parameters $\mu_{Aib,bonded}$ and $\mu_{Aib,nonbonded}$ are adjusted such that the Aib diagonal signal of the simulated and the experimental spectra fit with good agreement. The determined values then are $\mu_{Aib,bonded} = 1.3$ and $\mu_{Aib,nonbonded} = 1.0$ (see Figure 9.8 c for transient 2D-IR spectrum).

To investigate the origin of the observed cross peak due to the Ala(1) band in the long-time (1 ns time delay) transient 2D-IR spectrum of thioxopeptide **1a** after pumping the Aib band (see Figure 9.4 f), the coupling properties of the initial (no UV irradiation, hydrogen-bonded species) and the final (UV-irradiation followed by the 1 ns time delayed 2D-IR pulses, non hydrogen-bonded species) spectrum are varied. Following assumptions are considered:

- coupling (-6 cm^{-1}) in the initial state and no coupling in the final state (Figure 9.8 c),

- coupling (-6 cm^{-1}) in the initial state and coupling (-6 cm^{-1}) in the final state (Figure 9.8 d),

- No coupling in the initial state and no coupling in the final state (Figure 9.8 b), where no change of coupling should appear.

Figure 9.8 (b)-(d) show the simulated transient 2D-IR spectra for the different situations mentioned above which seem to fit well to the experimental spectrum (see 9.8 a). For better comparison, cuts are taken at different IR-pump frequencies. The dashed blue lines in Figure 9.8 e and f show the case for no coupling in the initial state and coupling in the final state (-6 cm^{-1}) as it has been assumed for the simulations of the 2D-IR spectra. They show good agreement with the experimental cuts (9.8) as well. The off-diagonal peak (at the Ala(1) position when pumping the Aib band) which already has been found in the experimental spectrum appears as well in the simulated spectrum. Comparing these cuts to the dashed red lines in Figure 9.8 (e) and (f) which are due to the case of the same coupling in the initial and the final state (-6 cm^{-1}), only little difference is obtained. Nevertheless, one would expect to see no change of the cross peak intensity in the situation with no coupling in the initial and the final state because there is no cross peak neither for the initial nor for the final state (see chapter 2). But the cuts of the simulated transient 2D-IR spectrum still show an off-diagonal peak at the amide I position of Ala(1) when pumping the Aib band (see Figure 9.8 f, dashed black line). The peak found in this case

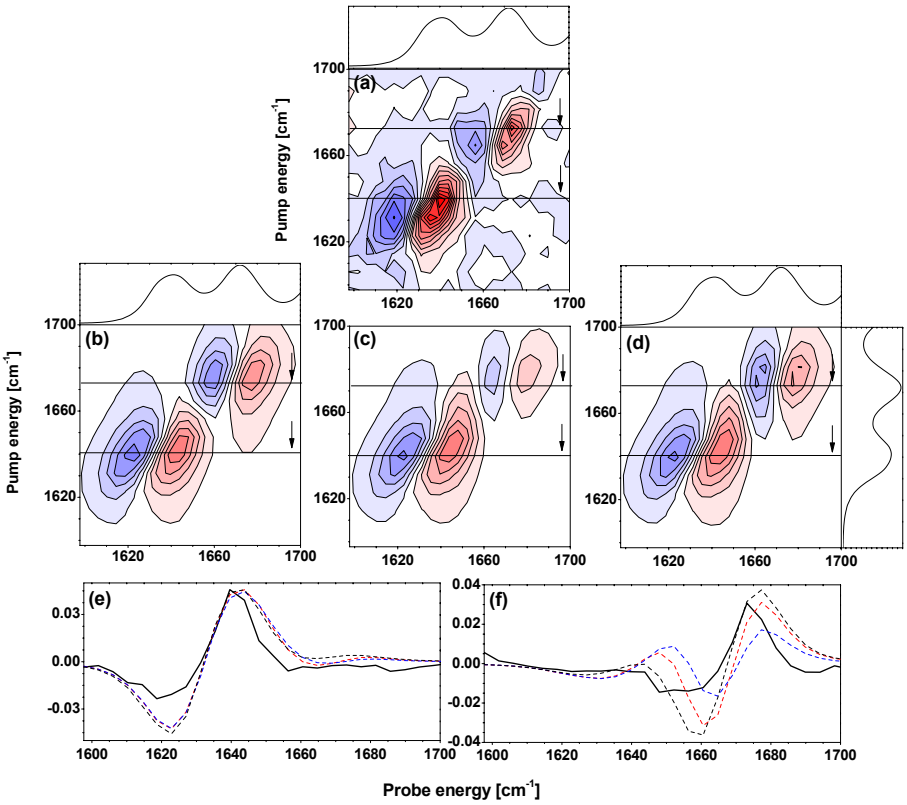

Figure 9.8: (a): Experimental transient 2D-IR spectrum with parallel polarization and 1.2 ps time delay between the IR-pump and IR-probe pulse and with perpendicular polarization and 1 ns time delay between the UV-pump and IR-pump pulse of thioxopeptide **1a**. Middle: Simulated transient 2D-IR spectrum with parallel polarization and 1.2 ps time delay between the IR-pump and IR-probe pulse and with perpendicular polarization and 1 ns time delay between the UV-pump and IR-pump pulse of thioxopeptide **1a** with (b) no coupling in the initial state and no coupling in the final state, (c) coupling (-6 cm^{-1}) in the initial state and no coupling in the final state and (d) coupling (-6 cm^{-1}) in the initial state and coupling (-6 cm^{-1}) in the final state. Bottom: Cuts taken at IR-pump pulse frequencies of 1640 (e) and 1673 cm^{-1} (f) in the experimental (solid black lines) and simulated (dashed lines) transient 2D-IR spectrum with (black) no coupling in the initial state and no coupling in the final state, (blue) coupling (-6 cm^{-1}) in the initial state and no coupling in the final state and (red) coupling (-6 cm^{-1}) in the initial state and coupling (-6 cm^{-1}) in the final state.

has its origin most probably in the direct excitation of the non hydrogen-bonded Ala(1) band with the IR-pump pulse. Thus, it can not be proofed if the supposed change of cross peak intensity of the Ala(1) band, which is found in the experimental transient 2D-IR spectrum (see Figure 9.4 f), has its origin in the coupling to the pumped Aib band or in its direct excitation by the IR-pump pulse.

To neglect possible direct excitation the IR-pump pulse, a long-time (1 ns time de-

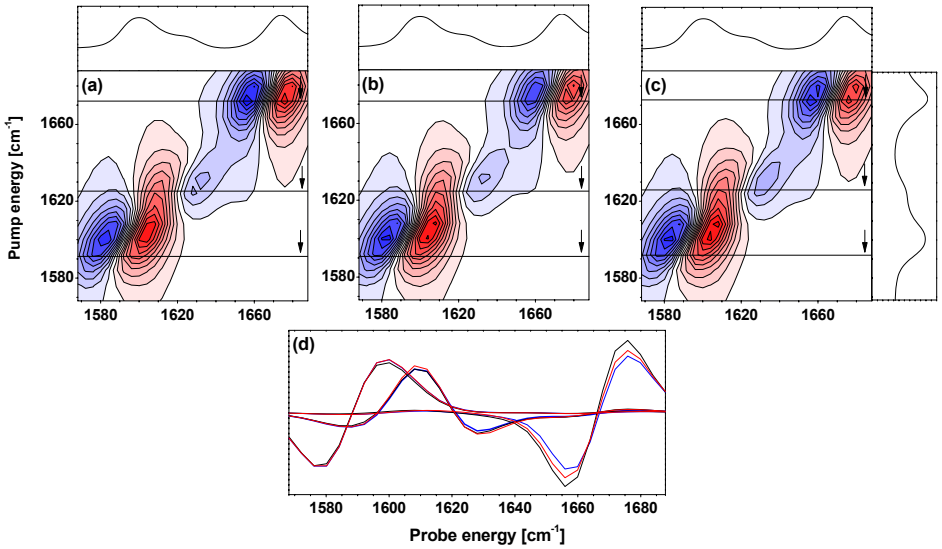

Figure 9.9: Top: Simulated transient 2D-IR spectrum with parallel polarization and 1.2 ps time delay between the IR-pump and IR-probe pulse and with perpendicular polarization and 1 ns time delay between the UV-pump and IR-pump pulse of thioxopeptide **1b** with (a) no coupling in the initial state and no coupling in the final state, (b) coupling (-6 cm^{-1}) in the initial state and no coupling in the final state and (c) coupling (-6 cm^{-1}) in the initial state and coupling (-6 cm^{-1}) in the final state. (d): Cuts taken at IR-pump pulse frequencies of 1593, 1624 and 1672 cm^{-1} in the simulated transient 2D-IR spectrum with (black) no coupling in the initial state and no coupling in the final state, (blue) coupling (-6 cm^{-1}) in the initial state and no coupling in the final state and (red) coupling (-6 cm^{-1}) in the initial state and coupling (-6 cm^{-1}) in the final state.

lay) transient 2D-IR spectrum of thioxopeptide **1b** for the different coupling assumptions mentioned above is simulated (see Figure 9.9 a-c). The cuts show no significant differences between the three line shapes (see Figure 9.9 d). On one hand, the Ala(1) and Aib band are further apart from each other than in thioxopeptide **1a** (73 and 49 cm^{-1} for the hydrogen-bonded and no hydrogen-bonded Ala(1) band respectively), and thus there is no direct excitation of the Ala(1) band when pumping at the spectral position of the Aib band and vice-versa. On the other hand, the bands seem to be insensitive to the coupling between them due to the large spectral distance they have. Up to a coupling constant β = $\pm$12 cm^{-1} no distinct differences for the different coupling situations are observed with this spectral distance between the bands.

9.4 Conclusion

Transient 2D-IR measurements have been performed on Boc-Ala-Pro-ψ(SC-NH)-Aib-Ala-OMe. The long-time spectrum (1 ns time delay between the UV-pump and the IR pulses)

indicates a change of the cross peak intensity between the Aib and the Ala(1) band due to $i \rightarrow i{+}3$ hydrogen-bond breaking. However, interference with the diagonal peak is strong.

Therefore, computer simulations of the inner part of the thioxopeptide have been performed. It has been shown that the simulations are most sensitive on the choice of the relative transition dipole strengths of the different bands and their changes due to isomerization.

Comparison between the simulated and experimental transient 2D-IR spectra point out that one has to be careful interpreting the spectra. The transient 2D-IR spectrum could not be unambiguously related to a change in coupling across the hydrogen-bond. One obstacle is the spectral overlap between the amide I bands, which can be neglected by using a system where the IR bands are further apart from each other. The cross peak intensity between two bands decreases significantly. Taking this into account, the measurement of transient 2D-IR spectra will remain a challenging task in the future and their correct interpretation need very detailed investigation of the system of interest by complementary techniques.

Chapter 10

Summary and Outlook

In this work, the potential of time-resolved infrared spectroscopy to reveal structural changes during peptide dynamics has been explored. For this purpose a -Pro-Aib- and thioamide-containing peptide, Boc-Ala-Pro-ψ(SC-NH)-Aib-Ala-OMe, has been synthesized. Using a variation of the 'Azirine/Oxazolone method' with an overall yield of 8 %. On one hand the -Pro-Aib- amino acid sequence is known to induce a well-defined β-turn conformation in a peptide which is characterized by a $i \rightarrow i{+}3$ hydrogen-bond. On the other hand a conformational change can be induced in the peptide by isomerizing the thioamide bond. Time-resolved IR-studies have shown that the isomerization of NMTAA, which is the simplest isomerizable thioamide analogue, is completed after 1 ns and has a trans $\rightarrow$ cis quantum yield of 30 - 40 %. The amino acid sequence has been chosen in a way that the amide I bands are well-resolved. Therefore, this thioxopeptide is an optimal model peptide for transient 2D-IR measurements.

The conformations of the synthesized thioxopeptide have been analyzed by linear and two-dimensional IR spectroscopy, as well as by NMR methods. It has been shown that in acetonitrile solution at room temperature a hydrogen-bonded structure, in which the amide proton of Aib forms a hydrogen-bond with the C=O carbonyl of the Ala(1) moiety, is present in coexistence with non hydrogen-bonded conformations, which remain unresolved. At higher temperatures the equilibrium is shifted away from the hydrogen-bonded conformation. β-turn opening and -closing happens on a timescale much slower than 4 ps, and can therefore not be detected by 2D-IR exchange spectroscopy.

Transient infrared spectroscopy could be used to follow the $i \rightarrow i{+}3$ hydrogen-bond breaking. The whole process is completed within 1 ns. The hydrogen-bond breaking results in a strong blue-shift of the Ala(1) amide I band and a corresponding smaller blue-shift of the Aib amide I band.

In addition, partial $i{+}3 \rightarrow i$ hydrogen-bonding with Ala(1) as a proton donor is indicated by the NMR data. Nevertheless, the spectral changes observed upon photoiso-

merization of the thioxopeptide do not confirm this hypothesis. In fact, spectral changes observed upon photoisomerization are much more specific for identifying intramolecular hydrogen-bonds than steady state absorption and temperature-dependent NMR data.

Transient infrared measurements on other -Aib-containing thioxopeptides (already Aib without Pro can induce a β-turn conformation) have been performed for comparison with Boc-Ala-Pro-ψ(SC-NH)-Aib-Ala-OMe. All thioxopeptides show very similar isomerization dynamics, whereas the relaxation in the thermal ground state after isomerization differs significantly, strongly depending on the steric interaction of the side chain of the thio-substituted residue *i+1* and Aib.

Additionally, angles between transitions dipole moments could be measured by using polarization-dependent time-resolve pump/probe spectroscopy. The structural information of the different thioxopeptides have been compared. The most rigid structure is found between moieties adjacent to the Aib amino acid, which is known to define peptide geometry with little margin. A conserved thioamide-Aib core structure was found in all thioxopeptides, while the tails of the thioxopeptides are very flexible. The anisotropies of Boc-Ala-Pro-ψ(SC-NH)-Aib-Ala-OMe consistent with β-turn structure and *ab initio* calculations.

From the comparison of the different thioxopeptides, conclusions about the isomerization mechanism and relaxation mechanism in the thermal ground state could be drawn. The current picture of the mechanism by which efficient photoisomerization is possible in a large number of monosubstituted thioxopeptides, involves a diffusive torsional motion about a thioamide single bond during the $\approx$ 200 ps lifetime of the lowest lying electronically excited state, followed by strongly driven motion in the electronic ground state. Further theoretical work would now be needed in order to establish if a sufficiently large region of conformational space can be sampled by the photo-excited peptides within 200 ps to reach the favorable conical intersections or intersystem crossing points, which, in the gas phase, have been predicted to lead to the cis photoproduct.

Transient 2D-IR measurements have been performed on Boc-Ala-Pro-ψ(SC-NH)-Aib-Ala-OMe. The long-time spectrum (1 ns time delay between the UV-pump and the IR pulses) indicates a change of the cross peak intensity between the Aib and the Ala(1) band due to $i \rightarrow i+3$ hydrogen-bond breaking. However, interference with the diagonal peak is strong. Therefore, computer simulations of the inner part of the thioxopeptide have been performed. It has been shown that the simulations are most sensitive on the choice of the relative transition dipole strengths of the different bands and their changes due to isomerization. Comparison between the simulated and experimental transient 2D-IR spectra point out that one has to be careful interpreting the spectra. The transient 2D-IR spectrum could not be unambiguously related to a change in coupling across the

hydrogen-bond. One obstacle is the spectral overlap between the amide I bands, which can be neglected by using a system where the IR bands are further apart from each other. The cross peak intensity between two bands decreases significantly. Taking this into account, the measurement of transient 2D-IR spectra will remain a challenging task in the future and their correct interpretation need very detailed investigation of the system interested by complementary techniques.

Appendix A

Parameter Determination

To simulate (transient) 2D-IR spectra different parameters have to be determined which are summarized in Table 9.1. In the following sections, detailed information about the derivation of the parameters is presented.

Fixed parameters - IR-pump width ω_{pump}, homogeneous width ω_{hom}

The measured spectral width of the IR-pump pulse ω_{pump} is 10 cm^{-1}.

The homogeneous width of all IR bands is fixed at 10 cm^{-1} which is in good agreement with previous results [14].

From the FT-IR spectrum - Spectral positions E_i, inhomogeneous widths ω_i

The values for the center frequencies $E_{Ala,bonded,\mathbf{1b}}$, $E_{Ala,nonbonded,\mathbf{1b}}$ and $E_{Aib,\mathbf{1b}}$ in the exciton basis, their inhomogeneous widths $\omega_{Ala,bonded,\mathbf{1b}}$, $\omega_{Ala,nonbonded,\mathbf{1b}}$ and $\omega_{Aib,\mathbf{1b}}$ are revealed from the FT-IR absorption spectrum of thioxopeptide **1b**. Additionally, 2D-IR spectra are simulated with small variations of these parameters and fitted to the experimental 2D-IR spectrum to define the optimal values.

From Long-time UV-pump/IR-probe spectrum - Relative transitions dipole strengths $\mid \overrightarrow{\mu}_i \mid$

It has to be considered that the area of the hydrogen-bonded (1600 cm^{-1}, negative) Ala(1) band (which is proportional to μ^2) in the long-time transient Uv-pump/IR-probe

spectrum of thioxopeptide **1b** (1 ns time delay) is approximately 1.55 times stronger than the one of the non hydrogen-bonded (1623 cm^{-1}, positive) Ala(1) band (see Figure 6.2). Thus, the transition dipole strength of the hydrogen-bonded band $\mu_{Ala,bonded}$ is set $1.24 \times \mu_{Ala,nonbonded}$ ($\mu_{Aib,bonded} = \mu_{Aib,nonbonded} = \mu_{Ala,nonbonded}$).

From anisotropy and *ab initio* calculations - Angle θ and dipole-dipole coupling β between the transition dipole moments

Ab inition normal mode calculations are performed on a MeCO-Pro-ψ(SC-NH)-Aib-NHMe moiety which corresponds to the core structure of thioxopeptide **1**. The input structure is revealed by the corresponding part of the crystal structure of Boc-Pro-(Aib-Δ^ZPhe)$_2$-Aib-OMe is used [129]. The carbonyl group of Pro amino acid is then substituted by a C=S group. The calculations are performed in Gaussian '03 on the B3LYP level using a two-layered 6-311++g**: b3lyp/6-31++g** basis set [130]. The first layer consists of all atoms except the ones of the sidechains. Consequently, the second layer consists of two CH_3-groups (Aib) and one C_3H_6-group.

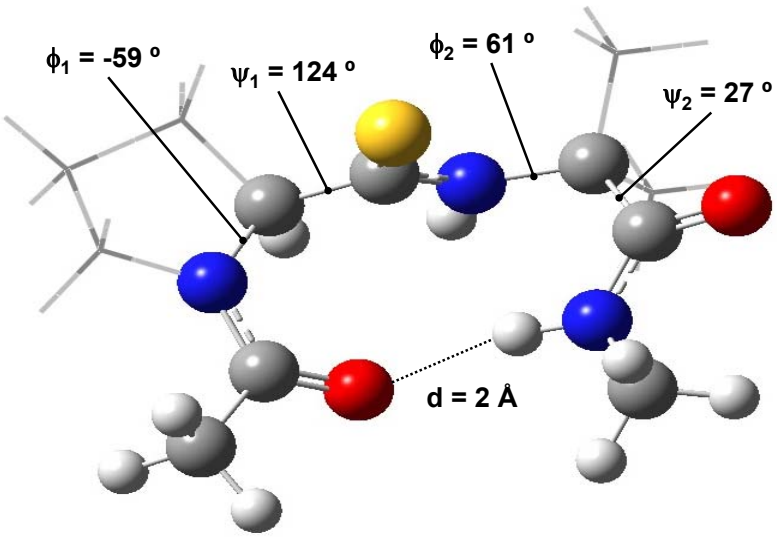

Figure A.1: Optimized structure of a MeCO-Pro-ψ(SC-NH)-Aib-NHMe moiety with their ϕ and ψ angles, revealed by Gaussian '03 calculations with a two-layered oniom(b3lyp/6-311++g**:b3lyp/6-31++g**) basis. Atoms due to first layer are indicated with balls, the ones due to second layer with sticks.

The optimized structure with the corresponding ϕ- and ψ-angles is shown in Figure

A.1. Comparing the angles with characteristic β-turn angles, the structure is closest to a type II β-turn (ϕ_1 = -60 °, ψ_1 = 120 °, ϕ_2 = 90 °, ψ_2 = 0 °) [126]. The anisotropies and corresponding angles between transitions dipole moments are listed in Table A.1 and compared to the ones of thioxopeptide **1**, determined by anisotropy measurements (see chapter 8. The values are very similar to each other. Therefore, it can be considered that the calculated structure is close to the one of thioxopeptide **1** in acetonitrile and the determined θ and β can be considered for the simulation of the (transient) 2D-IR spectra.

Thioxopeptide		**1**	Gauss
Anisotropy	Ala(1) (*i*)/ Pro(*i+1*, thio)	-0.02	-0.04
	Ala(1) (*i*)/ Aib (*i+2*)	-0.06[a]	-0.14
	Pro (*i+1*, thio)/ Aib (*i+2*)	-0.14	-0.17
Angle	Ala(1) (*i*)/ Pro(*i+1*, thio)	123	121
	Ala(1) (*i*)/ Aib (*i+2*)	65[a]	71
	Pro (*i+1*, thio)/ Aib (*i+2*)	71	77

Table A.1: Anisotropy and angle values between IR/UV-transition dipole moments of the thioxopeptide **1** and the optimized MeCO-Pro-ψ(SC-NH)-Aib-Me structure revealed by Gaussian '03 calculations based on the crystal structure of Inai et al. [129]. *a*: Hydrogen-bonded band at 1600 cm^{-1} of thioxopeptide **1b**.

The dipole-dipole coupling β between the two infrared transition dipole moments are obtained by using the so-called Hessian matrix reconstruction method (see chapter 2, equation 2.5) [94, 95]:

$$\begin{pmatrix} \varepsilon_1 & \beta_{12} \\ \beta_{12} & \varepsilon_2 \end{pmatrix} = U^{-1} \begin{pmatrix} E_1 & 0 \\ 0 & E_2 \end{pmatrix} U.$$

The calculations predict a coupling constant β = -6 cm^{-1}.

To check the plausibility of the calculated parameters β and θ, a series of simulated 2D-IR spectra (for perpendicular and parallel orientation of the IR-pump and IR-probe pulse) are performed by varying β from -16 to 16 cm^{-1} and θ from 0 to 180°. The frequencies ε in the site basis have been chosen such that the resulting frequencies E in the exciton basis remain constant for the different coupling values β_{12}. The spectra then are compared to the experimental 2D-IR spectra of thioxopeptide **1a**[1] by adding the squared differences (χ^2) between the simulated and experimental intensities at each spectral position for both perpendicular and parallel datasets (see Figure A.2). The smaller χ^2 the better the fit. Going from black to dark red increases the value from 35.0 to 81.0. In the region at β = -6 cm^{-1} and θ = 70 ° a local minimum is found (circled in Figure A.2) in agreement

[1]Thioxopeptide **1a** is taken because the bands are closer to each other than in thioxopeptide **1b**. Therefore the coupling has more influence on the shape of the spectra.

with the *ab initio* results. Thus, the calculated parameters β = -6 cm^{-1} and θ = 70 ° are adopted for the simulations of the (transient) 2D-IR spectra.

For the simulations of the 2D-spectra, it is assumed that the average coupling between Ala(1) and Aib amide I modes is significantly smaller in the non hydrogen-bonded species than in the hydrogen-bonded species. Therefore, the coupling between the non hydrogen-bonded Ala(1)and the Aib band is set to 0.

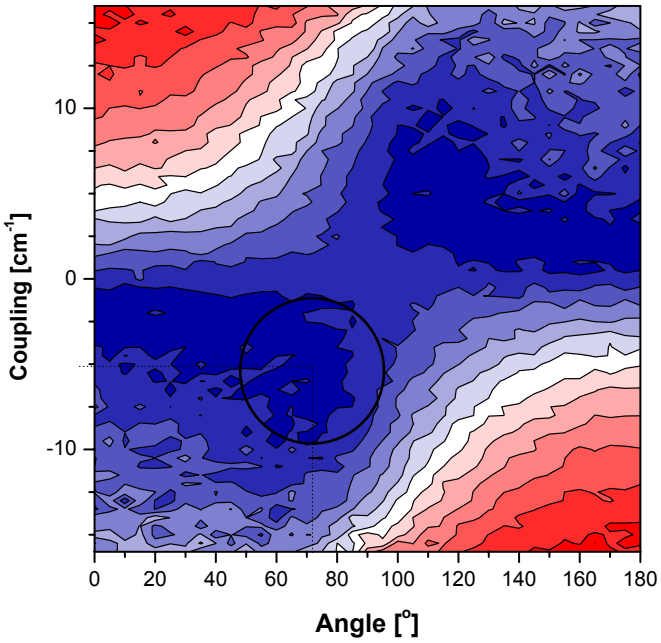

Figure A.2: 2D-plot of the fit between the experimental and calculated 2D-IR spectra with perpendicular and parallel polarization of thioxopeptide **1a** with varying the parameters β from -16 to 16 cm^{-1} and θ from 0 to 180 ° with fixed frequencies E in the exciton basis. The values - from 35.0 (black) to 81.0 (dark red), contour intervals are 1.5- are calculated by taking the squared differences (χ^2) between the simulated and experimental intensities at each spectral position.

From 2D-IR simulations - Hydrogen-bonded/non hydrogen-bonded ratio τ

The relative ratio τ of the non hydrogen-bonded and the hydrogen-bonded species of the thioxopeptide **1b** in the thermal ground state is obtained by adding the two 2D-IR spectra with different weights and then comparing to the experimental 2D-IR spectrum of thioxopeptide **1b**.

Bibliography

[1] E. Fischer. *Ber. Dtsch. Chem. Ges.*, 27:2985, 1894.

[2] M. Schliwa and G. Woehlke. *Nature*, 422:759, 2003.

[3] R. D. Vale and R. A. Milligan. *Science*, 288:88, 2000.

[4] J. Monod, J. Wyman, and J.-P. Changeux. *J. Mol. Biol.*, 12:88, 1965.

[5] L. T. May, K. Leach, P. M. Sexton, and A. Christopoulos. *Annu. Rev. Pharmacol. Toxicol.*, 47:1, 2006.

[6] A. Christopoulos, L. T. May, V. A. Avlani, and P. M. Sexton. *Biochem. Soc. Trans.*, 32:873, 2004.

[7] R. M. Daniel, R. V. Dunn, J. L. Finney, and J. C. Smith. *Annu. Rev. Biophys Biomol. Struct.*, 32:69, 2003.

[8] D. Kern and E. Zuiderweg. *Curr. Opin. Struct. Biol.*, 13:748, 2003.

[9] H. J. C. Berendsen and S. Hayward. *Curr. Opin. Struct. Biol.*, 10:165, 2000.

[10] K. Wüthrich. *NMR of proteins and nucleic acids, Wiley*, 1986.

[11] J. Drenth. *Principles of protein x-ray crystallography, Springer*, 1999.

[12] Y. Duan and P. A. Kollman. *Science*, 282:740, 1998.

[13] S. Woutersen, R. Pfister, P. Hamm, Y. Mu, D. S. Kosov, and G. Stock. *J. Chem. Phys.*, 117:6833, 2002.

[14] S. Woutersen and P. Hamm. *J. Phys.: Condens. Matter*, 14:1035, 2002.

[15] N. Hui and R. Hochstrasser. *PhysChemComm*, 5:1035, 2002.

[16] M. Khalil, N. Demirdöven, and A. Tokmakoff. *J. Phys. Chem. A*, 107:5258, 2003.

[17] M. T. Zanni, M. C. Asplund, and R. M. Hochstrasser. *J. Chem. Phys.*, 114:4579, 2001.

[18] S. Woutersen and P. Hamm. *J. Phys. Chem. B*, 47:11316, 2000.

[19] S. Woutersen, G. Stock, and P. Hamm. *Proc. Natl. Acad. Sci. U.S.A.*, 98:11254, 2001.

[20] S. Woutersen and P. Hamm. *J. Chem. Phys.*, 114:2727, 2001.

[21] J. Bredenbeck and P. Hamm. *J. Chem. Phys.*, 119:1569, 2003.

[22] J. Bredenbeck, J. Helbing, and P. Hamm. *J. Am. Chem. Soc.*, 126:990, 2004.

[23] V. Cervetto, P. Hamm, and J. Helbing. *J. Phys. Chem. B*, 112:8398, 2008.

[24] T. Wang, Y. Zhu, Z. Getahun, D. Du, C.-Y. Huang, W. F. DeGrado, and F. Gai. *J. Phys. Chem. B*, 108:15310, 2004.

[25] S. A. Petty and M. Volk. *Phys. Chem. Chem. Phys.*, 6:1022, 2004.

[26] S. Williams, T. P. Causgrove, R. Gilmanshin, K. S. Fang, R. H. Callender, W. H. Woodruff, and R. B. Dyer. *Biochemistry*, 35:691, 1996.

[27] V. Muñoz, P. A. Thompson, J. Hofrichter, and W. A. Eaton. *Nature*, 390:196, 1997.

[28] T. Nägele, R. Hoche, W. Zinth, and J. Wachtveitl. *Chem. Phys. Lett.*, 272:489, 1997.

[29] C. Renner, R. Behrendt, S. Sprlein, J. Wachtveitl, and L. Moroder. *Biopolymers*, 54:489, 2000.

[30] C. Renner, J. Cramer, R. Behrendt, and L. Moroder. *Biopolymers*, 54:501, 2000.

[31] A. Aemisegger, P. H. Huenenberger, D. Hilvert, T. Hansson, and W. F. Van Gunsteren. *J. Am. Chem. Soc.*, 127:4935, 2005.

[32] A. Aemisegger, V. Kraeutler, W. F. van Gunsteren, and D. Hilvert. *J. Am. Chem. Soc.*, 127:2929, 2005.

[33] A. Aemisegger and D. Hilvert. *Nat. Protocols*, 2:161, 2007.

[34] J. R. Kumita, O. S. Smart, and G. A. Wolley. *Proc. Natl. Acad. Sci. U.S.A.*, 97:2771, 2000.

[35] R. Behrendt, C. Renner, M. Schenk, F. Wang, J. Wachtveitl, D. Oesterhelt, and L. Moroder. *Angew. Chem. Int. Ed.*, 38:2771, 1999.

[36] J. Bredenbeck, J. Helbing, A. Sieg, T. Schrader, W. Zinth, C. Renner, R. Behrendt, L. Moroder, J. Wachtveitl, and P. Hamm. *Proc. Natl. Acad. Sci. U.S.A.*, 100:6452, 2003.

[37] J. Bredenbeck, J. Helbing, J. R. Kumita, G. A. Wolley, and P. Hamm. *Proc. Natl. Acad. Sci. U.S.A.*, 102:2379, 2005.

[38] J. A. Ihalainen, J. Bredenbeck, R. Pfister, J. Helbing, , L. Chiy, I. H. M. Van Stokum, G. A. Woolley, and P. Hamm. *Proc. Natl. Acad. Sci. U.S.A.*, 104:5383, 2007.

[39] J. Wachtveitl, S. Spörlein, H. Satzger, B. Fonrobert, C. Renner, R. Behrendt, D. Oesterhelt, L. Moroder, and W. Zinth. *Biophys. J.*, 86:2350, 2004.

[40] G. Mayer and A. Heckel. *Angew. Chem. Int. Ed.*, 45:4900, 2006.

[41] T. E. Schrader, W. J. Schreier, T. Cordes, F. O. Koller, G. Babitzki, R. Denschlag, C. Renner, M. Loweneck, S.-L. Dong, L. Moroder, P. Tavan, and W. Zinth. *Proc. Natl. Acad. Sci. U.S.A.*, 104:15729, 2007.

[42] J. Bredenbeck, J. Helbing, R. Behrendt, C. Renner, L. Moroder, J. Wachtveitl, and P. Hamm. *J. Phys. Chem. B*, 107:8654, 2003.

[43] M. Volk, Y. Kholodenko, H. S. M. Lu, E. A. Gooding, W. F. DeGrado, and R. M. Hochstrasser. *J. Phys. Chem. B*, 101:8607, 1997.

[44] H. S. M. Lu, M. Volk, Y. Kholodenko, E. Gooding, R. M. Hochstrasser, and W. F. DeGrado. *J. Am. Chem. Soc.*, 119:7173, 1997.

[45] C. Kolano, K. Gomann, and W. Sander. *Eur. J. Org. Chem.*, 20:4167, 2004.

[46] C. Kolano, J. Helbing, G. Bucher, W. Sander, and P. Hamm. *J. Phys. Chem. B*, 111:11297, 2007.

[47] C. Kolano, J. Helbing, M. Kozinski, W. Sander, and P. Hamm. *Nature*, 444:469, 2006.

[48] Song S, S. A. Asher, S. Krimm, and K. D. Shaw. *J. Am. Chem. Soc.*, 113:1155, 1991.

[49] I. Harada and M. Tasumi. *Chem. Phys. Lett.*, 70:279, 1980.

[50] E. B. Nielsen and J. A. Scellman. *J. Phys. Chem.*, 71:2297, 1967.

[51] J. H. Miwa, A. K. Patel, N. Vivatrat, S. M. Popek, and A. M. Meyer. *Org. Lett.*, 3:3373, 2001.

[52] J. H. Miwa, L. Pallivathucal, S. Gowda, and K. E. Lee. *Org. Lett.*, 4:4655, 2002.

[53] J. Zhao, D. Wildemann, M. Jakob, C. Vargas, and C. Schiene-Fischer. *Chem. Commun.*, page 2810, 2003.

[54] J. Zhao, J.-C. Micheau, C. Vargas, and C. Schiene-Fischer. *Chem. Eur. J.*, 10:6093, 2004.

[55] H. Satzger, C. Root, P. Gilch, W. Zinth, D. Wildemann, and G. Fischer. *J. Phys. Chem. B*, 109:4770, 2005.

[56] V. Cervetto, R.Pfister, and J. Helbing. *J. Phys. Chem. B*, 112:3540, 2008.

[57] V. Cervetto. *PhD thesis, University of Zürich*, 2007.

[58] L. Lankiewicz, C. Y. Bowers, G. A. Reynolds, V. Labroo, L. A. Cohen, S. Vonhof, A.-L. Sirén, and A. F. Spatola. *Biochem. Biophys. Res. Commun.*, 184:359, 1992.

[59] M. Schutowski, K. Neubert, and G. Fischer. *Eur. J. Biochem.*, 221:455, 1994.

[60] Y. Hitotsuyanagi, J. Suzuki, Y. Matsumoto, K. Takeya, and H. Itokawa. *J. Chem. Soc, Perkin Trans. 1*, page 1887, 1994.

[61] D. Wildemann, C. Schiene-Fischer, T. Aumüller, A. Bachmann, T. Kiefhaber, C. Lücke, and G. Fischer. *J. Am. Chem. Soc.*, 129:4910, 2007.

[62] M. P. Cava and M. I. Levinsnon. *Tetrahedron*, 41:5061, 1985.

[63] I. Thomsen, K. Clausen, S. Scheibye, and S.-O. Lawesson. *Org. Synth.*, 62:158, 1984.

[64] R. Frank, M. Jakob, F. Thunecke, G. Fischer, and M. Schutkowski. *Angew. Chem. Int. Ed*, 39:1120, 2000.

[65] M. A. Shalaby, C. W. grote, and H. Rapoport. *J. Org. Chem.*, 61:9045, 1996.

[66] K. Clausen, M. Thorsen, and S.-O. Lawesson. *Tetrahedron*, 37:3635, 1981.

[67] M. Thorsen, U. Pedersen, K. Clausen, and S.-O. Lawesson. *Tetrahedron*, 39:3429, 1983.

[68] G. Lajoie, F. Lépine, L. Maziak, and B. Belleau. *Tetrahedron Lett.*, 24:3815, 1983.

[69] K. Clausen, M. Thorsen, S.-O. Lawesson, and A. F. Spatola. *J. Chem. Soc, Perkin Trans. 1*, page 785, 1984.

[70] T. Sifferlen, M. Rueping, K. Gademann, B. Jaun, and D. Seebach. *Helv. Chim. Acta*, 82:2067, 1999.

[71] R. Frank and M. Schutkowski. *Chem. Commun.*, page 2509, 1996.

[72] R. Nagaraj and P. Balaram. *Acc. Chem. Phys.*, 14:356, 1981.

[73] P. Wipf and H. Heimgartner. *Helv. Chim. Acta*, 70:354, 1987.

[74] H. Heimgartner. *Angew. Chem.*, 103:271, 1991.

[75] R. A. Breitenmoser, A. Linden, and H. Heimgartner. *Helv. Chim. Acta*, 85:990, 2002.

[76] J. P. Lehmann. *PhD thesis, University of Zürich*, 1998.

[77] J. Lehmann, A. Linden, and H. Heimgartner. *Tetrahedron*, 55:5359, 1999.

[78] J. Zheng, K. Kwak, J. Asbury, X. Chen, I. R. Piletic, and M. D.Fayer. *Science*, 309:1338, 2005.

[79] Y. S. Kim and R. M. Hochstrasser. *Proc. Natl. Acad. Sci. U.S.A.*, 102:11185, 2005.

[80] J. B. Asbury, T. Steinel, C. Stromberg, K. J. Gaffney, I. R. Piletic, A. Goun, and M. D. Fayer. *Phys. Rev. Lett.*, 91:237402, 2003.

[81] S. Yeremenko, M. S. Pschenichnikov, and D. A. Wiersma. *Chem. Phys. Lett.*, 369:107, 2003.

[82] M. L. Cowan, B. D. Bruner, N. Huse, J. R. Dwyer, B. Chugh, E. T. J. Nibbering, T. Elsaesser, and R. J. D. Miller. *Nature*, 434:199, 2005.

[83] J. D. Eaves, J. J. Loparo, C. J. Fecko, S. T. Roberts, A. Tokmakoff, and P. L.Geissler. *Proc. Natl. Acad. Sci. U.S.A.*, 102:13019, 2005.

[84] O. Golonzka, N. Demirdöven, M. Khalili, and A. Tokmakoff. *J. Chem. Phys.*, 113:9893, 2000.

[85] C. J. Milne, Y. L. Li, T. L. C. Jansen, L. Huang, and R. J. D. Miller. *J. Phys. Chem. B*, 110:19867, 2006.

[86] L. J. Kaufman, J. Heo, L. D. Ziegler, and G. R. Fleming. *Phys. Rev. Lett.*, 88:207402, 2002.

[87] W. Zhao and J. C. Wright. *Phys. Rev. Lett.*, 84:1411, 2000.

[88] P. M. Donaldson, R. Guo, F. Fournier, E. M. Gardner, L. M. C. Barter, C. J. Barnett, I. R. Gould, D. R. Klug, P. D. Jason, and K. R. Willison. *J. Chem. Phys.*, 127:114513, 2007.

[89] E. Jr. Bright Wilson, J. C. Decius, and P. C. Cross. *Molecular Vibrations (New York: McGraw-Hill)*, 1955.

[90] P. Hamm, M. Lim, and R. M. Hochstrasser. *J. Phys. Chem. B*, 102:6123, 1998.

[91] P. Hamm, W. F. DeGrado, and R. M. Hochstrasser. *Proc. Natl. Acad. Sci. U.S.A.*, 96:2036, 1999.

[92] S. Krimm and J. Bandekar. *Adv. Prot. Chem.*, 38:181, 1986.

[93] H. Torii and M. Tasumi. *J. Chem. Phys.*, 96:3379, 1992.

[94] S. Ham and M. Cho. *J. Chem. Phys.*, 118:6915, 2003.

[95] P. Hamm and S. Woutersen. *Bull. Chem. Soc. Jpn*, 75:985, 2002.

[96] R. G. Gordon. *J. Chem. Phys.*, 45:1643, 1966.

[97] M. Dantus, R. M. Bowman, J. S. Baskin, and A. H. Zewail. *Chem. Phys. Lett.*, 159:406, 1989.

[98] K. Dietliker and H. Heimgartner. *Helv. Chim. Acta*, 66:262, 1983.

[99] J. Bredenbeck and P. Hamm. *Rev. Sci. Instrum.*, 74:3188, 2003.

[100] D. E. Spence, P. N. Kean, and W. Sibbett. *Opt. Lett.*, 16:42, 1991.

[101] N. H. Rizvi, P. M. W. French, and J. R. Taylor. *Opt. Lett.*, 17:279, 1992.

[102] D. Stickland and G. Mourou. *Opt. Commun.*, 55:447, 1985.

[103] P. Hamm, C. Lauterwasser, and W. Zinth. *Opt. Lett.*, 18:1943, 1993.

[104] J. Stenger. *PhD thesis, Logos Verlag, Berlin*, 2002.

[105] P. Hamm, R. A. Kaindel, and J. Stenger. *Opt. Lett.*, 25:1798, 2000.

[106] S. Ataka, H. Takechi, I. Harada, and M. Tasumi. *J. Phys. Chem.*, 88:449, 1984.

[107] C. Kato, H. Hamaguchi, and M. Tasumi. *J. Phys. Chem.*, 89:407, 1985.

[108] J. Helbing, H. Bregy, J. Bredenbeck, R. Pfister, P. Hamm, R. Huber, J. Wachtveitl, L. DeVico, and M. Olivucci. *J. Am. Chem. Soc.*, 126:8823, 2004.

[109] V. Cervetto, H. Bregy, P. Hamm, and J. Helbing. *J. Phys. Chem. A*, 110:11473, 2006.

[110] P. Hamm, M. Lim, and R. M. Hochstrasser. *J. Chem. Phys.*, 107:10523, 1997.

[111] P. Hamm, S. M. Ohline, and W. Zinth. *J. Chem. Phys.*, 106:519, 1997.

[112] G. Sieler and R. Schweitzer-Stenner. *J. Am. Chem. Soc.*, 119:1720, 1997.

[113] X. G. Chen, S. A. Asher, R. Schweitzer-Stenner, N. G. Mirkin, and S. Krimm. *J. Am. Chem. Soc.*, 117:2884, 1995.

[114] M. A. El-Sayed. *J. Chem. Phys.*, 38:2834, 1963.

[115] R. A. Shaw, E. Kollat, M. Hollosi, and H. H. Mantsch. *Spectrochimica Acta Part I*, 51:1399, 1995.

[116] O. E. Jensen, S.-O. Lawesson, R. Bardi, A. M. Piazzesi, and C. Toniolo. *Tetrahedron*, 23:5595, 1985.

[117] R. Bosch, G. Jung, and W. Winter. *Liebigs Ann. Chem.*, 1982:1322, 1982.

[118] M. Branik and H. Kessler. *Tetrahedron*, 30:781, 1974.

[119] H. Kessler. *Angew. Chem. Int. Ed.*, 21:512, 1982.

[120] D. V. Kurochkin, S. R. G. Naraharisetty, and I. V. Rubtsov. *Proc. Natl. Acad. Sci. U.S.A.*, 104:14209, 2007.

[121] V. Cervetto, R. Pfister, C. Kolano, H. Bregy, H. Heimgartner, and J. Helbing. *Chem. Eur. J.*, 13:9004, 2007.

[122] E. Benedetti, B. Di Blasio, V. Pavone, C. Pedone, C. Toniolo, and G. M. Bonora. *Int. J. Biol. Macromol.*, 2:217, 1980.

[123] J. W. Bats, H. Fuess, H. Kessler, and R. Schuck. *Chem. Ber.*, 113:520, 1980.

[124] S. Woutersen and P. Hamm. *Bull. Chem. Soc. Jpn.*, 75:985, 2002.

[125] L. DeVico. *priv. comm.*, 2005.

[126] E. G. Hutchinson and J. M. Thornton. *Protein Sci.*, 3:2207, 1994.

[127] S. Woutersen and P. Hamm. *J. Chem. Phys.*, 115:7737, 2001.

[128] V. Cervetto, J. Helbing, J. Bredenbeck, and P. Hamm. *J. Chem. Phys.*, 121:5935, 2004.

[129] Y. Inai, T. Oshikawa, M. Yamashita, T. Hirabayashi, and S. Ashitaka. *J. Chem. Soc., Perkin Trans. 2*, page 892, 2001.

[130] M. J. Frisch, G. W. Trucks, H. B. Schlegel, G. E. Scuseria, M. A. Robb, J. R. Cheeseman, Jr. J. A. Montgomery, T. Vreven, K. N. Kudin, J. C. Burant, J. M. Millam, S. S. Iyengar, J. Tomasi, V. Barone, B. Mennucci, M. Cossi, G. Scalmani, N. Rega, G. A. Petersson, H. Nakatsuji, M. Hada, M. Ehara, K. Toyota, R. Fukuda, J. Hasegawa, M. Ishida, T. Nakajima, Y. Honda, O. Kitao, H. Nakai, M. Klene, X. Li, J. E. Knox, H. P. Hratchian, J. B. Cross, V. Bakken, C. Adamo, J. Jaramillo, R. Gomperts, R. E. Stratmann, O. Yazyev, A. J. Austin, R. Cammi, C. Pomelli, J. W. Ochterski, P. Y. Ayala, K. Morokuma, G. A. Voth, P. Salvador, J. J. Dannenberg, V. G. Zakrzewski, S. Dapprich, A. D. Daniels, M. C. Strain, O. Farkas, D. K. Malick, A. D. Rabuck, K. Raghavachari, J. B. Foresman, J. V. Ortiz, Q. Cui, A. G. Baboul, S. Clifford, J. Cioslowski, B. B. Stefanov, G. Liu, A. Liashenko, P. Piskorz, I. Komaromi, R. L. Martin, D. J. Fox, T. Keith, M. A. Al-Laham, C. Y. Peng, A. Nanayakkara, M. Challacombe, P. M. W. Gill, B. Johnson, W. Chen, M. W. Wong, C. Gonzalez, and J. A. Pople. *Gaussian, Inc., Wallingford CT*, 2004.

Acknowledgements

First of all, I want to thank Dr. Jan Helbing. I have profited a lot from his knowledge about various issues concerning working in a laser lab. Further thanks goes to Prof. Dr. Peter Hamm for giving me the opportunity to realize my PhD thesis in his group. I also want to thank Dr. Christoph Kolano for supporting me during my peptide synthesis and my roommate Dr. Sean Garrett-Roe for helping me writing the thesis. Further, I want to thank Prof. Dr. Heinz Heimgartner for providing a number of thioxopeptides from his group. Of course, my thanks for a pleasant time in the group go to all group members I have met during the last years: Dr. Jens Bredenbeck, Dr. Julian Edler, Dr. Victor Volkov, Dr. Roland Schanz, Dr. Paul Kocian, Rolf Pfister, Dr. Virgiliu Botan, Dr. Valentina Cervetto, Mathias Bonmarin, Dr. Mariusz Kozinski, Dr. Ellen Backus, Dr. Janne Ihalainen, Adrian Jud, Andreas Messmer, Marco Schade, Fivos Perakis, Julien Réhault, Espen Andresen, Alexander Rodenberg, Mateusz Donten and Robbert Bloem.

Furthermore, I want to thank Armin Kühne, Roland Zehnder and Horst Blasi for their precision mechanical pieces, Ueli Feusi and Jens Jacobs for their excellent computer support, Hermann Schwarz for his electronic devices and last but not least Maja Gossweiler for handling all the administrative stuff.

My special thanks go to my parents which have supported me during my PhD thesis and moreover during my whole life. I also want to thank my brother Achim, his wife Corinne and their cute daughters Joanne and Tabea for the days we could spend together by now. Finally, my thanks go to all my relatives and friends, specifically to Tobi and his girlfriend Loo, Simone, Schretz, Sabrina, my godfather Marcel and his wife Olgi.

Curriculum vitae

Name:	Harald
Surname:	Bregy
Place and date of birth:	Zürich, Switzerland, 23.08.1979
Citizenship:	Swiss

Education:

2004-pres.	*PhD Program* University of Zürich, Switzerland
1999-2004	*Diploma in Chemistry (majored in Physical Chemistry)* University of Zürich, Switzerland
	Diploma Thesis Title : Zeitaufgelöste Infrarotabsorptionsspektroskopie der *trans/cis*-Isomerisierung von *N*-Methylacetamid
1992-1999	*High school* Kantonsschule Oerlikon, Zürich, Switzerland